

# University of Alberta

Probing the Molecular Interactions of Asphaltenes in Organic Solvents Using a Surface Forces Apparatus

by

Anand Natarajan

A thesis submitted to the Faculty of Graduate Studies and Research  
in partial fulfillment of the requirements for the degree of

Doctor of Philosophy

in

Materials Engineering

Department of Chemical and Materials Engineering

© Anand Natarajan  
Spring 2014  
Edmonton, Alberta

Permission is hereby granted to the University of Alberta Libraries to reproduce single copies of this thesis and to lend or sell such copies for private, scholarly or scientific research purposes only. Where the thesis is converted to, or otherwise made available in digital form, the University of Alberta will advise potential users of the thesis of these terms.

The author reserves all other publication and other rights in association with the copyright in the thesis and, except as herein before provided, neither the thesis nor any substantial portion thereof maybe printed or otherwise reproduced in any material form whatsoever without the author's prior written permission.

*To Family, Friends, Music and Zeal.*

## Abstract

A fundamental understanding of the stability of water-in-bitumen emulsions stabilized by surface active agents requires a good description of the molecular interactions between the different materials in contact. Of these surface active agents, asphaltenes and oil contaminated fine solids are major contributors to a stable emulsion. In this thesis, the molecular interactions of asphaltene surfaces in model oils, toluene and heptane, were measured using a surface forces apparatus. Adsorption of asphaltenes on mica surfaces was studied to understand the interactions that can occur between crude oil components and oil-contaminated fine solids during the extraction process.

The repulsive force measured between two asphaltene surfaces in toluene is attributed to steric repulsion, whereas the weak attractive force measured in heptane can be described by van der Waals forces. By fitting the measured force-distance profiles with theoretical models, the presence of secondary structures of asphaltenes in toluene was observed, stemming from the polydispersity/complexity of asphaltene molecules/aggregates. The adsorption results show that asphaltene adsorption onto mica is highly dependent on adsorption time and concentration of the solution. The adsorption process was identified to be controlled by diffusion of asphaltenes from the bulk solution to the mica surface.

Ethyl Cellulose (EC) is an effective demulsifier for water-in-bitumen emulsions. The interactions between asphaltenes, mica and EC were measured to understand the molecular mechanisms involved in destabilizing water-in-bitumen emulsions. Both EC and asphaltenes were observed to irreversibly adsorb on mica surface. The repulsive interaction forces measured during approach between EC and asphaltene surfaces in toluene were shown to have a steric nature, while the adhesive force measured between them during separation are attributed to attractive bridging forces between mica surfaces. Asphaltenes were observed to physisorb on EC coated surfaces and contribute to bridging adhesion. On the other hand, EC molecules were observed to gradually displace the irreversibly coated asphaltene films from mica surface, in which the asphaltenes are pushed into globule structures or nanoaggregates.

The above results provide an insight into the basic interaction mechanisms of asphaltenes in organic media and hence in crude oil and bitumen production.

## Acknowledgements

The work described in this thesis could not have been accomplished without the help of several parties that deserve recognition. First and foremost, I have to thank Dr. Zhenghe Xu, Dr. Jacob Masliyah and Dr. Hongbo Zeng for their continuous advice and support during the entire course of this work. I know that I have grown tremendously under their tutelage, not only as an engineer and research scientist, but also as a human being. They have always treated me with respect and challenged me with responsibilities, and have been a wonderful influence over the past five years. I wish them nothing but success, and I expect our personal and professional relationships to last for many years to come. I thank Dr. David Harbottle for all his help and advice during the last stages of my thesis and paper writing. Thank you for the countless hours of discussions face to face as well as over phone/skype.

I must also thank the various funding agencies throughout my time here at U of A, namely the members of the NSERC IRC in Oil Sands Engineering. To the various members of the Oil Sands Research group and Surface Science Research group over the years, I emphatically say thank you, particularly to Sharath Mahavadi, Benjamin Xie, Fucheng, Ali Faghihnejad, Jim Skwarok, Shau Yin, Jie Ru, Lisa Carreiro, and Leanne Swekla. Sharath, you helped to “get my lab coat dirty” in the lab, teaching me the basics of asphaltene chemistry. Benjamin, I will never forget the countless hours we spent in the lab trying to get good fringes. Fucheng

and Ali: thank you for teaching me the basics of MATLAB analysis and for the many hours of fruitful discussions. Jim, Shau Yin, Jie, Lisa and Leanne: Thank you so much for all your support and patience through the last five years.

To the staff of the Department of Chemical and Materials Engineering at U of A, I say THANK YOU! In particular, Les Dean, Walter Boddez, Kevin Heidebrecht, Lily Laser, Tina Baker, Gayle Hatchard, and Shiraz Merali have all been instrumental in many behind-the-scenes aspects of graduate school that you don't read about in the brochure.

To my many friends at U of A, I could not have survived without you. Simply having the opportunity to spend time with so many wonderful people kept me sane through the most challenging times. There are so many to list, and I hope I don't forget any. To Mridula, Michael, Ashish, Swetha, Akila, Barath, Sriram, Santhosh, Joy, and Fan, you all have made my time at U of A fun and memorable.

I must thank my family profusely for their endless support. Mom and Dad, without you, I wouldn't be here today. Mom, I will never forget the sacrifices you made for me. Dad, your passion for science and "learning by doing" is very inspiring and all I have achieved is derived from you. To my brother, Arjun, thank you for all your support during my years away from home. Finally, I dedicate this work to my wife, Priyanka, "the wind beneath my wings."

# Table of Contents

Chapter 1 Fundamentals of Oil Sands Extraction.....	- 1 -
1.1 Introduction .....	- 1 -
1.1.1 Bitumen Extraction. ....	- 2 -
1.1.2 Bitumen Froth Treatment.....	- 3 -
1.2 Asphaltenes – Definition, Composition and Molecular Aggregation ..	- 6 -
1.3 Emulsion and Emulsion Stability.....	- 10 -
1.4 Objective of the Thesis.....	- 12 -
1.5 Thesis Outline .....	- 15 -
1.6 References .....	- 17 -
Chapter 2 Molecular Forces.....	- 22 -
2.1 Theory of Adhesion.....	- 22 -
2.2 Adhesion at the Molecular Level .....	- 23 -
2.3 Jumping into Contact .....	- 25 -
2.4 Adhesion in Surface Forces Apparatus .....	- 26 -

2.5	Force Measurements .....	- 27 -
2.5.1	Mica Preparation .....	- 31 -
2.6	References .....	- 33 -
Chapter 3	Understanding Molecular Interactions of Asphaltenes in Organic Solvents Using a Surface Forces Apparatus .....	- 35 -
3.1	Introduction .....	- 35 -
3.2	Materials and Experimental Methods .....	- 39 -
3.2.1	Materials .....	- 39 -
3.2.2	Sample Preparation .....	- 39 -
3.2.3	Surface Forces Apparatus Technique .....	- 40 -
3.3	Results and Discussion.....	- 41 -
3.3.1	Interaction Forces in Toluene (Good Solvent).....	- 44 -
3.3.2	Interaction Forces in Heptane (Poor Solvent).....	- 57 -
3.3.3	Stability of Water-In-Oil Emulsions.....	- 60 -
3.4	Conclusion.....	- 62 -
3.5	References .....	- 64 -

Chapter 4 Understanding Mechanisms of Asphaltene Adsorption from Organic Solvent on Mica .....	- 70 -
4.1 Introduction .....	- 70 -
4.2 Materials and Experimental Methods .....	- 75 -
4.3 Sample Preparation .....	- 75 -
4.4 Surface Forces Measurements.....	- 76 -
4.4.1 AFM Imaging.....	- 77 -
4.5 Results and Discussion.....	- 77 -
4.5.1 Adsorption of Asphaltenes on Mica .....	- 78 -
4.6 Conclusion.....	- 92 -
4.7 Reference.....	- 94 -
Chapter 5 Understanding Molecular Interactions between Asphaltenes and Ethyl Cellulose immobilized on Hydrophilic Solids in Organic Solvent.....	- 98 -
5.1 Introduction .....	- 98 -
5.2 Materials and Experimental Methods .....	- 101 -
5.2.1 Materials .....	- 101 -

5.2.2	Sample Preparation .....	- 101 -
5.2.3	Force Measurement.....	- 102 -
5.3	Results and Discussion.....	- 104 -
5.3.1	Topography of Sample Surfaces .....	- 104 -
5.3.2	Adsorption of Ethyl Cellulose to Mica .....	- 105 -
5.3.3	Interaction between Asphaltene and EC Surfaces in Toluene ..	- 107 -
5.3.4	EC Coated Substrate and Asphaltene Solution.....	- 112 -
5.3.5	Asphaltene Coated Substrate and EC Solution.....	- 116 -
5.4	Conclusion.....	- 124 -
5.5	References .....	- 126 -
Chapter 6 Summary .....		- 130 -
6.1	Overall Summary .....	- 130 -
6.2	Major Contributions .....	- 132 -
6.3	Suggestions for Future Work .....	- 133 -
Appendix 1.....		- 135 -
Preparation of Solid and Hollow Asphaltene Fibers by Single Step Electrospinning .....		- 135 -

## List of Tables

Table 1-1 Comparison of operation conditions of paraffin and naphtha based forth treatment process .....	- 5 -
Table 3-1 Fitting parameters using the Alexander-de Gennes scaling theory ..	- 55 -
Table 5-1 Fitting parameters using the AdG scaling model. ....	- 111 -

# List of Figures

Figure 1-1 Asphaltene molecular structures. Shown here are two of the many possible structures of asphaltenes, which are a class of molecules composed of grouped aromatic rings (blue) with alkane chains. Some rings may be nonaromatic. Many of the rings are fused, meaning the rings share at least one side. Heteroatoms such as sulfur, nitrogen, oxygen, vanadium and nickel may reside in the aromatic rings. The molecule on the right contains a heteroatom in the form of sulfur [S]..... - 7 -

Figure 1-2 Image of emulsified water droplets and solids in 0.5 wt% asphaltene in toluene solution. Note the arrows pointing to the dark and rigid interfacial film formed by surface active agents adsorbed at the water-oil interface preventing water droplets from coalescing and thereby stabilizing the water-in-oil emulsion..... - 12 -

Figure 2-1 SFA experimental setup. (Reproduced from Dr. Hongbo Zeng's presentation at Petrophase conference, June 2010)..... - 28 -

Figure 2-2 Schematics of energy and force vs distance plot of two surfaces. (a) Separate intermolecular and spring potential functions. (b) Total energy curves at different molecule-surface separations. Spontaneous inward and outward jumps occur from  $J_{in}$  and  $J_{out}$ . (c) Spontaneous inward and outward jumps occur when  $dF(D)/dD \geq k_s$ . (Reproduced from Dr. Hongbo Zeng's Dissertation.<sup>13</sup>)..... - 30 -

Figure 2-3 Schematic drawings of the procedure to prepare mica sheets having the same thickness. (Reproduced from Dr. Hongbo Zeng's dissertation<sup>13</sup>). - 32 -

Figure 3-1 AFM images of (a) bare mica surface and (b) coated asphaltene film on mica surface. (c) FECO of mica surfaces in contact in air (d) FECO of a coated asphaltene film in contact with a mica surface in air. Note the shift in the wavelength of FECO and change in the shape (contact area) of the fringes, indicating the presence of asphaltene layers and change of adhesion due to the presence of asphaltenes as anticipated. FECO can be used to measure the surfaces deformations, surfaces separation and refractive index of the medium. .... - 43 -

Figure 3-2 Experimental configurations for studying the surface interactions of asphaltenes in organic solvents: (a) an asphaltene film vs. bare mica (asymmetric case) and (b) two asphaltene films (symmetric case). .... - 44 -

Figure 3-3 Force profiles of a coated asphaltene film on surface interacting with a bare mica surface across toluene: a) two bare mica surfaces in pure toluene (b) measurement after the asphaltene film being exposed in toluene for ~1 hr, and (c) successive measurement in which the asphaltene film was kept in contact with mica surface for about 10 min before separation. When the surfaces are compressed, the hard wall shifted to about 5 nm indicating that asphaltene film in toluene swell and is flexible instead of rigid. In this figure and all subsequent figures, "Approach" indicates bringing the two surfaces close together and "Retract" indicates separation of the two surfaces. ... - 46 -

Figure 3-4 Force profiles of (a) asphaltene coated surfaces in toluene immediately after toluene injection, and (b) asphaltene coated surfaces in toluene after 30 min. The vertical dashed lines indicate the hard wall distance of two asphaltene surfaces in air..... - 49 -

Figure 3-5 AFM image of asphaltene coated on mica surfaces. (a) Coated asphaltene film on mica in air, (b) coated asphaltene film on mica after incubation in toluene for 30 min, showing significant aggregation, and (c) coated asphaltene film incubated in heptane for 30 min, showing less significant aggregation than in toluene..... - 50 -

Figure 3-6 Force profiles of (a) mica surfaces in asphaltene-toluene solution measured immediately after injection, (b) same system as (a) but after the asphaltene-toluene solution is flushed out and replaced by pure toluene and measured after 30 min. .... - 52 -

Figure 3-7 Experimentally measured repulsion forces and best fitted curves using the Alexander-de Gennes theory for approach of (a) two asphaltene films and (b) an asphaltene film against a bare mica surface in toluene. .... - 56 -

Figure 3-8 Force profiles of two asphaltene films in heptane: (a) force-distance curves measured immediately after heptane injection and (b) force-distance curves measured after ~30 min immersion in heptane. .... - 59 -

Figure 3-9 Schematic illustration of a rigid interfacial film formed by asphaltenes, resins, fine particles etc., adsorbed at the water/oil interface, preventing

water droplets from coalescing and thereby stabilizing the water-in-oil emulsions, which is highly undesirable in petroleum processes. .... - 62 -

Figure 4-1 Experimental configuration and illustration of the adsorption process of asphaltenes onto mica in organic solvent: (a) mica surfaces in asphaltene solution, and (b) asphaltene layers gradually built up on mica associated with the adsorption. .... - 78 -

Figure 4-2 Approach and separation force-distance profiles of two mica surfaces in asphaltene-toluene solutions of different concentrations and at different time intervals: (a) 0.01 wt %, (b) 0.1 wt%, and (c) 1.0 wt% asphaltenes in toluene. The reference distance ( $D = 0$ ) was set as the adhesive contact between the two bare mica surfaces in air prior to injecting the asphaltene solution between the surfaces. In this figure, “Approach” indicates bringing the two surfaces close together and “Retract” indicates separation of the two surfaces. .... - 82 -

Figure 4-3 AFM images in air for (a) bare mica surface, and asphaltene layer adsorbed on mica surface for (b) 5 min, (c) 15 min, (d) 45 min, (e) 105 min and (f) 225 min immersion time in 0.1 wt% asphaltene-toluene solution. Note that the surfaces were gently dried with nitrogen before imaging. Image size:  $1\mu\text{m} \times 1\mu\text{m}$ . .... - 85 -

Figure 4-4 Adhesion energy  $W_{ad}$  between mica surfaces in different concentrations of asphaltene in toluene solution as a function of adsorption time at room temperature. .... - 87 -

Figure 4-5 Confined layer thickness plotted as a function of square root of adsorption time for the three different concentrations of asphaltene-toluene solution (wt %). Insert: Expanded plots for the 0.01 wt% and 0.1 wt% asphaltene-toluene solution. Note: Only 0.01 wt% follows a perfectly linear relationship with square root of adsorption time. .... - 89 -

Figure 4-6 Asphaltene (A) diffusion coefficient and (B) particle size, as a function of concentration (wt%). .... - 90 -

Figure 5-1 AFM images of (A) bare mica surface (B) coated EC film on mica surface (C) coated asphaltene film on mica surface. Note that the surfaces were gently dried with nitrogen before imaging. .... - 105 -

Figure 5-2 Force-distance profiles between two mica surfaces after immersed in 0.5 wt% EC-toluene solution for ~5 min. In this figure and all subsequent figures, “In” indicates approach of the two surfaces and “Out” indicates separation of the two surfaces. .... - 106 -

Figure 5-3 Experimental configuration for studying the surface interactions between asphaltene films and EC films coated mica surfaces in toluene (asymmetric case). .... - 107 -

Figure 5-4 Force-distance profile of EC and asphaltene films coated on mica (asymmetric surfaces). When the surfaces are compressed, the confined film thickness shifted to about 12 nm indicating that the coated films of EC and asphaltenes in toluene swell and are flexible instead of rigid. .... - 108 -

Figure 5-5 Experimentally measured repulsion forces and best fitted curves using the AdG theory for two EC films in toluene (E-E); asphaltene film against an EC film in toluene (A-E); and two asphaltene films in toluene (A-A)..... - 111 -

Figure 5-6 Experimental configuration for studying the surface interactions between EC films coated mica surfaces in asphaltene solution. .... - 112 -

Figure 5-7 (A) Approaching force profile of two EC surfaces in 0.5 wt% asphaltene-toluene solution. (B) Same data on a semi log plot to illustrate the exponentially repulsive force-distance regime. (C) Separation force profile of two EC surfaces in asphaltene-toluene solution. .... - 114 -

Figure 5-8 Adhesion energy  $W_{ad}$  between EC surfaces in asphaltene-toluene solution as a function of adsorption time at 24°C. .... - 116 -

Figure 5-9 Experimental configuration for studying the surface interactions between asphaltene films coated mica surfaces in EC solution. .... - 117 -

Figure 5-10 (A) Approaching force profile of two asphaltene surfaces in EC-toluene solution at different time intervals. (B) Same data on a semi log plot to illustrate the exponentially repulsive force-distance regime. (C) Separation force profile of two asphaltene surfaces in EC-toluene solution at different interval of time. .... - 119 -

Figure 5-11 AFM topography images of asphaltene surface in EC solution at different adsorption time. (A) asphaltene coated mica surface in air. (B) asphaltene coated mica surface in EC solution for 5 min. (C) asphaltene

coated mica surface in EC solution for 30 min. (D) asphaltene coated mica surface in EC solution for 280 min. Note: the time it takes for EC to displace asphaltene from the mica surface is very quick, within 5 min of adsorption time. The asphaltene height profile grows from ~10 nm to about ~20 nm in the first 5 min and remains almost consistent for the duration of the experiment. The dimension of images is  $1\ \mu\text{m} \times 1\ \mu\text{m}$ . ..... - 121 -

Figure 5-12 Adhesion energy  $W_{ad}$  between asphaltene surfaces in EC-toluene solution as a function of adsorption time at room temperature. .... - 123 -

Figure 5-13 Schematic representation of asphaltene on mica being displaced by EC from solution. .... - 124 -

# Chapter 1

## Fundamentals of Oil Sands Extraction

### 1.1 Introduction

The separation and recovery of oil from sand is a critical problem in a number of industries and crucial to the mitigation of environmental disasters such as those associated with oil spills. Canada's energy future lies in the oil sands. There are about 174 billion barrels of oil that can be recovered with today's technology. Out of that, 169 billion are located in the oil sands.<sup>1</sup> Oil sands are a complex mixture of sand, water, clay and bitumen. Bitumen is oil that is too heavy or thick to flow or be pumped without being diluted or heated. At 11°C bitumen is as hard as a hockey puck. Bitumen must therefore be upgraded and refined before it can be used as gasoline and other fuels.

There are two different methods of producing oil from oil sands: open-pit mining and in situ. Bitumen that is close to the surface is mined. Bitumen that occurs deep within the ground is produced in situ using specialized extraction techniques (e.g., steam-assisted gravity drainage, SAGD). In open-pit mining large shovels scoop the oil sands into trucks that then take it to crushers where large clumps of earth are broken down. This mixture is then thinned out with water and transported to a plant where bitumen is separated from other components and upgraded to create synthetic oil. Just 20% of the oil sands are recoverable through

open-pit mining. 80% of oil sands are recoverable through in situ technology like SAGD.<sup>2</sup> This method involves pumping steam underground through a horizontal well to liquefy the bitumen that is then pumped to the surface through a second well. Currently, about 60% of bitumen produced from oil sands is by open-pit mining and water based extraction technologies.<sup>2</sup>

### **1.1.1 Bitumen Extraction.**

In open-pit mining, the bitumen extraction process uses water-based extraction technologies.<sup>2,3</sup> The success of this technology lies in the key fact that the sand grains are hydrophilic. There is a theory that a thin layer (~10 nm) of formation water surrounds each individual sand grains separating them from the bitumen. The presence of this water layer has been postulated since early stage of oil sands development.<sup>2,3</sup> It is assumed, that were it not for the presence of this water layer around the sand grains, bitumen extraction process from the sand grains would be both difficult and economically unfeasible. The water film is assumed to be stabilized by electrostatic forces between the electric double layers that act between the oil-water and sand-water interfaces. The existence of the water layer, however, still remains to be experimentally proven.

Bitumen extraction process includes the crushing of oil sands lumps to smaller sizes with the help of crushers and mixed with warm process water and chemical additives, e.g., caustic soda, to form oil sands slurry. The temperature of the slurry is around 35-55°C and pH of 8-8.5.<sup>2,3</sup> Under these conditions, bitumen is liberated

from mineral solid's surface. Hydrotransport pipelines are used for bitumen conditioning process. During the conditioning, air at low doses is introduced into the slurry to facilitate bitumen aeration. The separation of the aerated bitumen droplets and solids are achieved using gravity separation vessels. The bitumen froth contains a considerable amount of water and solids that have to be removed in the bitumen froth treatment process prior to bitumen upgrading.

### **1.1.2 Bitumen Froth Treatment.**

Bitumen froth typically contains about 60 wt% bitumen, 30 wt% water and 10 wt% solids. The majority of the water is free water, but about 5 wt% of the water is in an emulsified form.<sup>4</sup> The solids are entrained in the bitumen phase or accumulated at the water/oil interface.<sup>5,6</sup> The process used to remove this water and solids is referred to froth treatment. Since bitumen has an almost identical density to that of water, the first step in the froth treatment process is the addition of a diluent (e.g., naphthenic or paraffinic solvent) to facilitate the density difference between oil phase and water phase. Water and solids are separated from the diluted bitumen froth by gravity settling, or by use of cyclones or centrifuges. Based on the types of diluents used, two froth treatment methods are commercially employed in the industry, known as naphtha-based froth treatment and paraffin-based froth treatment.<sup>5</sup>

In the naphtha-based froth treatment, mechanical separation equipment such as hydrocyclones and centrifuges are necessary for the separation of the water

droplets and solids. The water/oil droplets and solids usually form a rag layer that builds up at the water/oil interface, hindering effective phase separation.<sup>4</sup> Asphaltenes, which are a constituent of bitumen, do not precipitate in this process. After centrifugation, most of the water and solids can be removed. However, there are still about ~ 1.5 wt% to 2.5 wt% emulsified water and ~0.4 wt% to 0.8 wt% fine solids dispersed in the diluted-bitumen phase.<sup>3,5</sup> These solids and emulsified water droplets are only a few microns in diameter and are partly to wholly covered by layers of hydrocarbons, e.g., asphaltenes and natural surfactants in bitumen.<sup>7-14</sup> Consequently, they form stable emulsions that cause corrosion and fouling problems in downstream upgrading operations.<sup>2,3</sup> It is thus imperative to develop new technologies to remove these solids and emulsified water droplets.

Unlike the naphtha-based froth treatment process, the paraffin-based process produces a very clean bitumen product. When paraffinic solvents, like hexane, are added to bitumen at a sufficiently high diluent to bitumen ratio, about 1/3 to 1/2 of the asphaltenes would precipitate from bitumen due to low solubility of asphaltenes in alkane (paraffinic) solvents.<sup>3</sup> The precipitating asphaltenes can flocculate the dispersed water droplets and fine solids together to form complex floccules or clusters of water-solids-asphaltene precipitates that settle quickly under gravity to produce bitumen with a negligible amount of water and solids. Although this process produces high quality bitumen, entrapment of bitumen in the clusters of flocculated water-solids-asphaltene precipitates significantly reduces the recovery of bitumen in the froth cleaning process. In addition, low

recovery of solvents reduces the economic benefit of the paraffin-based process. A comparison of the operation conditions of the two froth treatment processes is listed in Table 1-1.

Table 1-1 Comparison of operation conditions of paraffin and naphtha based froth treatment process

	Paraffinic diluents	Naphthenic diluents
Solvents	Alkanes of C5-C6 mixture (e.g., hexane)	Naphtha
Aromatics content of diluent	0 wt%	~14 wt%
Critical solvent/bitumen ratio (S/B)	1.8-2	~4
S/B ratio in industrial operation	2.1-2.5	0.6-0.75
Temperature	30-32 C	75-78 C
Asphaltene precipitation	~50% asphaltenes in bitumen rejected	No asphaltene precipitation
Product quality	Solids & water < 0.1 wt%	Water: 1.0-2.5 wt% Solids: 0.3-0.8 wt%
Bitumen recovery	88-94%	~98%

Table is reproduced from Fundamentals of Oil Sands Extraction (ChE534 text book).<sup>2</sup>

## 1.2 Asphaltenes – Definition, Composition and Molecular Aggregation

Asphaltenes are a component of bitumen defined as the part of crude which is soluble in toluene and insoluble in alkanes, usually n-pentane or n-heptane.<sup>15,16</sup> Despite this definition, it is now well appreciated that there are individual molecular species in asphaltenes that are insoluble in toluene and there are others that are soluble in n-heptane.<sup>17,18</sup> This behavior of asphaltenes is not apparent as the physical state of asphaltenes in toluene, heptane and crude oil itself is as an aggregate, molecularly self-assembled; unless they are either diluted to a very high dilution or separated from other asphaltenic species. Nevertheless, molecular and functional group composition of asphaltene fractions suggests that their molecular structures are composed of condensed polyaromatic hydrocarbons with variable (length and substitution) alkyl chains and contain heteroatoms (N, S, and O) and sometimes, trace metals (e.g. V, Ni, and Fe).<sup>2,3,19</sup> The functional groups are typically hydrophilic while the hydrocarbon structure of asphaltenes is hydrophobic. Hence, asphaltenes are considered surface active and are able to adsorb at water–oil interfaces.

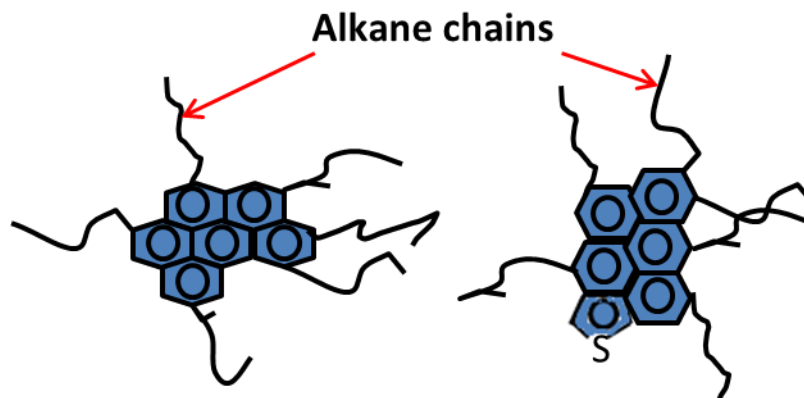


Figure 1-1 Asphaltene molecular structures. Shown here are two of the many possible structures of asphaltenes, which are a class of molecules composed of grouped aromatic rings (blue) with alkane chains. Some rings may be nonaromatic. Many of the rings are fused, meaning the rings share at least one side. Heteroatoms such as sulfur, nitrogen, oxygen, vanadium and nickel may reside in the aromatic rings. The molecule on the right contains a heteroatom in the form of sulfur [S]

Various analytical techniques have been used to characterize the structure and functional groups of asphaltenes.<sup>20-26</sup> X-Ray diffraction revealed that the aromatic rings could stack in a few layers through  $\pi$ - $\pi$  interaction to form condensed aromatic sheets but their packing was loosened by the aliphatic chains.<sup>20,27</sup> Many other techniques including infrared spectroscopy were applied to study the functional groups in asphaltenes.<sup>21,26</sup> All these analytical results of asphaltenes only represent the average structural characteristics of asphaltenes. Nevertheless, two model structures were proposed: the continental and the archipelago models.<sup>3</sup> Asphaltene in the continental model are made up of large condensed poly-aromatic rings with aliphatic chains in the end. The archipelago model assumes asphaltene as containing several poly-aromatic rings connected by aliphatic

chains or heteroatoms. Both models are successful in explaining certain properties of asphaltenes but neither is a complete model. As an example, the continental model agrees well to an asphaltene molecular weight of ~750 g/mol while the archipelago model does not. However, the archipelago model supports the polymeric properties of asphaltenes as observed by some researchers.<sup>28</sup>

Asphaltenes are best known for the problems they cause in many petroleum processes.<sup>3</sup> The main reason is their tendency to flocculate and precipitate. In petroleum processes precipitation of asphaltenes is detrimental and is an obvious phenomenon to be prevented. The precursor to precipitation is flocculation. Hence numerous studies have been conducted to understand flocculation in order to predict precipitation.<sup>29-31</sup> The precursor to precipitation is the formation of micrometer/nanometer sized particles. It is believed that these particles are formed due to asphaltene self-association. Yen proposed his model that describes the evolution of the particle size from nanoscale aggregates to macroscopic particles.<sup>32</sup> Yen's model is based on length scale and suggests that these nanoaggregates form from self-association of asphaltenes.

Asphaltene aggregation has been the subject of numerous studies.<sup>2,3,33-35</sup> It is well documented that asphaltenes aggregate in solvent when the concentration exceeds a threshold value. Time-resolved fluorescence depolarization (FD) studies have shown that the most key molecular parameter controlling asphaltene solubility is intermolecular binding of the aromatic ring systems versus steric repulsion of this

binding by alkane chains.<sup>36</sup> It is suggested that aggregation occurs when the aromatic ring systems of different asphaltene molecules stack up like pancakes to form nanoaggregates.<sup>32</sup> However, the alkane steric repulsion would limit the number of molecules in the stack. Further increase in asphaltene concentration will not increase the size of the existing nanoaggregates but rather result in new nanoaggregates. Eventually, at very high concentration, the nanoaggregates undergo clustering; the binding energy of one nanoaggregate to another is much lower than the binding energy in the interior of the nanoaggregates.

Asphaltene molecular weight has been the subject of huge controversy.<sup>37-41</sup> Asphaltene molecular weight varies from a few hundred Daltons to more than ten thousand Daltons, depending on the analytical techniques, solvent, temperature and the concentration of asphaltene solution. This large variation in the molecular weight data is not unexpected recognizing the polydispersity of asphaltene components. Furthermore, the tendency of asphaltenes to self-associate and aggregate in solvents complicates the interpretation of the results. The association state of asphaltenes is closely related to the solution condition (e.g., solvency, temperature, pressure) as well as existence of solids and water.

Asphaltenes also cause other challenges to fluid flow: not only do they increase fluid viscosity and density,<sup>19,42-47</sup> but they also stabilize oil-water emulsions. Emulsions form when oil and water mix under conditions of agitation. Usually, the mixture is more viscous than its components, and flows less easily. Separating

emulsified water and oil is difficult, and requires more than the gravitational methods used in most separators. A better understanding of the effect of asphaltenes may be the key to preventing the formation of emulsions or tempering the harmful effects of these mixtures.

### **1.3 Emulsion and Emulsion Stability**

An emulsion is composed of two immiscible or partially immiscible liquids in a dispersed system.<sup>2,3</sup> For example; one liquid could be water and the other a hydrocarbon liquid. One of the liquids forms a continuous phase, while the other is dispersed into small droplets. The droplet size ranges from a fraction of micrometer to over 10  $\mu\text{m}$ .

Adding water to the product to increase its recovery is an essential first step in extraction procedures. Water aids in the removal of water-soluble salts and facilitates transport of bitumen through the operation pipelines by lowering viscosity. Emulsion formation (water-in-oil, oil-in-water and multiple emulsions) can occur at nearly any point throughout this process. However, downstream operations require the removal of water prior to refinery and petroleum product recovery. The salts in the water and solids cause corrosion problems for the downstream operations and result in production losses. Furthermore, the added cost associated with using chemicals to break water and oil emulsions are expensive for the petroleum industry.

The most important property of an emulsion is its stability.<sup>3</sup> In general, emulsions are unstable. The large interfacial area increases the total energy of the system. Hence a decrease in system energy, called phase separation or emulsion breaking, should occur spontaneously. But this rate of phase separation could be extremely slow such that the emulsion appears to be infinitely stable. The stability is governed by the properties of a thin film which is a part of the continuous phase liquid that separates dispersed droplets on their close approach. It eventually becomes so thin that the droplets start to interact with each other via surface forces, such as van der Waals attractive forces, repulsive forces resulting from double layer overlapping, or forces resulting from steric effects. For the emulsion droplets to coalesce they must overcome repulsive forces. Therefore, emulsion stability is controlled by surface forces.<sup>3</sup>

Stable emulsions may be required in some food and cosmetic products, or can be regarded as highly detrimental in processes such as when removing water from oil in froth treatment operations. There are different emulsion stabilization processes but the most common process is due to the adsorption of surfactants on the water-oil interface. Ionic surfactants may stabilize emulsions by providing an electric charge to emulsion droplets. Charged droplets repel each other, which prevents them from colliding and coalescing. Non-ionic surfactant may stabilize emulsions by forming a steric stabilization layer, i.e., a layer that prevents a close droplet-to-droplet approach due to the protruding parts of the surfactant molecules.

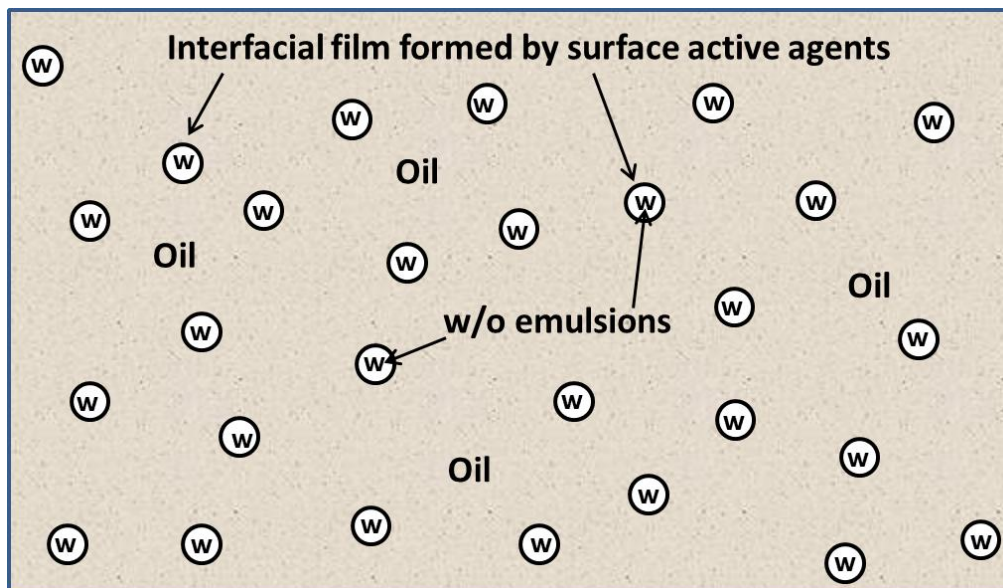


Figure 1-2 Image of emulsified water droplets and solids in 0.5 wt% asphaltene in toluene solution. Note the arrows pointing to the dark and rigid interfacial film formed by surface active agents adsorbed at the water-oil interface preventing water droplets from coalescing and thereby stabilizing the water-in-oil emulsion.

#### 1.4 Objective of the Thesis

The objectives of this thesis are as follows:

*1) To measure the molecular interactions between asphaltene surfaces in organic solvents using a surface forces apparatus to gain a fundamental understanding on the stability of water-in-diluted bitumen emulsions.*

This study focuses on understanding the interaction of two asphaltene films in good and poor solvents (toluene and heptane). Direct measurement of surface forces of asphaltene surfaces in aqueous solutions have been studied using an

atomic force microscope (AFM).<sup>48,49</sup> Reports on surface forces for crude oil systems in aqueous solutions using surface forces apparatus (SFA) and AFM are available.<sup>50-52</sup> But until now only very few experiments were ever conducted to measure the forces between asphaltene films in organic solutions.<sup>53,54</sup> This is not surprising for a fact that the force measurement of asphaltenes in organic solvent is not easy. The reason for this lies in asphaltenes definition. Being a solubility class, asphaltenes are a mixture of a large number of heavy hydrocarbons and they aggregate even in good solvents.<sup>55-57</sup> The molecular structure of various compounds in asphaltenes are still debated. Therefore, it is not practical to determine experimentally the interaction forces between individual components in asphaltene solutions. Theoretically, computer-based computation (e.g., molecular dynamics simulation) provides some information on molecular interactions of model compounds of asphaltenes.<sup>58,59</sup> However, molecular simulation results cannot represent the real conditions, especially when the structure and molecular weight of asphaltenes remain ill-defined.

In this study, the intermolecular interactions of asphaltene molecules are measured using a SFA to provide the interfacial forces as a function of the absolute separation distances. The forces between two asphaltene surfaces are a statistical combination of the interactions between various components in asphaltenes. The results thus represent the “general” or “average” asphaltene behavior.

*2) To measure the molecular interactions acting between a demulsifier, asphaltene film and representative clay surface (mica) using a surface forces apparatus to understand the molecular mechanisms involved in destabilizing water-in-bitumen emulsions.*

In heavy oil processing, demulsification of water-in-oil emulsions and removal of organic contaminated solids are the two main issues. The organic rich solids and emulsified water droplets, remaining in oil, are detrimental to downstream upgrading/refining operations and need to be removed from the oil phase.<sup>9,13</sup> These solids along with the heavy components of bitumen such as asphaltenes readily partition at the water-oil interface forming a film that hinders droplet coalescence.<sup>6-9</sup> The hindered breakdown of emulsions can result in the formation of rag layers that are a complex mixture of oil, water and solids.<sup>60</sup> A fundamental understanding of the emulsion stabilization mechanism and the subsequent destabilization of the emulsion by demulsifier can only be realized by a good description of the interaction forces that act between interfacial asphaltene films and demulsifiers.

## 1.5 Thesis Outline

This thesis consists of six chapters. The following outlines the structure of the thesis.

Chapter 1: This chapter provides a brief background of this study. The problematic nature of asphaltenes and its role in emulsion stabilization is presented. The objectives of this work are presented. Previous work on asphaltenes is briefly reviewed. A more detail review is presented in Chapters 3, 4 and 5.

Chapter 2: Molecular forces and surface forces are introduced as a foundation for future chapters in this thesis. The fundamental principle and operating procedures of the experimental work, especially the surface forces apparatus is presented.

Chapter 3: In this chapter, the results on molecular interaction forces between asphaltene surfaces in toluene and heptane measured using a SFA are presented. AFM was used to obtain complementary information on the morphology change of the asphaltene films in organic solvents with time. The results provide an insight into the role of surface-active chemicals to the stability of water-in-oil emulsions.

Chapter 4: This chapter focuses on the process of adsorption of asphaltene layers from solution onto molecularly smooth mica surfaces as a function of time using a

surface force apparatus. The measurements were carried out at varying concentration of asphaltene in toluene solution.

Chapter 5: In this chapter the molecular forces acting between a demulsifier, asphaltene film and representative clay surface (mica) in organic solvent using a surface force apparatus is measured to understand the molecular mechanisms involved in destabilizing water-in-oil emulsions.

Chapter 6: This chapter provides an overall summary of the thesis, major contributions, and suggestions for future work.

## 1.6 References

1. ERCB, Alberta Oil Sands Industry Quarterly Update, 2013.
2. Masliyah, J. H., Fundamentals of Oil Sands Extraction, ChE534 text book, 2006.
3. Masliyah, J. H.; Czarnecki, J.; Xu, Z. Handbook on Theory and Practice of Bitumen Recovery from Athabasca Oil Sands, volume 1, 2011, Kingsley Knowledge Publishing, Canada & USA.
4. Long, Y. C.; Dabros, T.; Hamza, H., Fuel 2002, 81, 1945.
5. Romanova, U. G.; Yarranton, H. W.; Schramm, L. L.; Shelfantook, W. E., Canadian Journal of Chemical Engineering 2004, 82, 710.
6. Saadatmand, M.; Yarranton, H. W.; Moran, K., Industrial & Engineering Chemistry Research 2008, 47, 8828.
7. Czarnecki, J.; Moran, K.; Yang, X. L., Canadian Journal of Chemical Engineering 2007, 85, 748.
8. Wu, X. A., Energy & Fuels 2008, 22, 2346.
9. Sparks, B. D.; Kotlyar, L. S.; O'Carroll, J. B.; Chung, K. H., Journal of Petroleum Science and Engineering 2003, 39, 417.
10. Kotlyar, L. S.; Sparks, B. D.; Woods, J. R.; Chung, K. H., Energy & Fuels 1999, 13, 346.
11. Kotlyar, L. S.; Sparks, B. D.; Woods, J. R.; Raymond, S.; Le Page, Y.; Shelfantook, W., Petroleum Science and Technology 1998, 16, 1.

12. Kilpatrick, P. K.; Spiecker, P. M., Encyclopedic handbook of emulsion technology. Johan Sjöblom Ed. ed.; Marcel Dekker, Inc.: New York, 2001.
13. Sjoblom, J.; Aske, N.; Auflem, I. H.; Brandal, O.; Havre, T. E.; Saether, O.; Westvik, A.; Johnsen, E. E.; Kallevik, H., *Advances in Colloid and Interface Science* 2003, 100, 399.
14. Sztukowski, D. M.; Jafari, M.; Alboudwarej, H.; Yarranton, H. W., *Journal of Colloid and Interface Science* 2003, 265, 179.
15. Mitchell, D. L.; Speight, J. G. *Fuel* 1973, 52, 149.
16. Yen, T. F.; Erdman, J. G.; Pollack, S. S. *Anal. Chem.* 1961, 33, 1587.
17. Spiecker, P. M.; Gawrys, K. L.; Kilpatrick, P. J. *Colloid Interface Sci.* 2003, 267, 178.
18. Alboudwarej, H.; Beck, J.; Svrcek, W. Y.; Yarranton, H. W. *Energy Fuels* 2002, 16, 462.
19. Hammami, A.; Ratulowski, J. In *Asphaltenes, Heavy Oils and Petroleomics*; Mullins, O. C., Sheu, E. Y., Hammami, A., Marshall, A. G., Eds.; Springer: New York, 2007; Vol. 1, pp 617-656.
20. Dickie, J. P.; Yen, T. F. *Analytical Chemistry* 1967, 39, 1847.
21. Strausz, O. P.; Mojelsky, T. W.; Faraji, F.; Lown, E. M.; Peng, P., *Energy & Fuels* 1999, 13, 207.
22. Strausz, O. P.; Mojelsky, T. W.; Lown, E. M., *Fuel* 1992, 71, 1355-1363.
23. Payzant, J. D.; Lown, E. M.; Strausz, O. P., *Energy & Fuels* 1991, 5, 445-453.

24. Sheu, E. Y., *Journal of Physics-Condensed Matter* 2006, 18, S2485-S2498.
25. Sirota, E. B., *Energy & Fuels* 2005, 19, 1290-1296.
26. Coelho, R. R.; Hovell, I., *Petroleum Science and Technology* 2007, 25, 41-54.
27. Zhang, Y.; Takanohashi, T.; Sato, S.; Saito, I.; Tanaka, R., *Journal of the Japan Petroleum Institute* 2004, 47, 32.
28. Long, J.; Xu, Z. H.; Masliyah, J. H., *Langmuir* 2007, 23, 6182.
29. Ekulu, G.; Rogalski, M.; Sadiki, A.; Bokolo, M. *Journal of Dispersion Science and Technology* 2013, 34, 1663.
30. Mansur, C. R. E.; de Melo, A. R.; Lucas, E. F. *Energy Fuels* 2012, 26, 4988.
31. Juyal, P.; Ho, V.; Yen, A.; Allenson, S. J. *Energy Fuels* 2012, 26, 2631.
32. Yen, T. F. In: M. Grayson and J. I. Krochwitz (eds.), *Encyclopedia of Polymer Science and Engineering*, 1988, 2nd edn., Vol. 1. Wiley, New York.
33. Safaie, K.; Nazar, A. R. S. *Journal of Dispersion Science and Technology*, 2013, 34, 1173.
34. Marcano, F.; Ranaudo, M. A.; Chirinos, J.; Castillo, J.; Daridon, J. L.; Carrier, H. *Energy Fuels* 2013, 27, 4598.
35. Haji-Akbari, N.; Masirisuk, P; Hoepfner, M. P.; Fogler, H. S. *Energy Fuels* 2013, 27, 2497.

36. Buenrostro-Gonzalez, E.; Groenzin, H.; Lira-Galeana, C.; Mullins, O. C. *Energy Fuels* 2001, 15, 972.
37. Strausz, O. P.; Peng, P.; Murgich, J., *Energy & Fuels* 2002, 16, 809-822.
38. Monte, M. B. M.; Coelho, R. R.; Middea, A., *Petroleum Science and Technology* 2004, 22, 991-1001.
39. Badre, S.; Goncalves, C. C.; Norinaga, K.; Gustavson, G.; Mullins, O. C., *Fuel* 2006, 85, 1-11.
40. Mullins, O. C.; Martinez-Haya, B.; Marshall, A. G., *Energy & Fuels* 2008, 22, 1765-1773.
41. Becker, C.; Qian, K. N.; Russell, D. H., *Analytical Chemistry* 2008, 80, 8592-8597.
42. Kilpatrick, P. K.; Spiecker, P. M. Asphaltene Emulsions. In *Encyclopaedic Handbook of Emulsion Technology*; Sjoblom, J., Ed.; Marcel Dekker: New York, 2001.
43. Yarranton, H. W.; Hussein, H.; Masliyah, J. H. J. *Colloid Interface Sci.* 2000, 228, 52.
44. Taylor, S. D.; Czarnecki, J.; Masliyah, J. J. *Colloid Interface Sci.* 2002, 252, 149.
45. Zhang, L. Y.; Xu, Z.; Masliyah, J. H. *Langmuir* 2003, 19, 9730.
46. Wu, X. *Energy Fuels* 2003, 17, 179.
47. Spiecker, P. M.; Kilpatrick, P. K. *Langmuir* 2004, 20, 4022.
48. Hartley, P. G.; Grieser, F.; Mulvaney, P.; Stevens, G. W. *Langmuir* 1999, 15, 7282.

49. Mulvaney, P.; Perera, J. M.; Biggs, S.; Grieser, F.; Stevens, G. W. J. *Colloid Interface Sci.* 1996, 183, 614.
50. Drummond, C.; Israelachvili. J. J. *Pet. Sci. Eng.* 2004, 45, 61.
51. Wu, X.; Czarnecki, J.; Hamza, N.; Masliyah, J. *Langmuir* 1999, 15, 5244.
52. Wu, X.; Dabros, T.; Czarnecki, J. *Langmuir* 1999, 15, 8706.
53. Wang, S.; Liu, J.; Zhang, L.; Xu, Z.; Masliyah, J. *Energy & Fuels*, 2009, 23, 862.
54. Vuillaume, K.; Giasson, S. J. *Phys. Chem. C* 2009, 113, 3660.
55. Yarranton, H. W., *Journal of Dispersion Science and Technology* 2005, 26, 5.
56. Merino-Garcia, D.; Murgich, J.; Andersen, S. I., *Petroleum Science and Technology* 2004, 22, 735.
57. Mohamed, R. S.; Ramos, A. C. S.; Loh, W., *Energy & Fuels* 1999, 13, 323.
58. Kuznicki, T.; Masliyah, J. H.; Bhattacharjee, S., *Energy & Fuels* 2009, 23, 5027.
59. Kuznicki, T.; Masliyah, J. H.; Bhattacharjee, S., *Energy & Fuels* 2008, 22, 2379.
60. Kupai, M. ; M. ; Yang, F. ; Harbottle, D. ; Moran, K. ; Masliyah, J. ; Xu, Z. *Canadian Journal of Chemical Engineering* 2013, 91, 1395.

## **Chapter 2**

### **Molecular Forces**

In chapter 1 we discussed the fundamentals of oil sands extraction and how asphaltenes and solids contaminated by hydrocarbons play an important role in the stabilization of w/o emulsions. Molecular forces are responsible for the stability of emulsions. Molecular forces act between objects that surround us in everyday life. Sometimes objects stick together with remarkable strength, for example a gecko. It can walk on any kind of surface at any orientation with strong adhesion between its legs and the surface. It can repeatedly apply the same adhesive force. Other times things fall apart with ease. For example, drug particles when consumed readily disintegrate in the mouth or stomach to give quick relief from discomfort. There are times when adhesion force is desired while at other times repulsive force is beneficial. The purpose of this chapter is to understand how molecular forces act, and to use this knowledge as foundation for the future chapters in this thesis.

#### **2.1 Theory of Adhesion**

The idea that things like to stick together was realized when man set his foot on the moon. Dust from the lunar surface settled on the windows of the space craft making it opaque. This proved the idea that clean surfaces in vacuum adhere much more strongly than the wet and contaminated surfaces on earth. Thus the importance of clean surfaces was realized in order to measure molecular adhesion.

Then again, although the surfaces were clean and smooth the contact between the bodies cannot be made easily at the molecular level. Firstly, the surfaces are contaminated by water vapor, oxygen and other foreign atoms that will prevent true atomic contact between the bodies. Secondly, the surfaces are not smooth but rough and jagged and large gaps exist that reduce contact and surface interaction. Hence, we can conclude that surface contamination and surface roughness are two important constraints that need to be overcome to realize true molecular interactions.<sup>1,2,3</sup> The surfaces in question must be clean and molecularly smooth. In addition to roughness, many other mechanisms such as hysteresis, restructuring, etc., exist, leading to a rich variety of adhesion phenomena, some of which are observed in future chapters of this thesis.

Summing up the above arguments, it is evident that molecular adhesion has several layers of complexity. Our macroscopic world of ordinary experience is seen to be false at the molecular level.

## **2.2 Adhesion at the Molecular Level**

Van der Waals was the first to propose a modification to the ideal gas law by considering molecular size and molecular interaction forces.<sup>4</sup> Later, London proposed his theory on why atoms attract each other and it is summarized in several books on intermolecular forces.<sup>4-7</sup> Atoms are bunches of electrons and an electron in an atom rotates rapidly around its nucleus. Because the electron is negative and the nucleus is positive, at any instant there is a separation of negative

and positive charge, even though the average charge separation is zero over a period of time. This is an instantaneous dipole, like a tiny magnet, which can line up a similar atom at some distance. This gives an instantaneous dipole-dipole interaction which is always attractive. Such a “London” force is responsible for majority of attractive adhesion between all atoms. This attractive energy decays with distance rapidly, with separation to the power of 6. This is the reason why molecular forces are short ranged and only act when the bodies are in close contact.

Apart from this London forces, there are two more forces such as dipole-dipole interaction and dipole-induced dipole interaction. These three forces are collectively called van der Waals forces. Regardless of the origin of interaction, whether it is due to a permanent dipole or induced dipole or dispersion forces, the average energy is always decaying with the 6<sup>th</sup> power of distance. This short range of action of molecular forces has made force measurement extremely difficult. Only in the past few years or so it has been possible to make the necessary measurements at the nanometer level. Two problems have been overcome. The first was the measurement technique. Optical methods such as multiple beam interferometry (MBI) and laser optical levers have been developed to measure atomic distances. Piezo-electric actuators were invented to control nano-movements. The second issue was surface smoothness. Smooth surface of oxides such as mica, silica or alumina have been found.

### **2.3 Jumping into Contact**

The concept of molecules jumping into contact is difficult to imagine. We don't see it in the macroscopic world. But at the atomic and molecular level this is pretty obvious and such events occur naturally. When two smooth spherical surfaces are brought close together, within several nanometers of contact, a sudden jump of the surfaces is observed. The contact diameter grows quickly to a large size under the influence of molecular adhesion. This flattening of the surfaces is the general mechanism of molecular adhesion. The size of the contact spot at this stage is a measure of molecular adhesion. A large spot is a measure of large adhesion.

In order to separate the surfaces apart, a tensile force is applied to overcome the adhesion force. As the tensile force becomes larger and larger, the contact diameter gets smaller and smaller. However, the contact diameter does not gradually decrease to zero. Instead, a point of instability is reached where the surfaces rapidly separate. This particular tension or "pull-off" force where the surfaces jump apart catastrophically, is another measure of the molecular adhesion between the surfaces. A large "pull-off" force or "jump out" indicates large adhesion. We will come across such examples throughout this thesis.

To summarize the above discussion: adhesion is not an isolated process but one which can be divided into three different parts – (1) jumping into contact, (2) contact diameter size, (3) separation when a tensile force is applied. In the first

part, jumping into contact, the adhesion can be measured by observing the distance of the jump. Further, a longer jump value indicates stronger adhesion. The second part is a true measure of molecular contact. A large spot means large adhesion. The third part is the test of adhesion. We define adhesion force as the tension force or pull-off force required to detach the surfaces apart. A large force means large adhesion.

## **2.4 Adhesion in Surface Forces Apparatus**

A typical Surface forces apparatus (SFA) experiment setup is shown in Figure 2-1. In the SFA, there are two molecularly smooth mica surfaces glued to cylindrical silica discs which are installed in the device. The two surfaces are in a crossed cylinder configuration which is locally equivalent to a sphere of radius  $R$  approaching a flat surface or two spheres close together. The lower surface can be moved over a range of about 3 mm with a precision of 1 nm. This is accomplished with a coarse and fine motor system, the latter of which is coupled to the surface via a motion reducing spring. The upper surface can be positioned within a few Å over a range of about 1000 Å by means of a piezoelectric crystal.<sup>7</sup> The actual surface separation during experiment is monitored and measured by use of an optical technique using MBI fringes called Fringes of Equal Chromatic Order (FECO).<sup>7,9</sup>

As shown in Figure 2-1, white light is passed vertically up through the two surfaces and the emerging beam is then focused onto the slit of a grating

spectrometer. From the positions and shapes of the FECO fringes which can be seen in the spectrogram, the distance between the two surfaces can be measured, from which we can get the exact shapes of the two surfaces and refractive index of the material between them. A detailed discussion on the design, history and working of a SFA can be found elsewhere.<sup>10</sup>

## 2.5 Force Measurements

The force between the two surfaces is measured according to Hooke's law,  $F = k\Delta x$ , where  $k$  is the spring constant supporting the lower surface, and  $\Delta x = D_{actual} - D_{applied}$  is the difference between applied and actual surface separations. The applied separation is a constant for each drive system and can be calibrated based on the calibration of the motor or piezocrystal-driven systems. The resolution of the force measurement in SFA experiments is about 10 nN and that of distance measurement is 1 Å.<sup>7</sup>

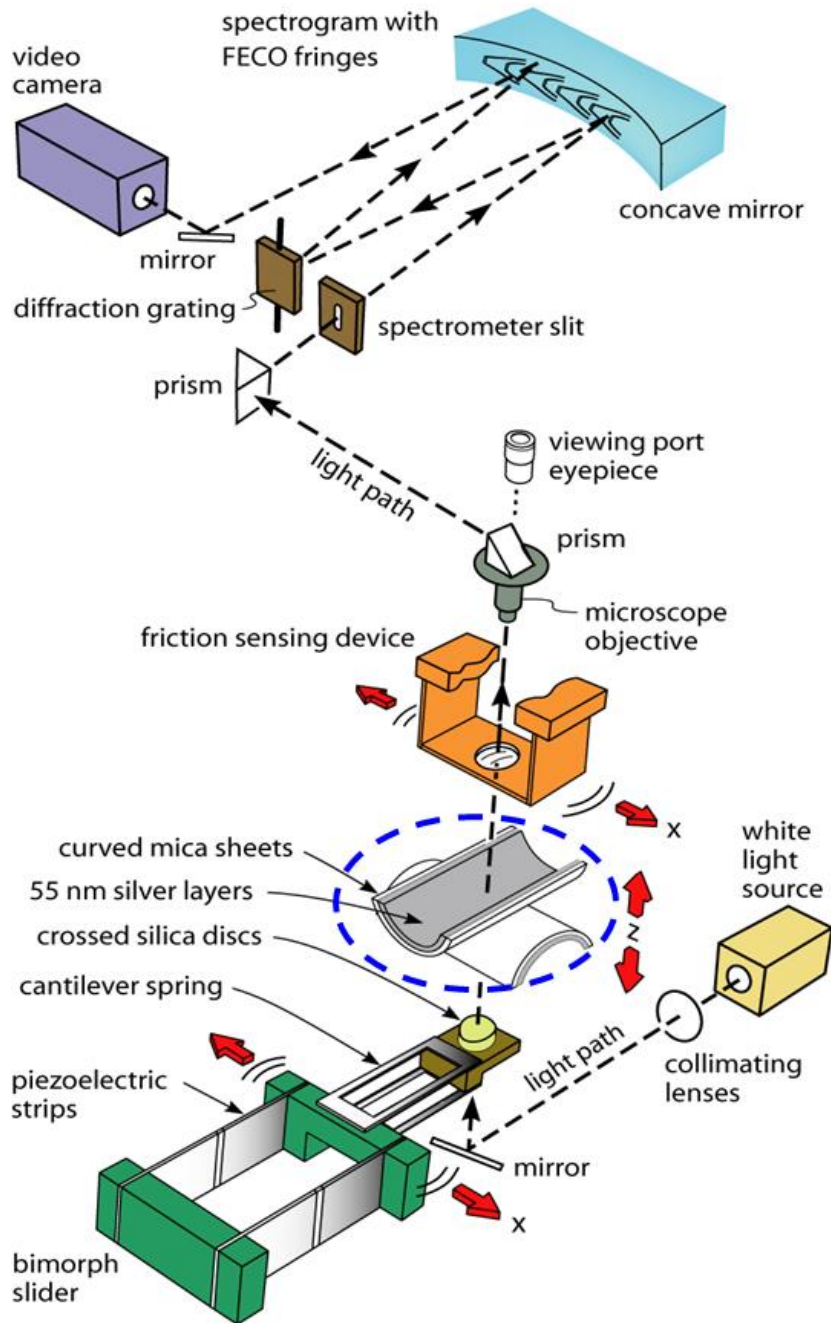


Figure 2-1 SFA experimental setup. (Reproduced from Dr. Hongbo Zeng's presentation at Petrophase conference, June 2010)

By plotting the force versus separation distance between two surfaces, one can get interactions between the sample surfaces such as van der Waals, electrostatic, and hydrophobic forces at various length scales. Furthermore, the adhesion or interfacial energy, per unit area between two flat surfaces  $E(D)$  is simply related to  $F(D)$  by Derjaguin approximation.<sup>7</sup>

The schematics of typical energy-distance plot of two surfaces in the SFA are shown in Figure 2-2 (a) and (b). The total interaction energy is the sum of the spring potential and intersurface potential.<sup>7</sup> Depending on the position of top surface in Figure 2-2 (c), i.e., moving-in or moving- out from the lower surface, the spring potential and the interface potential will change along with a change in total energy as shown in Figure 2-2 (b). When the top surface is approaching the bottom surface, at some critical point that the gradient of the force  $dF(D) / dD$  is equal to or exceeds the supporting spring stiffness  $k_s$ :  $dF(D)/dD \geq k_s$ , the two surfaces will jump into adhesive contact spontaneously. During separation, the two surfaces will jump apart spontaneously from a critical point when  $dF(D)/dD \geq k_s$ , as shown in Figure 2-2.<sup>11</sup> These spontaneous jumps are not reversible, and the critical jump-in distance and jumping positions are determined by the spring stiffness and the intersurface interaction strength.<sup>7, 11, 12</sup>

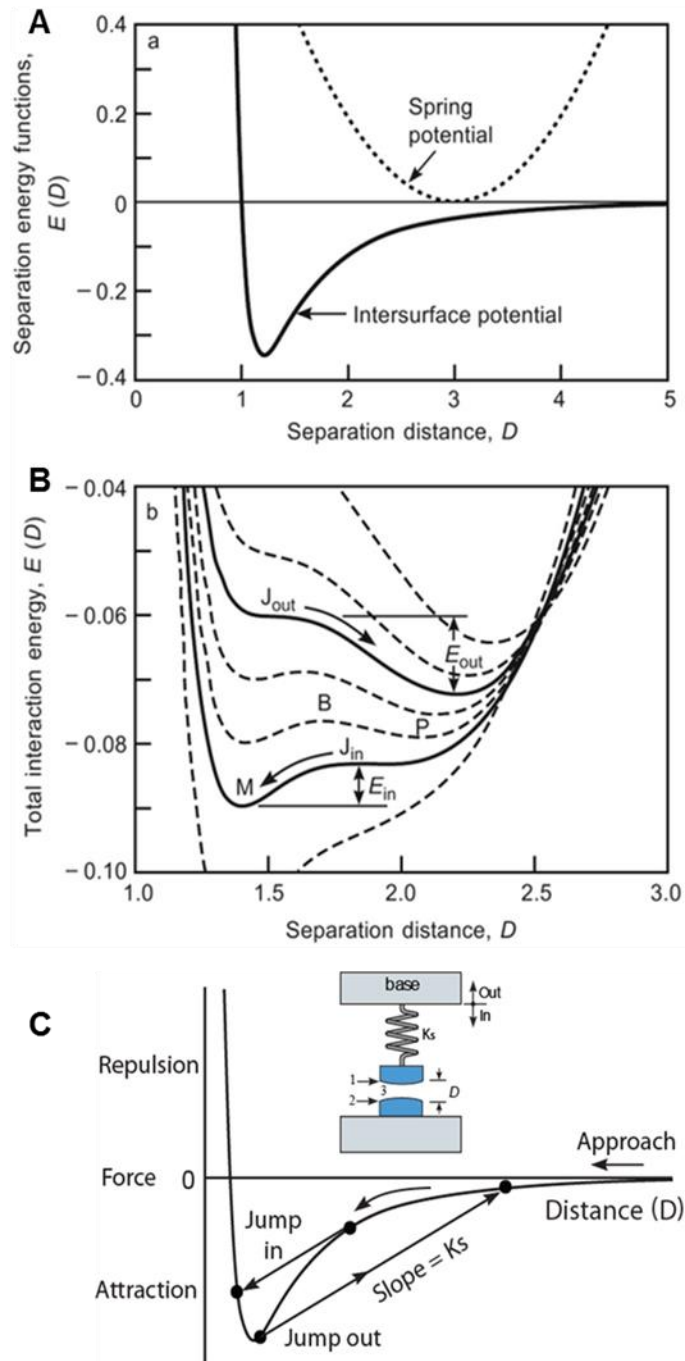


Figure 2-2 Schematics of energy and force vs distance plot of two surfaces. (a) Separate intermolecular and spring potential functions. (b) Total energy curves at different molecule-surface separations. Spontaneous inward and outward jumps occur from  $J_{in}$  and  $J_{out}$ . (c) Spontaneous inward and outward jumps occur when  $dF(D)/dD \geq k_s$ . (Reproduced from Dr. Hongbo Zeng's Dissertation.<sup>13</sup>)

### **2.5.1 Mica Preparation.**

The supporting substrate surfaces used in the SFA are generally freshly cleaved muscovite mica pieces. Other materials such as silica, silicon nitride, and alumina may also be used as supporting surfaces. The utility of mica lies in the fact that the sheets of the material can be obtained which are extremely smooth ( $\sim 0.2\text{nm}$ ) over macroscopic dimensions ( $\sim \text{cm}$ ). This useful property, along with its inertness and relative hardness makes it an ideal substrate for the study of a variety of surface phenomena. The quality of mica surface is significant to the success of any surface force experiment. Typically, the mica sheets must be very thin ( $1\text{--}5\ \mu\text{m}$ ) and be free of steps over large areas ( $1\text{--}2\ \text{cm}^2$ ), and must be kept very clean during preparation.

The procedure to prepare mica surfaces is shown in Figure 2-3. Commercially available mica comes in thick sheets and so they need to be trimmed, split and cleaved in a laminar flow cabinet. A big piece of freshly cleaved mica sheet is chosen as the backing sheet. Smaller cut pieces of thin and smooth mica sheets ( $1\text{--}5\ \mu\text{m}$ ) are placed onto the backing sheet. A uniform layer of pure silver ( $\sim 48\ \text{nm}$  thick in all my experiments, and/or about 98% reflectivity) is deposited on the mica surface, which acts as a mirror in the MBI during SFA experiments. After silvering, the large backing sheet is returned to the dust free laminar flow cabinet. Here, the smaller, thin and molecularly smooth mica sheets are removed and glued onto silica disks. Epoxy glue with different glass transition temperature and elastic modulus, or UV-curable glue can be used as glue. After gluing, the two

surfaces are mounted into the SFA chamber, and are brought into contact to measure the molecular interaction between the surfaces or thin films.

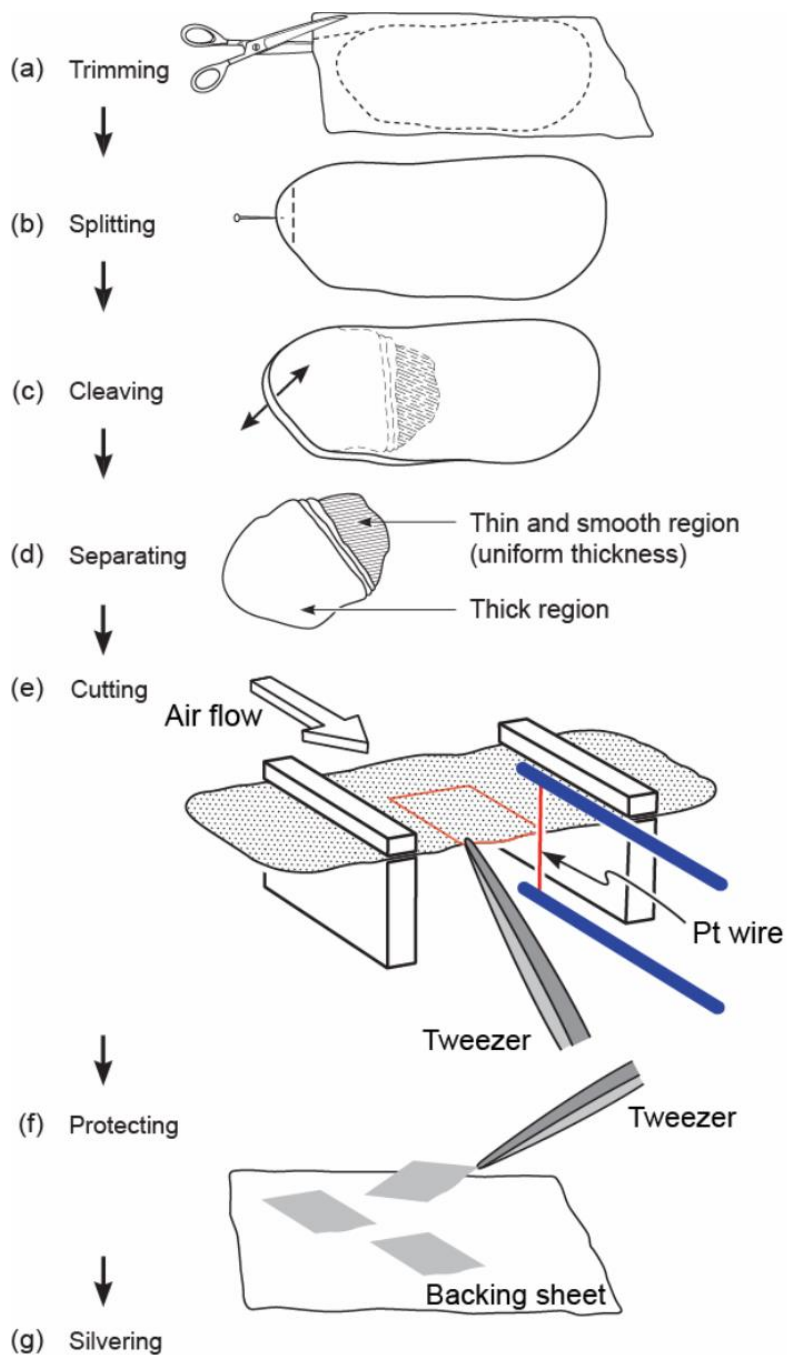


Figure 2-3 Schematic drawings of the procedure to prepare mica sheets having the same thickness. (Reproduced from Dr. Hongbo Zeng's dissertation<sup>13</sup>).

## 2.6 References

1. Lee, L-H.; In Fundamentals of Adhesion and Interfaces, eds. Rimai, D. S.; DeMejo, L. P. and Mittal, K. L.; VSP, Utrecht, 1995.
2. Bowden, F. P. and Tabor, D. T. Friction and Lubrication of Solids, Clarendon Press, Oxford, Part I, 1950, Part II 1964.
3. Kendall, K. Molecular Adhesion and Its Application – The Sticky Universe, Kluwer Academic / Plenum Publishers, New York, 2001.
4. Masliyah, J. H.; Czarnecki, J.; Xu, Z. Handbook on Theory and Practice of Bitumen Recovery from Athabasca Oil Sands, vol 1, Kingsley Knowledge Publishing, 2011.
5. Mahanty, J.; and Ninham, B. W. Dispersion Forces, Academic Press, New York, 1976.
6. Margenau, H. and Kestner, N. R. Theory of Intermolecular Forces, Pergamon, Oxford, 1971.
7. Israelachvili, J. N. Intermolecular and Surface Forces, 3rd Edition, Elsevier Inc. 2011.
8. Johnson, K. L.; Kendall, K. and Roberts, A. D. Proc. R. Soc. A 1971, 324, 301.
9. Israelachvili, J. N. J. Colloid Interface Sci. 1973, 44, 259.
10. Israelachvili, J. N.; Min, Y.; Akbulut, M.; Alig, A.; Carver, G.; Greene, W.; Kristiansen, K.; Meyer, E.; Pesika, N.; Rosenberg, K.; Zeng, H. Rep. Prog. Phys. 2010, 73 036601, 1.
11. Israelachvili, J.N.; Tabor, D. Proc. R. Soc. London, Ser A 1972, 331, 19.

12. Zeng, H. B.; Tian, Y.; Zhao, B. X.; Tirrell, M.; Israelachvili, J. *Langmuir* **2007**, 23, 612.
13. Zeng, H. Interactions of Polymer Surfaces and Thin Films. *Dissertation* **2007**, University of California, Santa Barbara, UMI Dissertations Publishing.

## **Chapter 3**

# **Understanding Molecular Interactions of Asphaltenes in Organic Solvents Using a Surface Forces Apparatus<sup>a</sup>**

As we saw in the previous chapters, stable emulsions are a big challenge to the oil sands industry and measuring the molecular forces between the various components will be the key to understanding the stabilization mechanism. In this chapter, we measure the molecular forces between asphaltene coated surfaces to study the interactions between the asphaltene layers coated on hydrophilic solids or water. This understanding will give us an insight into the basic interaction mechanisms of asphaltenes in organic media and hence in crude oil and bitumen production. A detailed history of the problem is given below.

### **3.1 Introduction**

Asphaltenes are normally defined as the part of the crude which is soluble in toluene and insoluble in alkanes, usually n-pentane or n-heptane.<sup>1,2</sup> The above definition indicates that asphaltenes do not comprise a chemically defined group of molecules, but rather a solubility class. In general, asphaltene molecules are large polyaromatic hydrocarbons containing a significant number of heteroatom

---

<sup>a</sup> A version of this chapter has been published: Natarajan, A.; Xie, J.; Wang, S.; Liu, Q.; Masliyah, J.; Zeng, H.; Xu, Z. *J. Phys. Chem. C* **2011**, 115, 16043-16051.

functional groups including both acids and bases.<sup>3</sup> The functional groups are typically hydrophilic while the hydrocarbon structure of asphaltenes is hydrophobic. Hence, asphaltenes are considered surface active and are able to adsorb at water–oil interfaces. The adsorbed asphaltenes, together with the accumulation of other surface active materials such as resins and nature surfactants with fine solids, form a protective interfacial film that prevents the dispersed water droplets from coalescence, thereby stabilizing water-in-oil (w/o) emulsions.<sup>4-17</sup> Stable emulsions are undesirable in petroleum processing because the presence of w/o emulsions leads to serious processing problems in downstream operations, i.e., corrosion, erosion and fouling in the heat exchangers, transportation device, and distillation equipment, causing a significant increase in operating cost. Despite the extensive research reported on w/o emulsions, the exact stabilization mechanism remains to be fully established. Many believe that asphaltenes are almost exclusively responsible for stabilizing w/o emulsions,<sup>18-20</sup> while others believe that only a small fraction of total asphaltenes is involved in stabilization mechanism.<sup>21,22</sup> Many other industrial problems such as wellbore or pipeline plugging, alteration of wettability of solids, and sedimentation during crude blending are all attributed, at least partly, to molecular aggregation of asphaltenes upon exposure to an unfavourable liquid environment, to an oil/water interface or to various solid-oil interfaces. Thus, understanding the role of asphaltenes in stabilization of w/o emulsions at the molecular level is of both fundamental and practical importance.

The behavior of asphaltenes in a crude oil is almost exclusively determined by interactions between asphaltene molecules/aggregates in the surrounding organic solvents. Significant efforts have been made during the past decade in this regard. Several microscopic and nanoscopic techniques, including micropipette and Langmuir trough have been applied to study the molecular interactions of asphaltenes and its relation to stability of w/o emulsions. The micropipette technique allows micrometer-size emulsion droplets to attach onto a small pipette, which has been used to study water-diluted bitumen interfacial properties such as interfacial tension, crumpling ratio and interfacial rheology.<sup>23, 24</sup> Langmuir trough was used to measure surface pressures of asphaltene monolayers formed at the water-toluene interface.<sup>25-27</sup> The Langmuir trough results showed that asphaltene monolayer is rigid and irreversibly adsorbed at the water-toluene interface, which accounts for the observed difficulties to disrupt the protective asphaltene layers surrounding the emulsified water droplets in diluted bitumen.

Surface forces between asphaltene surfaces in aqueous solutions have been measured directly using an atomic force microscope (AFM) and were reported in the literature, as were a number of quantitative studies conducted on colloidal force measurements between solids and model oil droplets.<sup>28-31</sup> Reports on surface forces for crude oil systems in aqueous solutions are also available.<sup>4,32-35</sup> To understand the colloidal interactions between oil sand components in aqueous solutions, a number of systematic studies were conducted using AFM to measure surface forces between bitumen and silica,<sup>36</sup> bitumen and clay,<sup>37</sup> bitumen and fine

solids,<sup>38</sup> bitumen and bitumen,<sup>39</sup> silica and clay,<sup>40</sup> and asphaltenes and asphaltenes.<sup>41</sup> These studies provided a better understanding of and scientific guidance to bitumen extraction and flotation during oil sand processing. Although there are many reports on direct surface force measurements in aqueous systems using AFM or SFA, less attention has been devoted to non-aqueous systems. Recently, Wang et al. reported measurements of interaction forces between asphaltene films or asphaltene films and a micron size silica sphere in oil media using an AFM,<sup>42,43</sup> while Vuillaume et al. used a SFA to measure interaction forces between mica surfaces across asphaltene solutions and crude oil in the presence and absence of water.<sup>44</sup> These measurements provided valuable information on stabilization mechanism of the water-in-diluted bitumen emulsions as of steric origin. Due to the complexity of the water-in-diluted bitumen emulsion systems and limitations of techniques described above, understanding of interfacial properties, intermolecular and surface interactions of asphaltenes and corresponding governing mechanisms on the stability of water-in-oil emulsions remains incomplete.

In the present study, we focus on understanding the interactions of two asphaltene films in good/poor solvents (toluene and heptane). Due to the unique ability of SFA to measure simultaneously the interaction force,  $F$ , as a function of the absolute surface separation,  $D$ , and the local geometry of two interacting surfaces (the local radius  $R$  or contact area) at a force sensitivity of  $\sim 10$  nN and an absolute distance resolution of 0.1 nm in situ and in real time, it has been widely used in

studying governing forces of many biological and non-biological systems.<sup>45</sup> SFA could be a unique and ideal technique for the research objective of this study. The force-distance curves or so-called force profiles obtained from SFA measurements would be able to provide valuable information on material properties such as interaction energies, Hamaker constant, and molecular conformation changes of the interacting asphaltene surfaces or films in a given solvent. AFM imaging was employed to provide complementary information on the surface morphology of the asphaltene films studied.

## **3.2 Materials and Experimental Methods**

### **3.2.1 Materials**

Vacuum distillation feed bitumen was provided by Syncrude Canada Ltd., Alberta, Canada. Asphaltenes were precipitated from bitumen by adding 40 times of n-heptane to bitumen by volume and repeatedly washed with n-heptane. Details on asphaltene precipitation were reported elsewhere.<sup>14</sup> High-performance liquid chromatography (HPLC)-grade toluene and heptane purchased from Fisher Scientific was used as received. Ruby mica sheets were purchased from S & J Trading Inc. (Glen Oaks, NY).

### **3.2.2 Sample Preparation**

Film-coating method was adopted to coat an asphaltene film on a mica surface. Briefly, after gluing a freshly cleaved thin mica sheet on a silica disk used in SFA, several drops of 0.5 wt% asphaltene in toluene solution were placed and spread on

the exposed mica surface. The solvent was evaporated for ~15 min to immobilize asphaltenes on the mica surface. The sample was then washed with pure toluene and blow-dried with ultra-pure nitrogen before it is loaded in the SFA chamber. The asphaltene coated mica surfaces were then used to measure interaction forces and image their topographic features by SFA and AFM, respectively.

### 3.2.3 Surface Forces Apparatus Technique

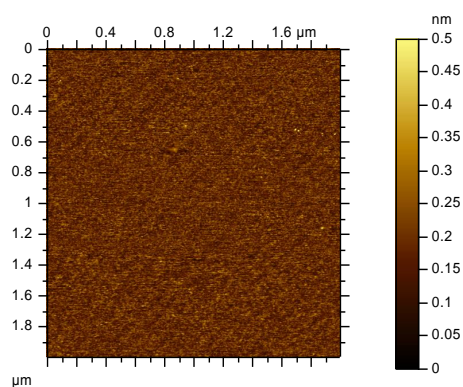
A surface forces apparatus (Surforce LLC, Santa Barbara, CA, USA) was used to measure the normal interaction forces between two asphaltene films immobilized on mica in organic solvents. Detailed setup of SFA experiments has been reported elsewhere.<sup>45,46</sup> Briefly, the back surface of a thin mica sheet (1-5  $\mu\text{m}$  thick) was coated with an ~50 nm thick semi reflective layer of silver, required to obtain multiple beam interference fringes of equal chromatic order (FECO). The FECO was used to determine the surface separation, surface geometry, deformations and the contact area in situ and in real time. The silver coated mica sheet was glued onto a cylindrical silica disk (radius  $R=2$  cm). The prepared silica disks were then mounted into the SFA chamber in a cross-cylinder geometry, which roughly corresponds to a sphere of radius  $R$  approaching a flat surface locally. With this arrangement, the measured force  $F(D)$  is converted to interaction energy per unit area between two flat surfaces  $W(D)$  using the Derjaguin approximation:<sup>46,47</sup>  $F(D) = 2\pi RW(D)$ . In each set of measurements, the reference distance ( $D = 0$ ) was determined at the adhesive contact between the two bare mica surfaces in air prior to introducing the solvents between the surfaces. For the force measurements, ~50

$\mu\text{L}$  of desired solvent/solution was injected between two closely placed coated mica surfaces in the SFA chamber. The chamber was sealed and saturated with the vapour of the same solvent. Normal forces between the two surfaces are measured by moving the lower surface supported on a double-cantilever ‘force springs’ towards the upper surface by a distance  $\Delta D_{\text{applied}}$ . The actual distance that the surfaces moved to each other,  $\Delta D_{\text{meas}}$ , is measured by multiple beam interferometry in real time.<sup>48</sup> The change in the force  $\Delta F$  between the surfaces, when they come to rest at a separation distance  $D$ , is calculated from the deflection of the cantilever spring by,  $\Delta F(D) = k (\Delta D_{\text{applied}} - \Delta D_{\text{meas}})$ , where  $k$  is the spring constant. When  $\partial F(D)/\partial D > k$ , there is a mechanical instability that causes the lower surface to jump either towards or away from the upper surface during approaching or separation process, respectively. During a typical force measurement, the normal force-distance ( $F$  vs.  $D$ ) profile is obtained by an initial approach to a “hard wall” followed by separation of the two surfaces (note the “hard wall” distance in this study is defined as the mica-mica separation distance or thickness of confined asphaltenes which barely changed with increasing the normal load or pressure).

### **3.3 Results and Discussion**

The topographical features of asphaltene films immobilized on mica surfaces were imaged in air by an AFM operating in tapping mode. As shown in Figure 3-1a, the AFM image of bare mica prior to asphaltene film deposition showed a

featureless flat surface with a root-mean-square (rms) roughness of 0.3 nm. The AFM image of coated asphaltene film on mica in Figure 3-1b shows an rms roughness of 0.9 nm. Typical FECO fringe of two mica surfaces in contact in air is shown in Figure 3-1c and FECO of an asphaltene film in contact with mica in air is shown in Figure 3-1d. Taking the distance of two mica surfaces as zero, the thickness of a film of asphaltene in air was determined to be ~5 nm. The intermolecular forces of asphaltenes immobilized on mica in organic solvents were measured using an SFA in two different configurations as shown in Figure 3-2. Figure 3-2a shows an asymmetric geometry of an asphaltene film coated on mica interacting with a bare mica surface in a solvent. Figure 3-2b shows a symmetric geometry of two asphaltene films coated on mica in a solvent of interest.



(a)

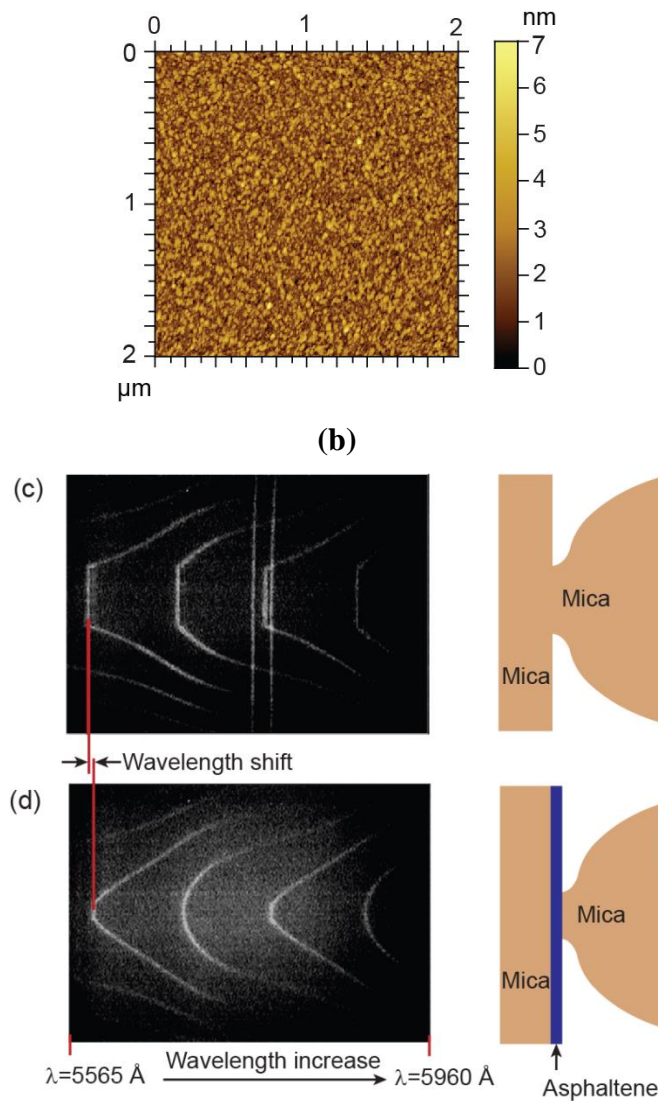


Figure 3-1 AFM images of (a) bare mica surface and (b) coated asphaltene film on mica surface. (c) FECO of mica surfaces in contact in air (d) FECO of a coated asphaltene film in contact with a mica surface in air. Note the shift in the wavelength of FECO and change in the shape (contact area) of the fringes, indicating the presence of asphaltene layers and change of adhesion due to the presence of asphaltenes as anticipated. FECO can be used to measure the surfaces deformations, surfaces separation and refractive index of the medium.

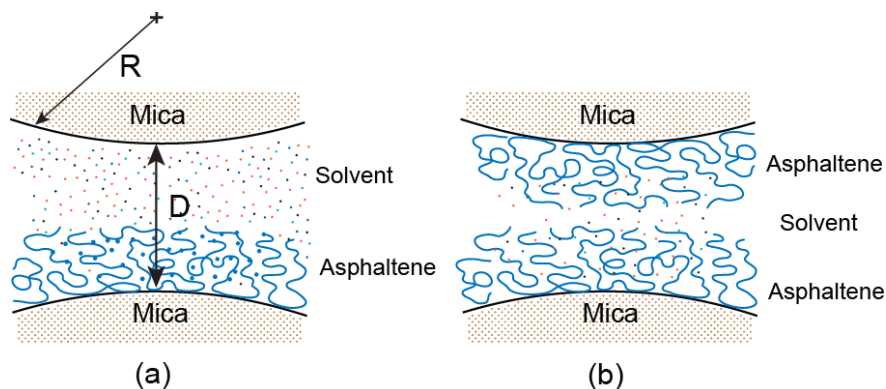


Figure 3-2 Experimental configurations for studying the surface interactions of asphaltenes in organic solvents: (a) an asphaltene film vs. bare mica (asymmetric case) and (b) two asphaltene films (symmetric case).

### 3.3.1 Interaction Forces in Toluene (Good Solvent)

Asphaltenes are soluble in toluene. To that end, toluene can be considered as a good solvent which significantly mediates the configuration of asphaltene molecules on a substrate and hence affects the interaction forces. In this study, the force profile of two bare mica surfaces in toluene was first determined. As shown in Figure 3-3a, an attractive interaction force was observed as the two mica surfaces approach each other. The two surfaces jumped at  $D_J \sim 7.5$  nm into contact. When the surfaces were separated, a very strong adhesive force was observed and the surfaces jumped apart from contact. For two surfaces 1 and 2 in a geometry of two crossed cylinders having the same radius  $R$  approaching each other in a medium 3, the attractive van der Waals force is given by Eq 3-1, and the critical jump-in distance  $D_J$  is given by Eq 3-2,

$$F_{\text{vdW}} = -\frac{A_{132}R}{6D^2} \quad (3-1)$$

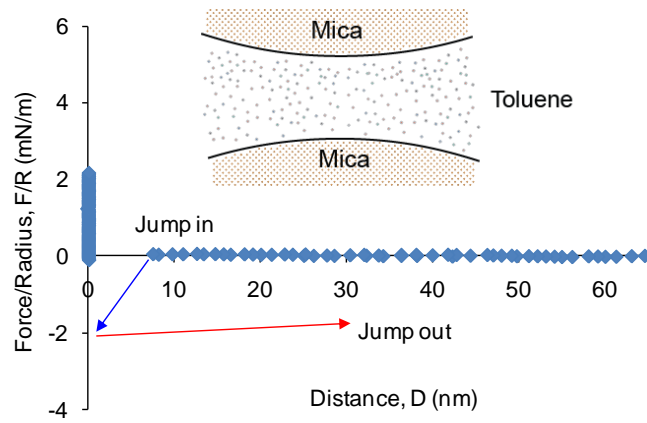
$$D_J = \left( \frac{A_{132}R}{3k} \right)^{1/3} \quad (3-2)$$

where  $D$  is the distance between the two curved surfaces,  $k$  is the force-measuring spring constant, and  $A_{132}$  is the combined Hamaker constant of the two surfaces 1 and 2 interacting across 3.<sup>49</sup>  $A_{132}$  can be estimated using Eq 3-3,

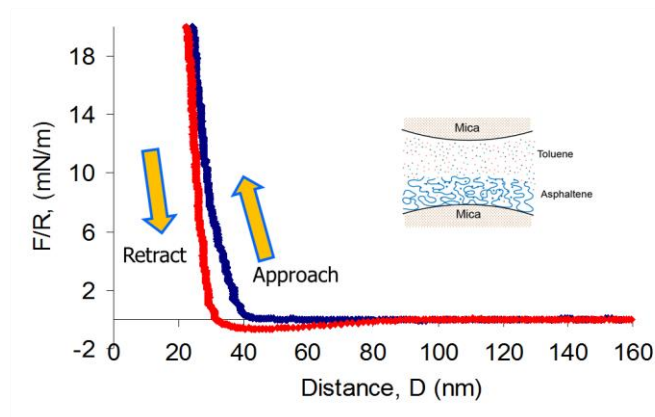
$$A_{132} \approx (\sqrt{A_1} - \sqrt{A_3})(\sqrt{A_2} - \sqrt{A_3}) \quad (3-3)$$

where  $A_1$ ,  $A_2$ ,  $A_3$  are the Hamaker constants of media 1, 2, and 3 in vacuum. In this experiment, two bare mica surfaces (surface 1 = surface 2) approach each other in toluene (medium 3) with a measured values of  $D_J \approx 7.5$  nm, and  $k \approx 500$  N/m. With these measured values, the Hamaker constant of  $A_{\text{mica-toluene-mica}} = 3KD_J^3/R$  is estimated to be  $3.2 \times 10^{-20}$  J.

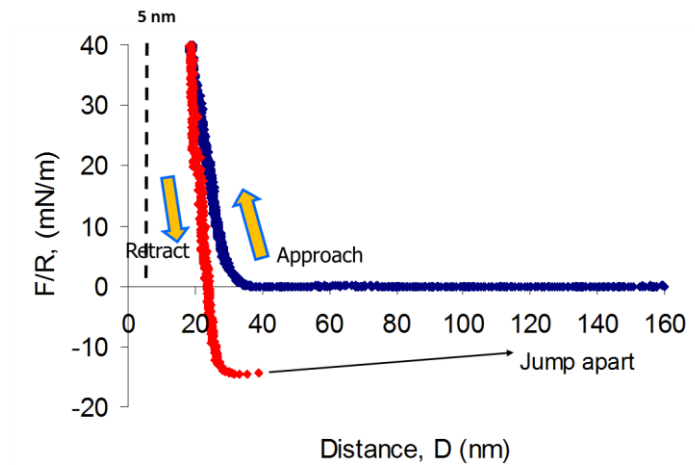
Using Hamaker constants  $A_{\text{mica}} \approx (15.8 \pm 2.5 \times 10^{-20} \text{J})$  and  $A_{\text{toluene}} \approx 5.4 \times 10^{-20} \text{J}$ , Eq 3-3 gives  $A_{\text{mica-toluene-mica}} \approx (\sqrt{A_{\text{mica}}} - \sqrt{A_{\text{toluene}}})^2 \approx 2.7 \times 10^{-20} \text{J}$ .<sup>46</sup> This value is in agreement with the above experimentally measured value, validating the experimental setup and accurate measurement in organic solvents.



(a)



(b)



(c)

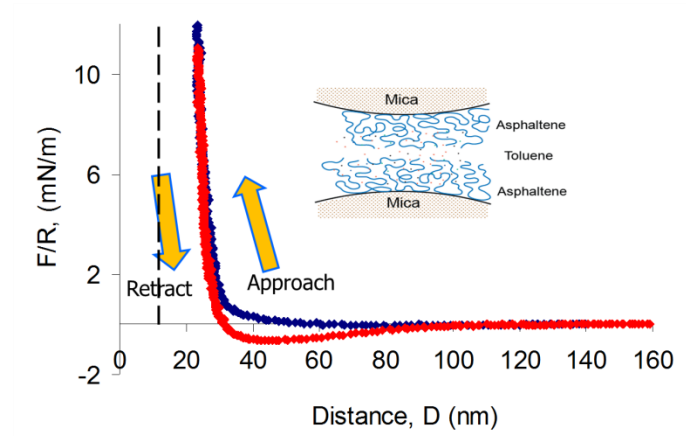
Figure 3-3 Force profiles of a coated asphaltene film on surface interacting with a bare mica surface across toluene: a) two bare mica surfaces in pure toluene (b) measurement

after the asphaltene film being exposed in toluene for ~1 hr, and (c) successive measurement in which the asphaltene film was kept in contact with mica surface for about 10 min before separation. When the surfaces are compressed, the hard wall shifted to about 5 nm indicating that asphaltene film in toluene swell and is flexible instead of rigid. In this figure and all subsequent figures, “Approach” indicates bringing the two surfaces close together and “Retract” indicates separation of the two surfaces.

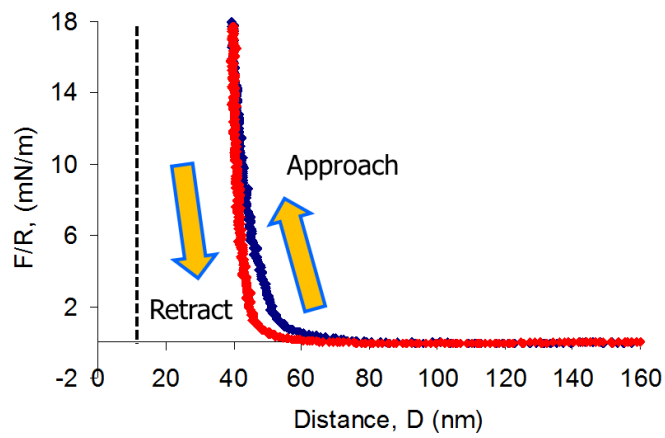
The interactions between a coated asphaltene film and a bare mica surface in toluene were measured. Figure 3-3b shows the interaction force measured after exposing asphaltenes to toluene for ~ 1 hour. The two surfaces were brought into contact and then separated immediately. Repulsive force was observed during approach at around 40 nm with a hard wall distance of ~ 22 nm. A weak adhesive force ( $F/R \sim -0.6$  mN/m) was observed during separation. On the next approach at the same position, shown in Figure 3-3c, a repulsive force was observed at about 5 nm closer than the previous approach, shown in Figure 3-3b, while the hard wall shifted to ~18 nm. Before the separation process, asphaltene film and mica surface were kept in contact in toluene for ~10 min, and a much stronger adhesion force was measured ( $F/R \sim -14.5$  mN/m). Under high compression of ~2 MPa, the hard wall separation shifted to ~5 nm, which corresponds to the thickness of one film of coated asphaltene in air on mica surface. The force profiles for coated asphaltene films in toluene are shown in Figure 3-4a (measured immediately after toluene injection) and Figure 3-4b (measured ~30 min after toluene injection). Weak adhesion was measured during the separation for the initial measurement, but disappeared when measured after 30 min

incubation of the system. Interestingly, the hard wall distance in reference to mica-mica separation distance in toluene, i.e., the thickness of the confined asphaltenes in toluene shifted from ~25 nm to ~40 nm between the two measurements. However, when a higher load/pressure (~1 MPa) was applied, the confined asphaltene thickness decreased to ~11 nm, which corresponds to two films of asphaltenes ~5.5 nm thick on each mica surface. This finding suggests that asphaltene layers in toluene swelled in 30 min by 60%, i.e., up to about ~15 nm on each surface. Also, the asphaltene layers are flexible and soft instead of being rigid.

Since the electric double-layer forces in toluene can be considered negligible, repulsive forces observed during the approaching of two asphaltene films in toluene as shown in Figure 3-4a and Figure 3-4b, are attributed to steric repulsion of swollen asphaltene chains.<sup>42</sup> The retracting force profile in Figure 3-4a shows a weak adhesion, mostly likely due to the interdigitation and bridging of the asphaltene molecules on the two surfaces when brought in contact for a few seconds during force measurements. Such interactions resulted in stretching of the asphaltene layers up to D~40 nm during separation before the two surfaces finally detached from each other. As shown in Figure 3-4b, this bridging adhesion force disappeared after 30 min incubation of asphaltene in toluene, accompanied by much longer range repulsion. It appears that asphaltenes are fully solvated during this period in a good solvent, leading to the conformational change which was confirmed by the AFM images of coated asphaltene surfaces before and after



(a)



(b)

Figure 3-4 Force profiles of (a) asphaltene coated surfaces in toluene immediately after toluene injection, and (b) asphaltene coated surfaces in toluene after 30 min. The vertical dashed lines indicate the hard wall distance of two asphaltene surfaces in air.

immersion in toluene for 30 min as shown in Figure 3-5a and Figure 3-5b. The RMS roughness of asphaltene surfaces increased from 0.9 nm to 2.8 nm and the aggregates become much larger after immersion of asphaltene films in toluene for half hour.

Such an increase in surface roughness by soaking asphaltene films in toluene leads to a greater hard wall distance as shown in Figure 4b. Since asphaltenes are amphiphilic and highly soluble in toluene, most of the polar functional groups stick to the mica surface with time, leaving the rest of the molecules being extended into toluene. In this manner, the side chains of asphaltene aggregates mimic a swollen brush and repelled each other when brought in contact. This argument is supported by repulsive forces and ~15 nm surface shift of the hard wall distance as shown in Figure 3-4a and Figure 3-4b. The hard wall can be pushed to about ~11 nm under a compressive load/pressure of ~1 MPa, indicating that the asphaltene layers are soft and that they swell in toluene.

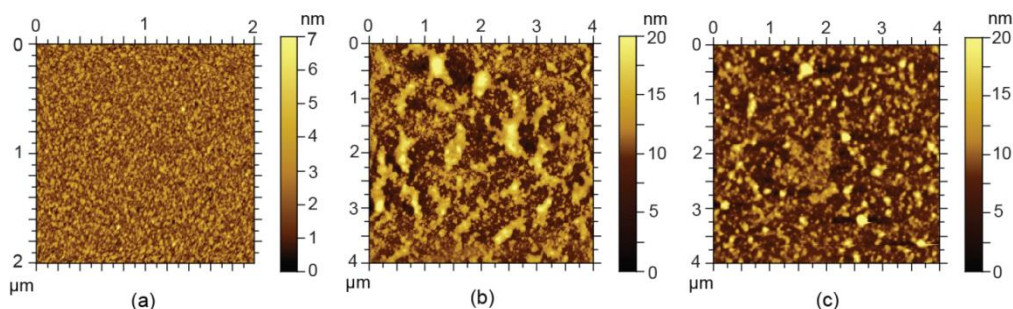
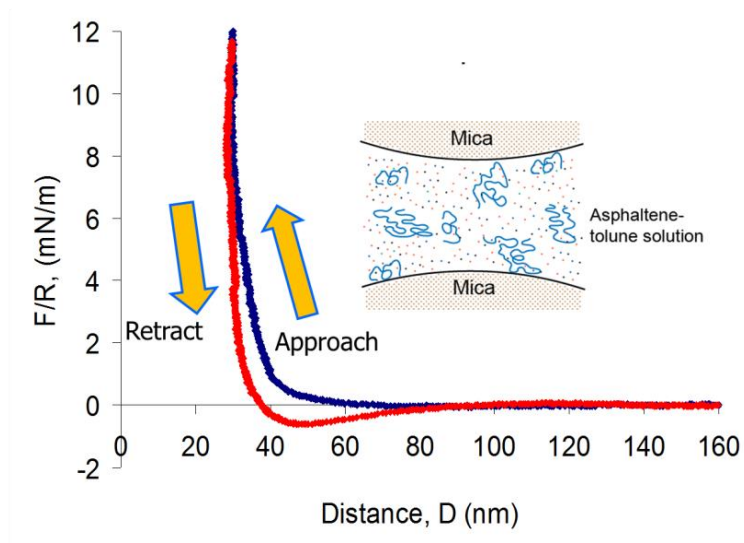


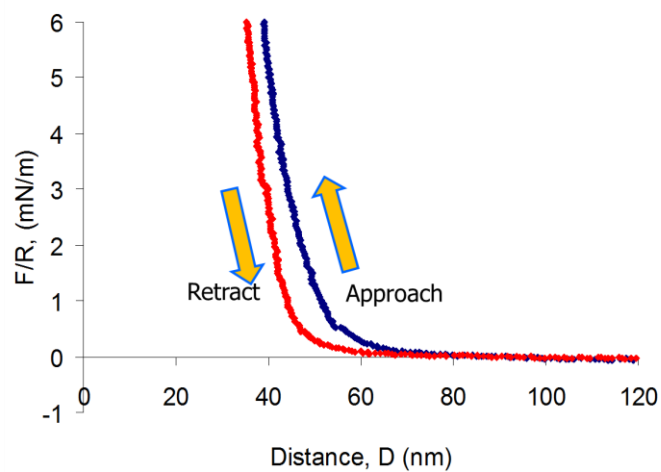
Figure 3-5 AFM image of asphaltene coated on mica surfaces. (a) Coated asphaltene film on mica in air, (b) coated asphaltene film on mica after incubation in toluene for 30 min, showing significant aggregation, and (c) coated asphaltene film incubated in heptane for 30 min, showing less significant aggregation than in toluene.

The force profile for the interaction between two mica surfaces immediately following the injection of 0.5 wt% asphaltene toluene solution is shown in Figure 3-6a. The asphaltenes in the solution adsorbed very quickly (less than 5 min) to the mica surfaces and the hard wall distance increased to  $\sim 30$  nm. A weak adhesive force of  $F/R \sim -1$  mN/m was observed during separation. The asphaltene-toluene solution was flushed out and replaced by pure HPLC toluene. The force profile in Figure 3-6b shows that only pure repulsive forces were observed with the hard wall distance shifted to  $\sim 40$  nm. This result is similar to the interaction between two coated asphaltene films on mica in toluene as shown in Figure 3-4.

As toluene is a good solvent for asphaltenes, the side chains/branches of the immobilized asphaltene molecules on mica surface tend to stretch and act as a swollen brush while the aggregated core could swell to become mushrooms. Consequently, the adsorbed asphaltene film on mica may be treated as a polymer brush, and the interaction between two such films could be described by the Alexander-de Gennes (AdG) theory on two interacting polymer brush layers.<sup>50-53</sup>



(a)



(b)

Figure 3-6 Force profiles of (a) mica surfaces in asphaltene-toluene solution measured immediately after injection, (b) same system as (a) but after the asphaltene-toluene solution is flushed out and replaced by pure toluene and measured after 30 min.

When two polymer brush surfaces approach each other, at some distance the brushes/films start to overlap. The increased local density of polymer segments lead to an increase in osmotic pressure and repulsive interaction energy. The repulsive pressure between two planar brush layers is given by<sup>54</sup>

$$P(D) \approx \frac{kT}{s^3} \left[ \left(\frac{2L}{D}\right)^{9/4} - \left(\frac{D}{2L}\right)^{3/4} \right] \text{ for } D < 2L \quad (3-4)$$

where  $s$  is the mean distance between anchoring (or grafting) sites on the surface,  $L$  is the brush layer thickness per surface,  $T$  is the temperature and  $k$  is Boltzmann constant. For the geometry of two crossed cylinders of radius  $R$  (used in our SFA measurements), the force between them is given by first integrating the above equation and then using the Derjaguin approximation as,<sup>46,54</sup>

$$\frac{F(D)}{R} = 2\pi \int P(D)dD = \frac{16\pi kTL}{35s^3} \left[ 7\left(\frac{2L}{D}\right)^{5/4} + 5\left(\frac{D}{2L}\right)^{7/4} - 12 \right] \quad (3-5)$$

For the asymmetric case (a brush layer against a solid substrate), the equation becomes

$$\frac{F(D)}{R} = \frac{8\pi kTL}{35s^3} \left[ 7\left(\frac{L}{D}\right)^{5/4} + 5\left(\frac{D}{L}\right)^{7/4} - 12 \right] \quad (3-6)$$

The fit of measured repulsive forces for two asphaltene films in toluene with the AdG theory (Eqs 5 and 6, solid curves) is shown in Figure 3-7a while for

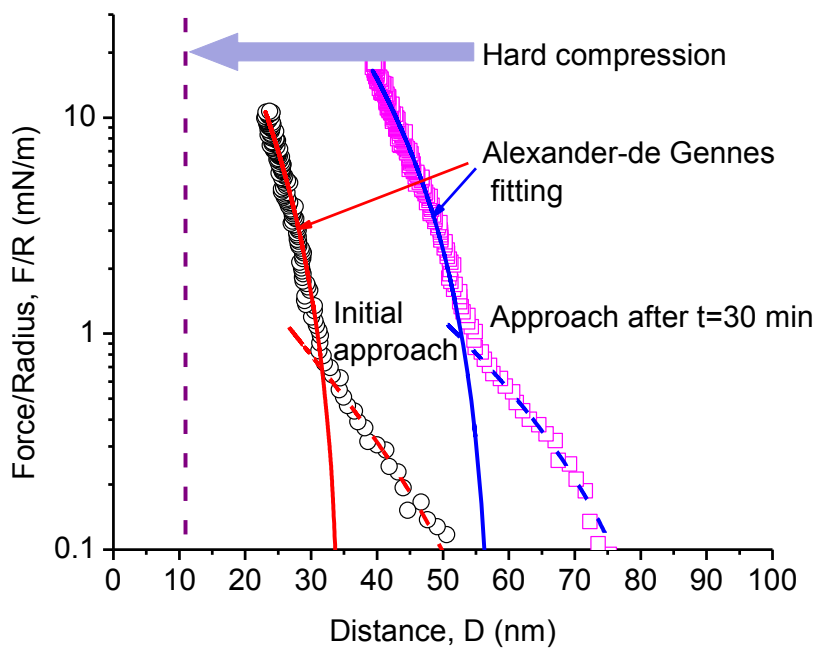
asphaltene film interacting with a mica surface in Figure 3-7b. As shown in Figure 3-7a, the AdG model fits the measured force profile well at short separation distances under high compression forces. However, a significant deviation is seen at longer separation distances under lower compression forces. It appears that the protrusion or undulation of aliphatic side chains on asphaltene brushes and aggregates in good solvent induces a weaker repulsive force over a much longer separation distance. This additional force is not considered in the AdG theory of monodisperse brushes. In fact, lower compression regime can be fitted with the AdG theory using an independent set of parameters as shown in Figure 3-7a, indicating the presence of possible secondary brushes in the current systems due to the polydispersity/complexity of asphaltene molecules/aggregates. The fitted parameters of  $s$  and  $L$  are listed in Table 3-1. It is interesting to note that for both the symmetric and asymmetric cases, the fitted mean distance between anchoring (or grafting) sites  $s$  are very close to each other as anticipated and also close to the size of nano-aggregates of asphaltenes in bulk toluene solutions.<sup>55</sup> The thickness of brush layer  $L$  depends on compression pressure and immersion time in toluene, which causes aggregation and swelling of asphaltene molecules and aggregates. This observation is consistent with surface morphological features revealed in AFM images shown in Figure 3-4. It is interesting to note that regardless of the swollen thickness in either symmetrical or asymmetrical cases, the final thickness of each asphaltene film after high pressure compression is the same of ~5 nm as anticipated.

Table 3-1 Fitting parameters using the Alexander-de Gennes scaling theory

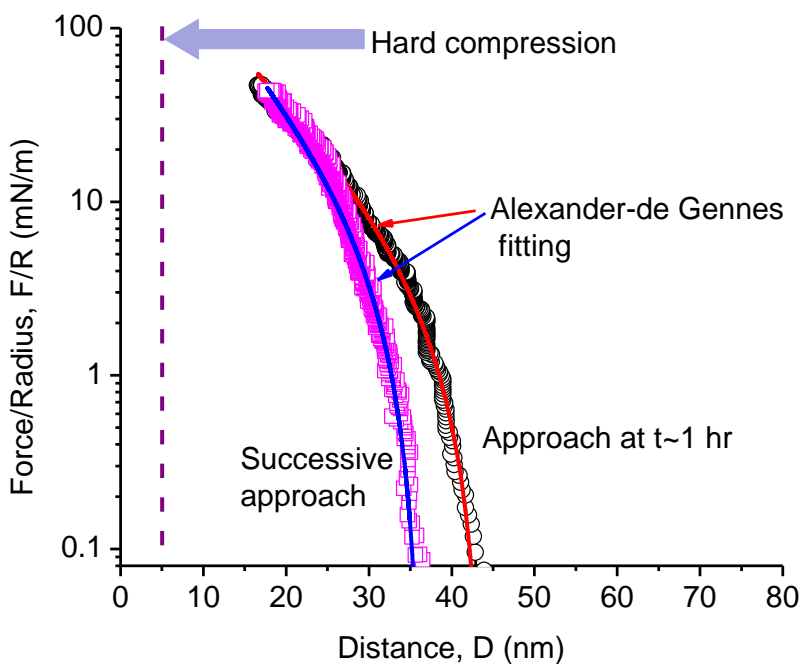
<i>Asphaltene surface vs. asphaltene surface</i>		
Time after asphaltenes immersed in toluene (min)	~5	~35
L, nm§	17.6	29.0
s, nm§	2.8	2.7
L, nm*	33	45.0
s, nm*	12.5	10.0
<i>Asphaltene surface vs. mica surface</i>		
Time after asphaltenes immersed in toluene (min)	~60	~70
L, nm	44.0	37.0
s, nm	3.2	2.5

§High compression and short separation distance regime (solid fitting curve in Figure 3-7a).

\*Low compression and long separation distance regime (dash fitting curve in Figure 3-7a).



(a)



(b)

Figure 3-7 Experimentally measured repulsion forces and best fitted curves using the Alexander-de Gennes theory for approach of (a) two asphaltene films and (b) an asphaltene film against a bare mica surface in toluene.

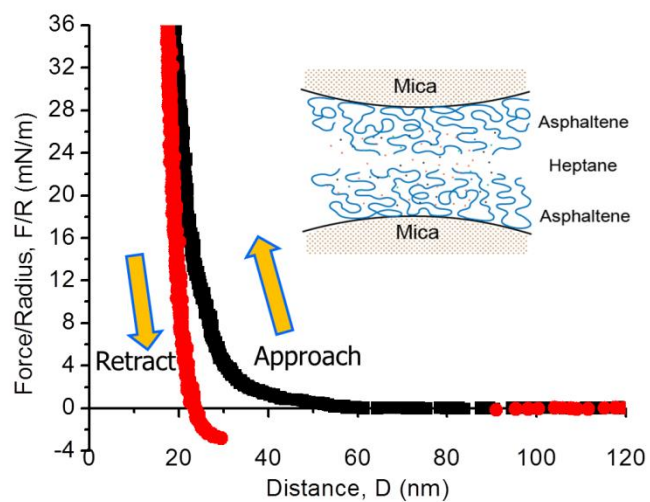
### 3.3.2 Interaction Forces in Heptane (Poor Solvent)

Heptane is a paraffinic and apolar organic solvent, while asphaltene molecules are highly aromatic with a significant number of heteroatoms. Therefore asphaltene and heptane are very different in their molecular structure. Heptane is known to be a poor solvent for polyaromatic asphaltenes. In heptane asphaltenes tend to self-aggregate and precipitate, which is very different from their state in toluene. The interaction force profile between two coated asphaltene films in heptane is shown in Figure 3-8. The effective Hamaker constant of two asphaltene films across a liquid heptane,  $A_{asphaltene-heptane-asphaltene} = 1.1 \times 10^{-21} J$ .<sup>43,46,56,57</sup> With the spring stiffness used for this experiment  $k \approx 880$  N/m, Eq. 2 predicts a jump-in distance  $D_j = (A_{asphaltene-heptane-asphaltene} R / 3k)^{1/3} \approx 2$  nm for two smooth asphaltene films in heptane. However, no jump-in was observed during the approach of the two asphaltene films. Wang et al.<sup>43</sup> observed a weak attractive adhesion force while the two asphaltene surfaces approached in heptane with an AFM. The difference in our results is attributed to surface roughness resulted from self-association of asphaltene molecules, as observed in the AFM image shown in Figure 3-5c, and also the strong spring constant that was used in the SFA experiments. Strong adhesion force of  $F/R \sim 3$  mN/m was however measured during the separation as shown in Figure 3-8a. The force profile of separation indicates a significant stretch of asphaltene films by  $\sim 10$  nm before the two surfaces detached from each other. Similar force profile was measured after 30 min immersion in heptane, as shown in Figure 3-8b, although a weaker adhesion

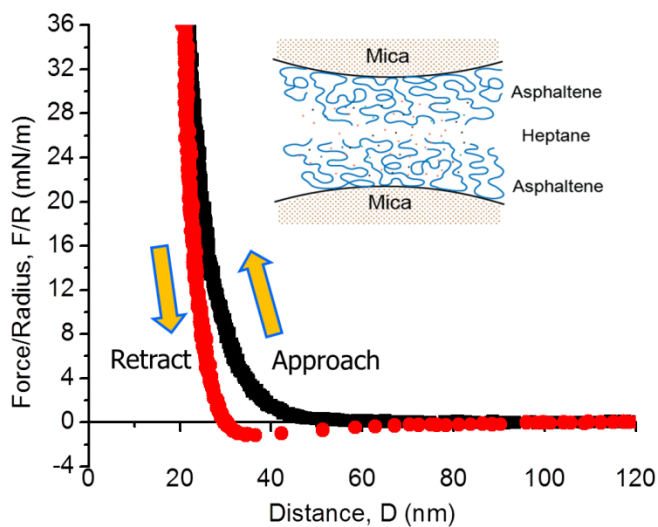
of  $F/R \sim 1$  mN/m and a slightly larger hard wall distance of  $\sim 20.5$  nm were determined, in comparison to  $\sim 16.5$  nm observed at initial approach shown in Figure 3-8a.

The adhesion forces measured between two asphaltene films in heptane are attributed to the van der Waals interactions,<sup>58,59</sup> which are stronger than that in toluene. The current study demonstrates that van der Waals forces are responsible for asphaltene flocculation in paraffinic solvents. Comparing Figure 3-4 and Figure 3-8, one can observe clearly that the hard wall shift after 30 min immersion in solvent is greater for two asphaltene films in toluene (Figure 3-4b) than in heptane (Figure 3-8b). The hard wall distance in the heptane system is  $\sim 20$  nm shorter, suggesting a much less significant swelling of asphaltene molecules in heptane than in toluene. Nevertheless, a small hard wall shift of  $\sim 4$  nm in heptane does indicate some morphology changes of the asphaltene films (limited swelling or molecular rearrangement) upon exposure to heptane. The AFM image of the asphaltene films immersed in heptane for half hour in Figure 3-5c shows many smaller asphaltene aggregates as compared with the initial smooth surface shown in Figure 3-5a. The results from both SFA force measurement and AFM imaging suggest that certain fractions of asphaltenes are able to have limited swelling in heptane, resulting in rearrangement and aggregation of these fractions of asphaltene molecules to minimize the total energy in the heptane system. The interactions between an asphaltene film and a bare mica surface in heptane were

also studied, and similar force profiles and adhesion forces were obtained as in asymmetrical toluene systems.



(a)



(b)

Figure 3-8 Force profiles of two asphaltene films in heptane: (a) force-distance curves measured immediately after heptane injection and (b) force-distance curves measured after ~30 min immersion in heptane.

### **3.3.3 Stability of Water-In-Oil Emulsions.**

Water-in-oil (W/O) emulsions are highly undesirable in petroleum processes as they lead to serious processing problems such as equipment fouling and corrosion and cause significant cost increase due to transportation difficulties and equipment corrosion. The stability of w/o emulsions is directly related to the water-oil interfacial properties.

Strong repulsive forces or the absence of adhesion between emulsified droplets usually corresponds to higher emulsion stability, while a weaker repulsion or a strong adhesion can lead to flocculation and instability of emulsions. The SFA measurements in this study show that asphaltene surfaces swell significantly in toluene, leading to strong steric repulsion. In contrast, asphaltenes show a strong adhesion between asphaltene and hydrophilic mica surfaces in toluene, providing an attractive force between the two surfaces. These findings suggest that fine hydrophilic solid/clay particles are able to aggregate with the asphaltene residues and with each other in toluene. Since asphaltenes are known to be amphiphilic, the asphaltene, and fine particle aggregates would prefer to stay at the water-oil interface, and form a semi rigid interfacial film. The presence of such rigid interfacial films and strong steric repulsion between two asphaltene surfaces lead to a strong energy barrier preventing the water droplets from attaching to each other and coalescing. This is the case of commercial process for the naphtha-based bitumen froth treatment (cleaning) process in the oil sand industry. Because naphtha is a mixture of aromatic and aliphatic/naphthenic hydrocarbons, which is

a relatively good solvent for asphaltenes (no asphaltene precipitation occurs at the industrial dilution ratio), 1-2 wt % residual emulsified water droplets are always present in the final diluted bitumen product. In this study we use the asphaltene films on the mica surface to mimic the stable interfacial film and the mica surfaces to mimic the clay surfaces as shown in Figure 3-9. Such approach has been used in a number of previous studies where a solid substrate supported polymers or surfactants layer was used to mimic the interface between two fluid-like phases/domains.<sup>41,44,60-64</sup> The results of this study provide an insight into the intermolecular interactions of asphaltene-asphaltene and asphaltenes-clay surfaces in organic media of varying solvent quality. To fully understand the stability of water-in-oil emulsions as encountered in heavy oil processing, however, other factors such as naphthenic acid, resins and moisture/water content need to be included. To break this stable w/o emulsion, demulsifiers are needed to eliminate the repulsive forces by destroying the asphaltene films adsorbed on the water surface. This part of discussion will be illustrated in a subsequent paper.

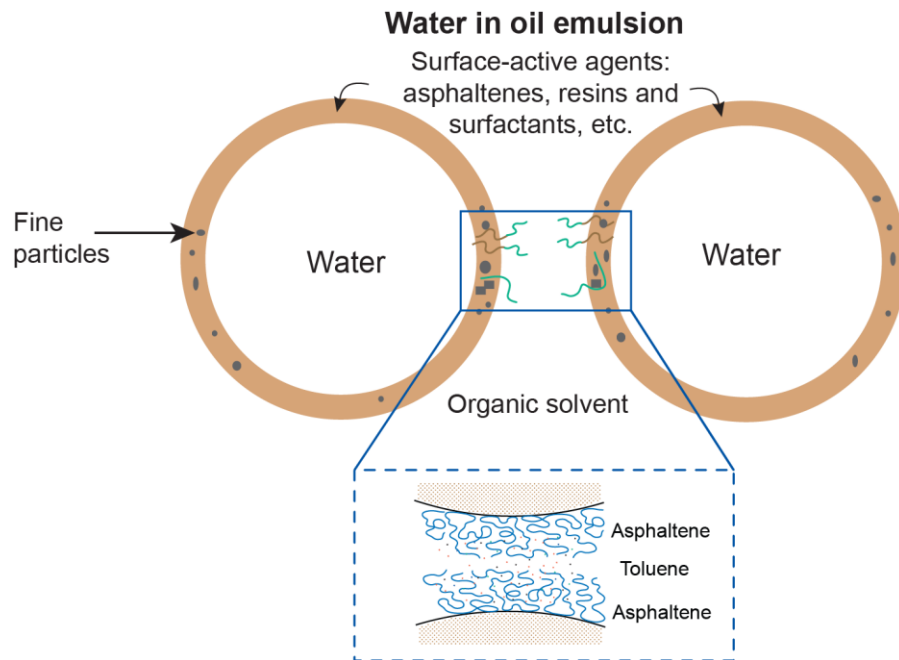


Figure 3-9 Schematic illustration of a rigid interfacial film formed by asphaltenes, resins, fine particles etc., adsorbed at the water/oil interface, preventing water droplets from coalescing and thereby stabilizing the water-in-oil emulsions, which is highly undesirable in petroleum processes.

### 3.4 Conclusion

The forces between coated asphaltene films in toluene and heptane were measured using a SFA. The SFA force measurements allowed a direct evaluation on molecular interactions of asphaltenes in organic solvents, providing insight of molecular aggregation, re-arrangements and swelling of asphaltenes in toluene and heptane. AFM was used to obtain complimentary information on the morphology change of the asphaltene films in organic solvents with time. The results of this study show that the surface interactions of asphaltenes strongly depend on the type of solvent, contact time and load (pressure) applied to the

asphaltene films during the force measurement. Adhesion forces were measured between asphaltene and mica in both toluene and heptane, as well as between two asphaltene films in heptane. Although small adhesion was initially observed for two asphaltene films in toluene, pure repulsion was observed with increasing film incubation time, which was attributed to steric repulsion of swollen asphaltene films. The steric repulsion at short separation distances under high compression forces fits well with the Alexander-de Gennes scaling theory of two interacting polymer brush layers. The deviation of steric repulsion at large separation distances under lower compression forces from the Alexander-de Gennes scaling theory suggests the presence of secondary structures of asphaltenes in good solvent, mostly likely stemming from the polydispersity/complexity of asphaltene molecules/aggregates. The AFM experiments showed significant changes with time, in conformation and morphology of asphaltene films in toluene, which were less significant in heptane, accounting for the observed results from the SFA force measurements. The steric repulsion between asphaltene films in toluene and adhesion force between asphaltene and mica surfaces contribute significantly to the stability of the water-in-oil emulsions encountered in bitumen and crude oil production.

### 3.5 References

1. Mitchell, D. L.; Speight, J. G. *Fuel* 1973, 52, 149-152.
2. Yen, T. F.; Erdman, J. G.; Pollack, S. S. *Anal. Chem.* 1961, 33, 1587-1594.
3. Speight, J. G. *Asphaltenes and Asphalts*, 1; Yen, T. F., Chilingarian, G. V., Eds.; Elsevier Science, Amsterdam, 1994, p 7.
4. Wu, X.; van de Ven, T. G. M.; and Czarnecki, J. *Colloids Surf. A.* 1999, 149, 577-583.
5. Sjöblom, J.; Urbahl, O.; Grete, K.; Børve, N.; Mingyuan, L.; Saeten, J. O.; Christy, A. A.; Gu, T. *Adv. Colloid Interface Sci.* 1992, 41, 241-271.
6. Sjöblom, J.; Mingyuan, L.; Christy, A. A.; Ronningsen, H. P. *Colloids Surf., A* 1995, 96, 261-272.
7. Yarranton, H. W.; Hussein, H.; Masliyah, J. H. *J. Colloid Interface Sci.* 2000, 228, 52-63.
8. Taylor, S. D.; Czarnecki, J.; Masliyah, J. J. *Colloid Interface Sci.* 2002, 252, 149-160.
9. Zhang, L. Y.; Xu, Z.; Masliyah, J. H. *Langmuir* 2003, 19, 9730-9741.
10. Wu, X. *Energy Fuels* 2003, 17, 179-190.
11. Spiecker, P. M.; Kilpatrick, P. K. *Langmuir* 2004, 20, 4022-4032.
12. Zhang, L. Y.; Xu, Z.; Masliyah, J. H. *Ind. Eng. Chem. Res.* 2005, 44, 1160-1174.

13. Abraham, T.; Christendat, D.; Karan, K.; Xu, Z.; Masliyah, J. *Ind. Eng. Chem. Res.* 2002, 41, 2170-2177.
14. Zhang, L. Y.; Lawrence, S.; Xu, Z.; Masliyah, J. H. J. *Colloid Interface Sci.* 2003, 264, 128-140.
15. Horva'th-Szabo', G.; Masliyah, J. H.; Elliott, J. A. W.; Yarranton, H. W.; Czarnecki, J. J. *Colloid Interface Sci.* 2005, 283, 5-17.
16. Friberg, S. E.; Yang, H. F.; Midttun, O.; Sjoblom, J.; Aikens, P. A. *Colloids Surf., A* 1998, 136, 43-49.
17. Yan, N. X.; Masliyah, J. H. J. *Colloid Interface Sci.* 1994, 168, 386-392.
18. Kilpatrick, P. K.; Spiecker, P. M. Asphaltene Emulsions. In *Encyclopaedic Handbook of Emulsion Technology*; Sjoblom, J., Ed.; Marcel Dekker: New York, 2001.
19. Sjoblom, J.; Johnsen, E. E.; Westvik, A.; Ese, M. H.; Djuve, J.; Auflem, I. H.; Kallevik, H. Demulsifiers in the oil industry. In *Encyclopaedic Handbook of Emulsion Technology*; Sjoblom, J., Ed.; Marcel Dekker: New York, 2001.
20. McLean, J. D.; Kilpatrick, P. K. *J. Colloid Interface Sci.* 1997, 189, 242-253.
21. Czarnecki, J.; Moran, K. *Energy Fuels* 2005, 19, 2074-2079.
22. Czarnecki, J. *Energy & Fuels* 2009, 23, 1253-1257.
23. Yeung, A.; Dabros, T.; Czarnecki, J.; Masliyah, J. *Proc. R. Soc. London. A.* 1999, 455, 3709-3723.

24. Tsamantakis, C.; Masliyah, J.; Yeung, A.; Gentzis, T. J. *Colloid Interface Sci.* 2005, 284, 176-183.
25. Zhang, L. Y.; Lawrence, S.; Xu, Z.; Masliyah, J. H. J. *Colloid Interface Sci.* 2003, 264, 128-140.
26. Zhang, L. Y.; Breen, P.; Xu, Z.; Masliyah, J. H. *Energy Fuels* 2007, 21, 274-285.
27. Nordgård, E. L.; Sørland, G.; Sjöblom, J. *Langmuir* 2010, 26, 2352-2360.
28. Aston, D. E.; Berg, J. C. J. *Pulp Pap. Sci.* 1998, 24, 121-125.
29. Hartley, P. G.; Grieser, F.; Mulvaney, P.; Stevens, G. W. *Langmuir* 1999, 15, 7282-7289.
30. Mulvaney, P.; Perera, J. M.; Biggs, S.; Grieser, F.; Stevens, G. W. J. *Colloid Interface Sci.* 1996, 183, 614-616.
31. Snyder, B. A.; Aston, D. E.; Berg, J. C. *Langmuir* 1997, 13, 590-593.
32. Drummond, C.; Israelachvili, J. J. *J. Pet. Sci. Eng.* 2004, 45, 61-81.
33. Wu, X.; Czarnecki, J.; Hamza, N.; Masliyah, J. *Langmuir* 1999, 15, 5244-5250.
34. Wu, X.; Dabros, T.; Czarnecki, J. *Langmuir* 1999, 15, 8706-8713.
35. Christenson, H. K.; Israelachvili, J. N. *J. Colloid Interface Sci.* 1987, 119, 194-202.
36. Liu, J. J.; Xu, Z. H.; Masliyah, J. *Langmuir* 2003, 19, 3911-3920.
37. Liu, J. J.; Xu, Z. H.; Masliyah, J. *AIChE J.* 2004, 50, 1917-1927.
38. Liu, J. J.; Xu, Z. H.; Masliyah, J. *Can. J. Chem. Eng.* 2004, 82, 655-666.

39. Liu, J. J.; Xu, Z. H.; Masliyah, J. *Colloids Surf., A* 2005, 260, 217–228.
40. Li, H.; Long, J.; Xu, Z.; Masliyah, J. H. *Energy Fuels* 2005, 19, 936–943.
41. Liu, J. J.; Zhang, L. Y.; Xu, Z. H.; Masliyah, J. *Langmuir* 2006, 22, 1485–1492.
42. Wang, S.; Liu, J.; Zhang, L.; Xu, Z.; Masliyah, J. *Energy Fuels* 2009, 23, 862-869.
43. Wang, S.; Liu, J.; Zhang, L.; Xu, Z.; Masliyah, J. *Langmuir* 2010, 26, 183-190.
44. Vuillaume, K.; Giasson, S. J. *Phys. Chem. C* 2009, 113, 3660-3665.
45. Israelachvili, J.; Min, Y.; Akbulut, M.; Alig, A.; Carver, G.; Greene, W.; Kristiansen, K.; Meyer, E.; Pesika, N.; Rosenberg, k.; Zeng, H. *Rep. Prog. Phys.* 2010, 73, 036601, 1-16.
46. Israelachvili, J. N. *Intermolecular and Surface Forces*, 2nd ed.; Academic Press: New York, 1991; p 291.
47. Akbulut, M.; Alig, A. R. G.; Min, Y.; Belman, N.; Reynolds, M.; Golan, Y.; Israelachvili, J. *Langmuir* 2007, 23, 3961-3969.
48. Israelachvili, J. N. *J. Colloid Interface Sci.* 1973, 44, 259-272.
49. Zeng, H.; Tian, Y.; Zhao, B.; Tirrell, M.; Israelachvili, J. *Macromolecules* 2007, 40, 8409-8422.
50. Degennes, P. G. *Adv. Colloid Interface Sci.* 1987, 27, 189-209.
51. Kuhl, T. L.; Leckband, D. E.; Lasic, D. D.; Israelachvili, J. N. *Biophys. J.* 1994, 66, 1479-1488.

52. Efremora, N. V.; Bondurant, B.; O'Brien, D. F.; Leckband, D. E. *Biochemistry* 2000, 39, 3441-3451.
53. Butt, H. J.; Kappl, M.; Mueller, H.; Raiteri, R.; Meyer, W.; Ruhe, J. *Langmuir* 1999, 15, 2559-2565.
54. Kamiyana, Y.; Israelachvili, J. *Macromolecules* 1992, 25, 5081-5088.
55. Mostowfi, F.; Indo, K.; Mullins, O. C.; McFarlane, R. *Energy Fuels*, 2009, 23, 1194-1200.
56. Masliyah, J. H.; Bhattacharjee, S. *Electrokinetics and Colloid Transport Phenomena*; John Wiley & Sons: New York, 2006.
57. Fotland, P.; Askvik, K. M. *Colloids Surf. A* 2008, 324, 22-27.
58. Stachowiak, C.; Viguie, J. R.; Grolier, J. P. E.; Rogalski, M. *Langmuir* 2005, 21, 4824-4829.
59. Takanohashi, T.; Sato, S.; Saito, I.; Tanaka, R. *Energy Fuels* 2003, 17, 135-139.
60. Anderson, T. H.; Donaldson, S. H.; Zeng, H.; Israelachvili, J. N. *Langmuir*, 2010, 26, 14458-14465.
61. Hwang, D. S.; Zeng, H.; Masic, A.; Harrington, M. J.; Israelachvili, J. N.; Waite, J. H. *J. Biol. Chem.* 2010, 285, 25850-25858.
62. Hwang, D. S.; Zeng, H.; Srivastava, A.; Krogstad, D. V.; Tirrell, M.; Israelachvili, J. N.; Waite, J. H. *Soft Matter* 2010, 6, 3232-3236.
63. Zeng, H.; Hwang, D. S.; Israelachvili, J. N.; Waite, J. H.; *Proc. Natl. Acad. Sci. U.S.A.* 2010, 107, 12850-12853.

64. Blomberg, E.; Claesson, P. M.; Warnheim, T. *Colloids Surf. A* 1999, 159, 149-157.

## Chapter 4

# Understanding Mechanisms of Asphaltene Adsorption from Organic Solvent on Mica<sup>b</sup>

In chapter 3 we discussed the interactions between asphaltene-asphaltene surfaces coated on mica (water droplet or solid) in organic solvent. In this chapter we study the interactions between asphaltene from the bulk solution and mica surface. The force measurements are carried out with increasing adsorption time. This study will enhance our understanding about the adsorption mechanisms of asphaltenes on hydrophilic surfaces. A brief summary of the problem is described below.

### 4.1 Introduction

Interfacial phenomena govern the properties of solids, liquids and gases in pharmaceuticals, food products, cosmetics, and petroleum processing, to name a few. From interfacial studies, one can determine the fundamental mechanisms and kinetics of film formation, surfactant adsorption, and film rupture that ultimately govern the behaviour of dispersion systems. Of extreme importance in the petroleum industry is the formation of stable water-in-oil (w/o) emulsions that result from the adsorption of bituminous compounds at an oil-water interface. The interactions and assembly of adsorbed molecules or their aggregates lead to

---

<sup>b</sup> A version of this chapter has been submitted for publication: Natarajan, A; Kuznicki, N.; Harbottle, D.; Zeng, H.; Xu, Z. *Langmuir* **2014**, submitted.

formation of a protective layer that resists droplet-droplet coalescence.<sup>1-9</sup> Stable emulsions have been a major challenge in petroleum production, affecting process throughput and downstream operations such as upgrading. It is necessary to develop knowledge on the formation of these protective layers to design suitable protocols for film disruption and prevention of stable emulsion formation.

Polyaromatic asphaltene containing a significant fraction of heteroatoms such as oxygen, nitrogen and sulphur are commonly considered the problematic component of crude oil and bitumen. They readily partition at the liquid-liquid and solid-liquid interfaces. The complex nature of asphaltene molecules makes it difficult to define their molecular structures. As a result asphaltenes are poorly defined as a solubility class material that is soluble in toluene but insoluble in alkanes such as *n*-heptane.<sup>10,11</sup> Due to the presence of heteroatoms, asphaltenes are partially polar, and have a tendency to adsorb at the oil-water and oil-solid interface.

The adsorption of asphaltene on solids such as pipelines and clay particles create added processing difficulties. While pipeline deposition can lead to pipe plugging, adsorption onto clay solids modifies their wettability, decreasing efficiency of oil liberation from the solids and increasing solids partitioning at the oil-water interface.<sup>12-15</sup> In oil production, the formation of a complex multiphase dispersion layer in the middle of oil-water separation vessel, known as rag layers, is frequently encountered.<sup>16</sup> The rag layers are extremely stable multiemulsions with

the stabilizing species identified as surfactants, asphaltenes and fine particles. The fines fraction is predominantly iron-containing solids that readily associate with organic compounds such as asphaltenes to form biwettable solids which preferentially stabilize w/o emulsions. The presence of this highly viscous rag layer with medium density prevents the separation of emulsified water from oil or vice versa.

Adsorption of asphaltenes on mineral surfaces has commonly been studied by quantitatively determining the amount of asphaltene adsorbed using i) solution depletion method,<sup>17,18</sup> ii) quartz crystal microbalance,<sup>19,20</sup> iii) photothermal surface deformation spectroscopy<sup>21</sup> and iv) thermal gravimetric method, or qualitatively by contact angle measurements.<sup>14,15</sup> In all of these studies, asphaltenes are extracted from crude oils and solubilised in mixtures of toluene and *n*-alkanes. According to Buckley,<sup>22</sup> the driving force for asphaltene adsorption on inorganic solids in the absence of water is mainly through polar interactions between oil and a solid, which leads to surface precipitation of asphaltenes.

Determining the organization of asphaltenes at a solid-liquid interface has been the subject of numerous studies generally involving determination of adsorption isotherms. Several authors have reported Langmuir-type adsorption isotherms, indicating the formation of a monolayer of asphaltenes at the toluene-quartz interface.<sup>15,23</sup> Whereas, others have found stepwise or linear increase in

adsorption, suggesting a multilayer adsorption process, for example, toluene to glass, and toluene to quartz/dolomite/kaolin/calcite.<sup>21,24,25</sup> Ellipsometry studies confirmed the presence of multilayer asphaltene adsorbed on solids.<sup>26</sup> Acevedo et al.<sup>21,27</sup> suggested that a weakly aromatic asphaltene that is stable in its crude oil would form a single layer whereas a strongly aromatic asphaltene, which exhibits a tendency to precipitate, would form a multilayer.

The kinetic aspect of asphaltene adsorption on metal surfaces has also been studied. With quartz crystal microbalance measurements, Xie and Karan<sup>28</sup> showed that the initial asphaltene adsorption process on gold surface is controlled by the diffusion of asphaltene from the bulk solution to the substrate surface. The equilibrium state is then reached only after an extended adsorption period, which can be as long as several days, as also observed by Acevedo et al.<sup>27</sup> Using solution depletion method, Goual et al.<sup>20</sup> determined two distinct regimes of asphaltene adsorption on silica surface as a function of asphaltene concentration: at low bitumen concentration, the system did not reach a steady-state of adsorption because the adsorbed amount of asphaltene was still increasing linearly even after 8 h of adsorption; whereas at high bitumen concentration a steady-state of adsorption was reached after just few min (<2 min). The authors proposed that the transition between these two regimes could be due to the stabilization of asphaltene by increased amount of resins at high bitumen concentrations, better solubilisation of asphaltene would prevent any further adsorption.

The above research provided valuable information on stabilization mechanisms and adsorption kinetics of asphaltenes. Due to the complexity of asphaltene molecules and limitations of the techniques described, probing molecular mechanisms of asphaltene adsorption on inorganic solid surfaces from organic solvents and subsequent association remains rather limited.

In a previous study,<sup>12</sup> we measured the interactions between asphaltene-asphaltene surfaces in toluene and heptane using a surface forces apparatus (SFA). Strong steric repulsion was observed between asphaltene surfaces which are responsible for preventing water droplets from coalescing and leading to a stable emulsion. In the present study, we investigate the adsorption mechanisms of asphaltenes (from bulk solution) to hydrophilic solid surface and the associated molecular interactions.

Due to its unique ability to measure simultaneously the interaction force,  $F$ , as a function of the absolute surface separation,  $D$ , and the local geometry of two interacting surfaces (the local radius  $R$  or contact area) at a force sensitivity of  $<10$  nN and an absolute distance resolution of  $\sim 0.1$  nm *in situ* and in real time, SFA has been extensively used in studying governing forces of many biological and non-biological systems.<sup>29</sup> SFA is one of the most powerful techniques for the research objective of this study. The force-distance curves or so-called force profiles obtained from SFA measurements could provide important information on build-up kinetics of adsorbed layers via film thickness measurement and

properties of adsorbed layers such as asphaltene-solvent interfacial energy and molecular conformation changes of the adsorbed asphaltene layers.

## **4.2 Materials and Experimental Methods**

Vacuum distillation feed bitumen was provided by Syncrude Canada Ltd., Alberta, Canada. Asphaltenes were precipitated from bitumen by adding 40 times of n-heptane to bitumen by volume. Details on asphaltene precipitation were reported elsewhere.<sup>30</sup> Asphaltene solutions were prepared using as received High-Performance Liquid Chromatography (HPLC)-grade toluene (Fisher). Solutions were prepared fresh prior to each measurement and mildly sonicated for 15 min. Muscovite mica sheets were purchased from S & J Trading Inc. (Glen Oaks, NY).

## **4.3 Sample Preparation**

Muscovite mica can be easily cleaved to obtain large atomically smooth surfaces whose exposed aluminosilicate lattice is similar to quartz and many clay surfaces. In that way, a clean reproducible substrate can be obtained. A thin layer ( $\sim 500 \text{ \AA}$ ) of silver was coated at the back side of the mica surface. With the silver face down, the mica was glued to cylindrically shaped silica glasses before loading it in the SFA chamber. For the SFA experiments, a desired asphaltene solution was injected to fill the gap between two closely placed mica surfaces in the SFA chamber. The chamber was sealed and saturated with the vapor of the same solvent.

#### 4.4 Surface Forces Measurements

The SFA<sup>31</sup> is an ideal technique for exploring the adsorption kinetics and interactions between asphaltene layers.<sup>12,32</sup> During the force measurements, if the surface separation  $D$  is much smaller than local radius of curvature  $R$ , the surface interaction of the crossed-cylinder configuration in SFA is equivalent to that between a sphere of the same radius and a flat surface.<sup>33</sup> The surface separation and deformation is monitored in real time and in situ by Multiple Beam Interferometry (MBI) using Fringes of Equal Chromatic Order (FECO).<sup>34</sup> The interaction forces are determined by probing the deflection of the force-measuring springs. The interaction force  $F(D)$  between two crossed-cylinder surfaces can be correlated to the interaction energy per unit area of two flat surfaces,  $W(D)$ , based on the Derjaguin approximation.<sup>33,35,36</sup>

$$F(D) = 2\pi RW(D) \quad (4-1)$$

The adhesion energy per unit area between two surfaces of the same materials,  $W_{ad}$ , can be determined from the pull-off force,  $F_{ad}$  (the force required to separate the surfaces from adhesive contact), given by:<sup>33,35,37</sup>

$$W_{ad} = 2\gamma = F_{ad}/1.5\pi R \quad (4-2)$$

In this study, the reference distance ( $D = 0$ ) was set as the adhesive contact between the two bare mica surfaces in air prior to injecting the asphaltene solution between the surfaces. During a typical force measurement, the normal force-distance profile ( $F$  vs.  $D$ ) was obtained by an initial approach to a “hard wall” or “confined layer thickness” followed by separation of the two surfaces (note: the “hard wall” distance or the “confined layer thickness” in this study is defined as the mica-mica separation distance or thickness of confined asphaltenes which barely changed with increasing the normal load or pressure).

#### **4.4.1 AFM Imaging.**

AFM topographical images of the sample surfaces were obtained using an Agilent 5500 Molecular Imaging Microscope (Agilent Technologies, Inc., Chandler, AZ) under AAC mode in air, to observe changes in surface structure, surface coverage, approximate layer thickness and aggregate size of adsorbed asphaltenes. Silicon nitrate cantilevers (RTESP, Veeco, Santa Barbara, CA) were used in the AFM experiments with a nominal resonance frequency of 300-350 kHz, and the amplitude set point was normally set at 95% - 98% of the free amplitude in order to avoid surface damage.

## **4.5 Results and Discussion**

The surface force measurements between two mica surfaces in asphaltene solution using SFA provided information on the adsorption and built-up of asphaltenes on mica. The typical experimental configuration and adsorption process of

asphaltenes on mica are shown in Figure 4-1. Figure 4-1a shows asphaltene solution confined between two bare mica surfaces. Figure 4-1b shows the evolution of the adsorption and accumulation of asphaltenes on mica to form a layer.

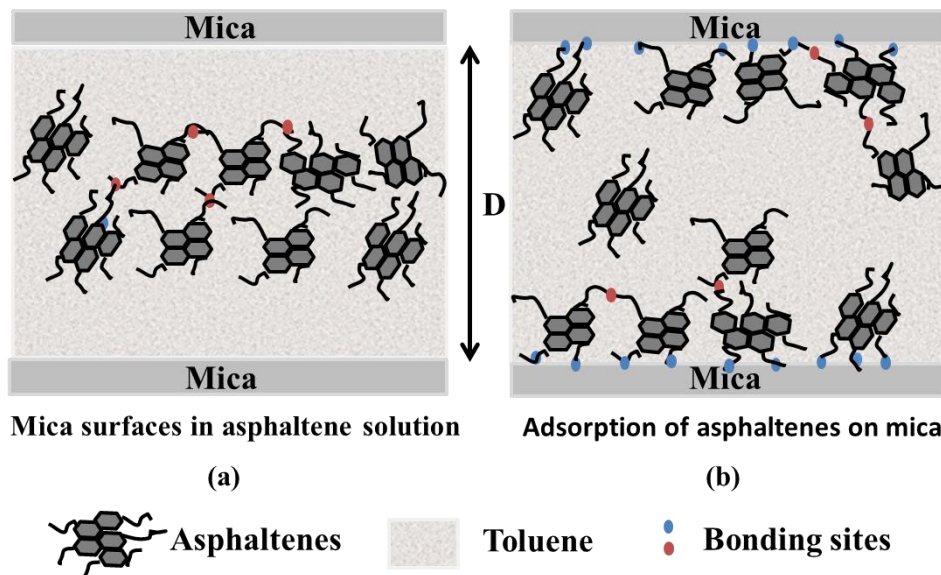
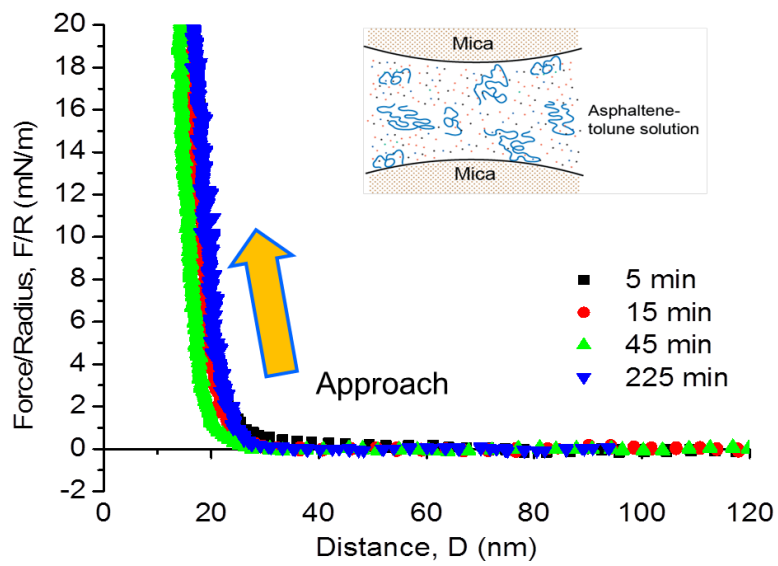


Figure 4-1 Experimental configuration and illustration of the adsorption process of asphaltenes onto mica in organic solvent: (a) mica surfaces in asphaltene solution, and (b) asphaltene layers gradually built up on mica associated with the adsorption.

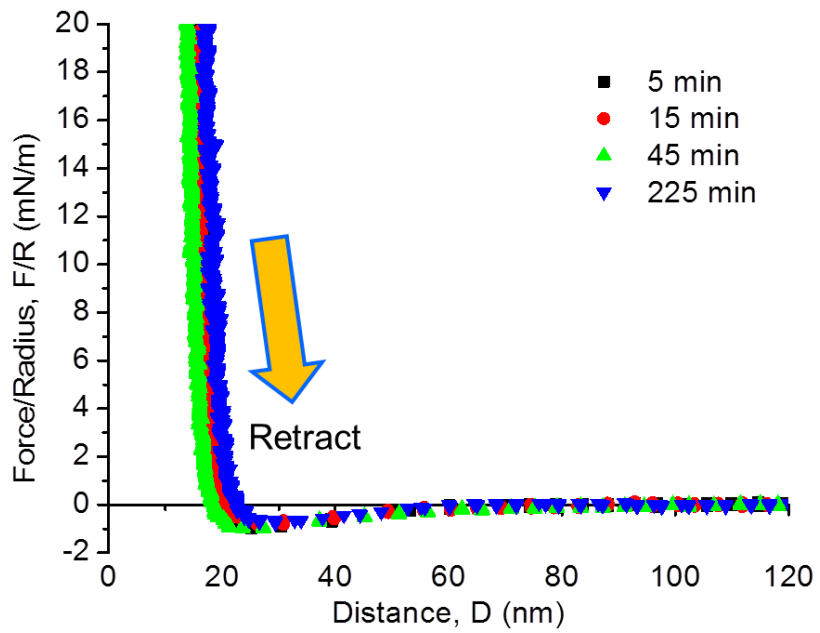
#### 4.5.1 Adsorption of Asphaltenes on Mica

Figure 4-2 shows the typical force-distance curves between two mica surfaces in 0.01 wt% [(a-In) & 1(a-Out)], 0.1 wt% [(b-In) & (b-Out)] and 1 wt% [(c-In) & (c-Out)] asphaltene solutions at different adsorption time, measured during approach (In) and separation (Out), respectively. The two surfaces were brought closer until the confined layer thickness barely changed with the increased normal load. The thickness of the adsorbed asphaltene layer on mica (T) was determined as half of

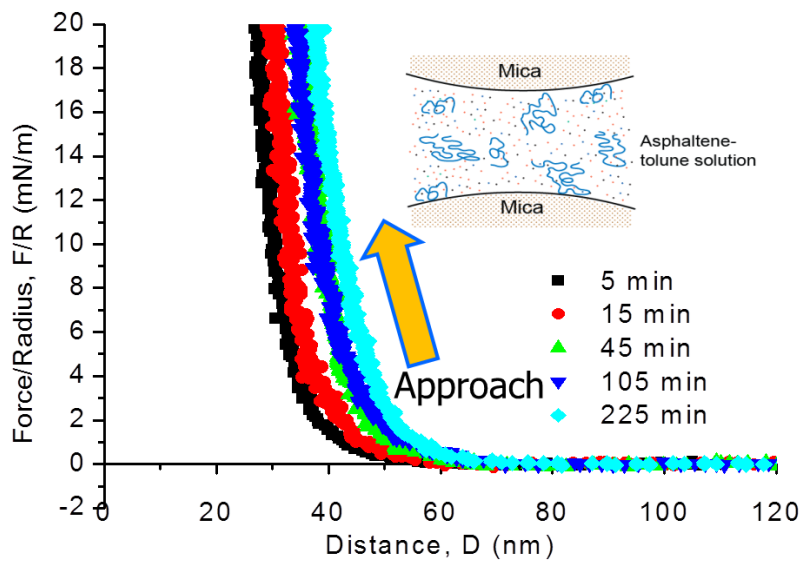
the confined layer thickness measured between the surfaces, i.e.,  $T = \frac{1}{2} D$ . The thickness of the asphaltene layers at different concentrations and time intervals were determined.



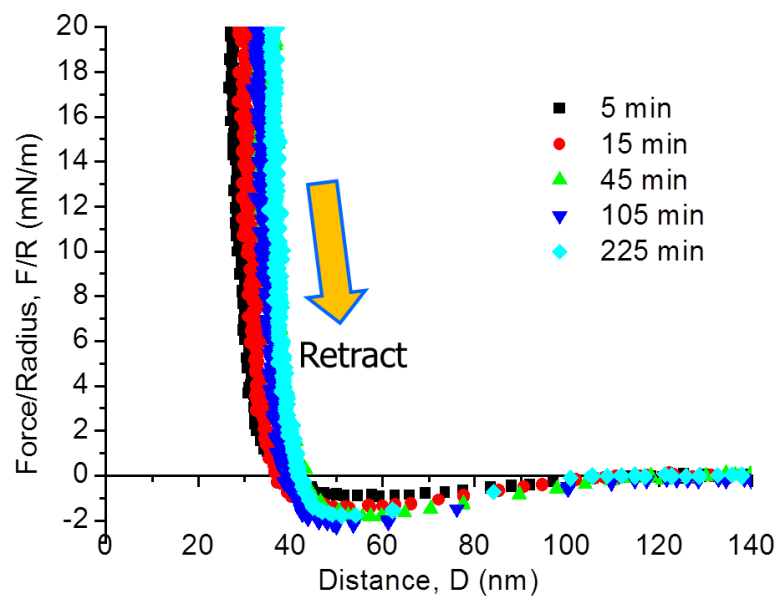
(a-In)



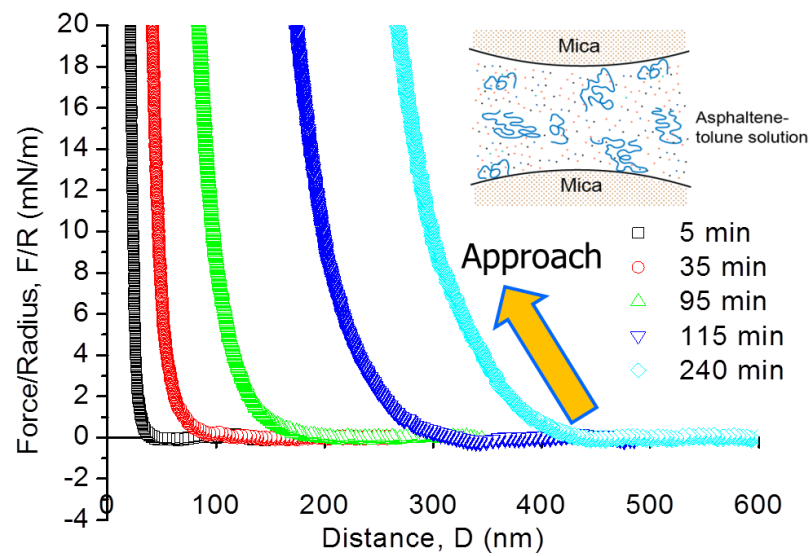
(a-Out)



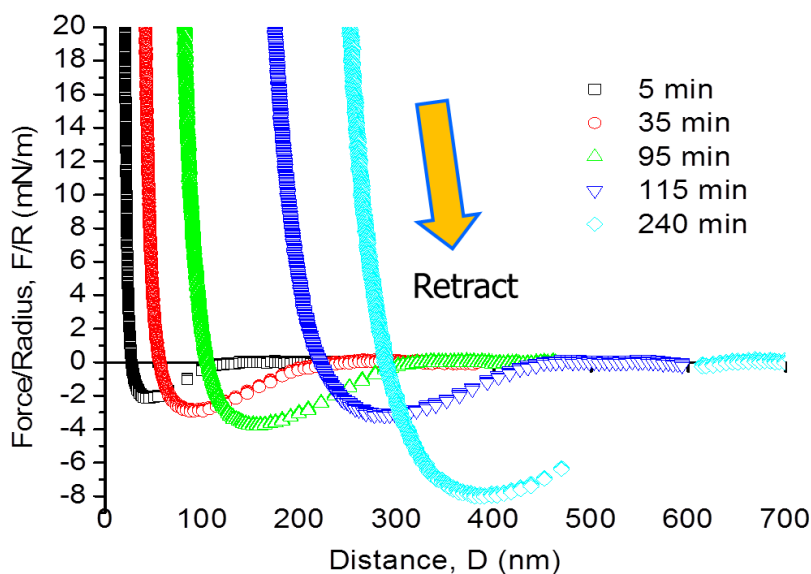
(b-In)



(b-Out)



(c-In)



(c-Out)

Figure 4-2 Approach and separation force-distance profiles of two mica surfaces in asphaltene-toluene solutions of different concentrations and at different time intervals: (a) 0.01 wt %, (b) 0.1 wt%, and (c) 1.0 wt% asphaltenes in toluene. The reference distance ( $D = 0$ ) was set as the adhesive contact between the two bare mica surfaces in air prior to injecting the asphaltene solution between the surfaces. In this figure, “Approach” indicates bringing the two surfaces close together and “Retract” indicates separation of the two surfaces.

Figure 4-2(a) shows the force-distance profile between two mica surfaces approaching each other in 0.01 wt% asphaltene solution. On approach after 5-min adsorption, there is a strong repulsion below  $\sim 10$ - $20$  nm separation. With increasing the normal load the confined layer is compressed to  $\sim 12$  nm which corresponds to an adsorbed layer thickness of  $\sim 6$  nm asphaltene layers on each mica surface and is in good agreement with the previously reported values.<sup>12,38,39</sup>

A slight increase in the thickness of confined asphaltene layer (as well as the

adsorbed asphaltene layer on mica) from ~12 nm to ~16 nm was observed as the adsorption time increased from 5 min to ~4 hr. Upon separation, an attraction of  $F_{ad}/R \sim -0.9 \text{ mN/m}$  ( $W_{ad} = 0.19 \text{ mJ/m}^2$ ), was detected. The adhesion did not vary significantly with increasing adsorption time. The repulsion measured during approach is attributed to steric interaction. The steep increase of repulsive force over a short range indicates that the adsorbed asphaltene layers were loosely packed and compressible. The attraction measured during the separation was due to the bridging interaction as a result of interdigitation of the confined asphaltenes between the two mica surfaces. It has been reported that asphaltenes tend to form nano-aggregates, even in a good solvent (e.g., toluene).<sup>40,41</sup> Though the present concentration is very low, under compression, the loosely adsorbed asphaltenes are likely to interdigitate, resulting in bridging attraction.

Increasing the solution concentration to 0.1 wt% and 1.0 wt%, the build-up of asphaltene layers becomes much faster with a significant increase in the confined layer thickness to ~100 nm within ~1.5 hours of adsorption in 1.0 wt% asphaltene in toluene solutions. It is also interesting to note that the repulsive forces become much longer ranged, with a corresponding increase in the confined layer thickness with increasing adsorption time. Such an effect is evident for the 1.0 wt% solution case shown in Figure 4-2(c), indicating a more compressible adsorbed asphaltene layer. The increase in the confined layer thickness suggests the build-up of 3-D structures of adsorbed asphaltenes on mica surfaces. Although the repulsion is experienced at a much larger separation distance with increasing asphaltene

concentration and adsorption time, the decay of the repulsion with decreasing the separation distance appears to be more or less the same, indicating the same nature of the steric repulsion.<sup>12</sup> This repulsive force rises more steeply at smaller separations once the layers become more compressed, indicating the dominate effect of the excluded volume.<sup>33</sup> In addition, during separation, we observe progressively increasing adhesive bridging forces with increasing asphaltene concentration and adsorption time, as well as at a given asphaltene solution concentration and adsorption time, as shown in Figure 4-2 (a-Out), (b-Out) and (c-out). All the separation force profiles show that the asphaltene layers were stretched before the two surfaces detached from each other. The above results indicate several aspects of the adsorption mechanism of asphaltenes on mica. First the asphaltenes exhibit a strong affinity to mica as such that the bridging force between two mica surfaces due to interdigitation of the adsorbed asphaltenes could be realized. Second, the adsorption of asphaltenes is a strong function of solution concentration of asphaltenes and adsorption time. Third the adsorbed layers of asphaltenes are soft and compressible under normal load, but with dangling branches to cause long range steric repulsion and high compressibility of the asphaltene layers.

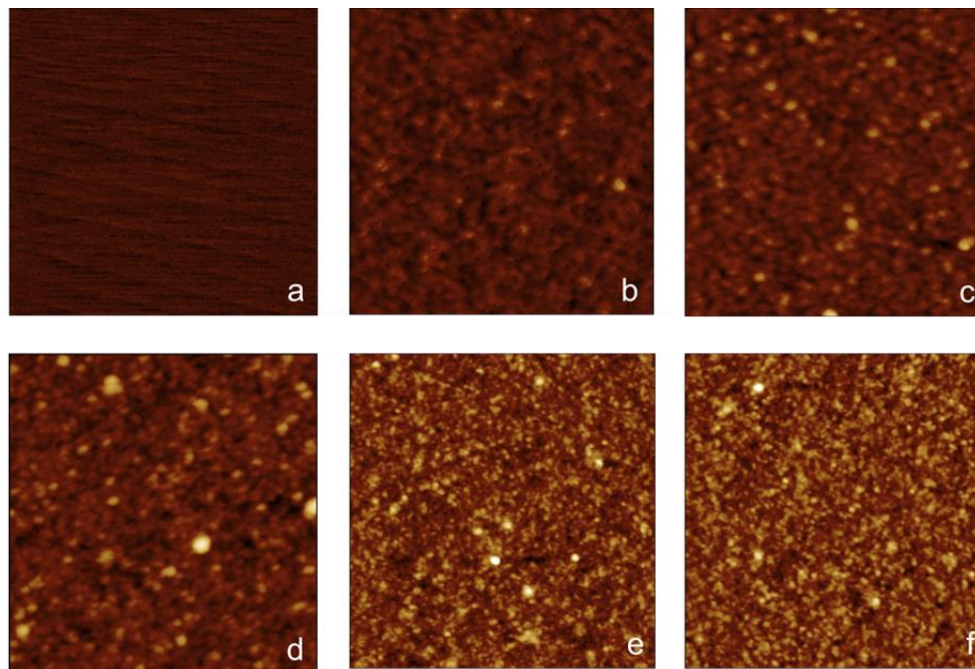


Figure 4-3 AFM images in air for (a) bare mica surface, and asphaltene layer adsorbed on mica surface for (b) 5 min, (c) 15 min, (d) 45 min, (e) 105 min and (f) 225 min immersion time in 0.1 wt% asphaltene-toluene solution. Note that the surfaces were gently dried with nitrogen before imaging. Image size:  $1\mu\text{m} \times 1\mu\text{m}$ .

Figure 4-3 shows the typical AFM images of mica and asphaltene films adsorbed on mica from asphaltene in toluene solutions. Freshly cleaved mica was submerged in 0.1 wt% asphaltene in toluene solution for different periods of times and then dried with blowing nitrogen before imaging. The root-mean-square (RMS) roughness of surfaces increased from 0.2 nm to about  $\sim 1$  nm (Figure 4-3(a) to (f)) in about  $\sim 4$  hours. The increase in surface roughness with increasing immersion (adsorption) time suggests that the asphaltene film is built up by nanoaggregation of asphaltene molecules. The topography of the adsorbed

asphaltene films exhibits heterogeneous nature. Similar heterogeneous patterns were observed for Langmuir-Blodgett deposited asphaltene films by others.<sup>32,42</sup>

Our results show that during separation, adhesive bridging forces dominate for all the cases at small distances, exhibiting an adhesive well at ‘contact’ (seen in Figure 4-2 (a-Out), (b-Out) and (c-Out)). The depth of the adhesive well is  $F_{ad}/R \approx -1$  mN/m (in Figure 4-2 (b-Out) at 5 min), which corresponds to an adhesion energy in the order of  $W_{ad} = F_{ad}/1.5\pi R \approx 0.21$  mJ/m<sup>2</sup>. The force curve at 5 min adsorption time at 0.1 wt% concentration has similar values to our previously reported confined layer thickness (~30 nm), repulsion range (~30 to 60 nm), and adhesion energy (0.2 mJ/m<sup>2</sup>) of two asphaltene films right after immersed in toluene (within ~5 min).<sup>12</sup> This validates the consistency in our measurements. Figure 4-4 shows that the adhesion energy increases steadily with increasing adsorption time for all concentrations, more significantly at higher asphaltene concentrations. The time and concentration dependent increase in the adhesion is due to an increased interdigitation of adsorbed asphaltene molecules across the interface, which increases the contact area of molecules from two interacting surfaces with increasing adsorption time. This type of effect is often seen in polymer and surfactant systems.<sup>33</sup>

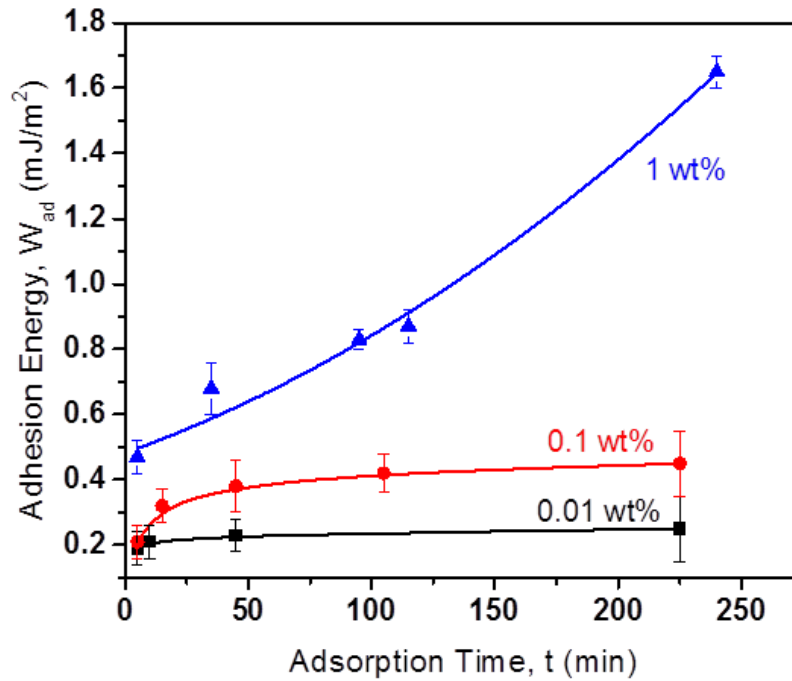


Figure 4-4 Adhesion energy  $W_{ad}$  between mica surfaces in different concentrations of asphaltene in toluene solution as a function of adsorption time at room temperature.

To determine the controlling mechanism of asphaltene adsorption from their toluene solutions, the thickness of confined asphaltene layers was plotted as a function of square root of time, as shown in Figure 4-5. The results in Figure 4-5 show that the confined layer thickness follows a linear relationship with the square root of adsorption time. For higher concentrations (0.1 wt% and 1 wt%) the confined layer thickness does not follow a linear relationship as well as the 0.01 wt% case. The increase in the range of repulsion observed from the force profiles above is mainly attributed to the compressibility of the adsorbed (loosely packed and patchy) asphaltene layers, which is pronounced at higher concentrations.

Figure 4-2 (a-In), (b-In) and (c-In) show that the confined layer thickness increases with increasing adsorption time for all the cases of different asphaltene concentrations and the increment is more pronounced at higher concentrations. The force-distance profiles measured at higher asphaltene concentrations suggest the formation of asphaltene aggregates. Therefore, we focus our discussions only on the case of lowest asphaltene concentration (i.e., 0.01 wt%) where the compressibility effect and the aggregation is minimum. Thus, for our experimental conditions, asphaltene adsorption from its lowest concentration solution, where layer compressibility was assumed to be negligible, is controlled by the diffusion of asphaltene molecules from the bulk solution to the substrate.

According to Ward and Tordai,<sup>43</sup> the initial rate of change of surface mass density is a linear function of the inverse of the square root of time, as given by:

$$\frac{d(\Gamma)}{dt} = C \left( \frac{D^*}{\pi t} \right)^{1/2} \quad (4-3)$$

where  $C$  is the concentration of species in the bulk solution,  $\Gamma$  is the adsorbed mass density,  $D^*$  is the diffusion coefficient, and  $t$  is time. The concentration of the species accumulated at the interface at any time is obtained by integrating the above equation. The apparent diffusion coefficient may be calculated from the initial slopes,  $S$ , of  $\Delta\Gamma / \Delta\Gamma_0$  versus  $\sqrt{t}$  curves, according to:<sup>44</sup>

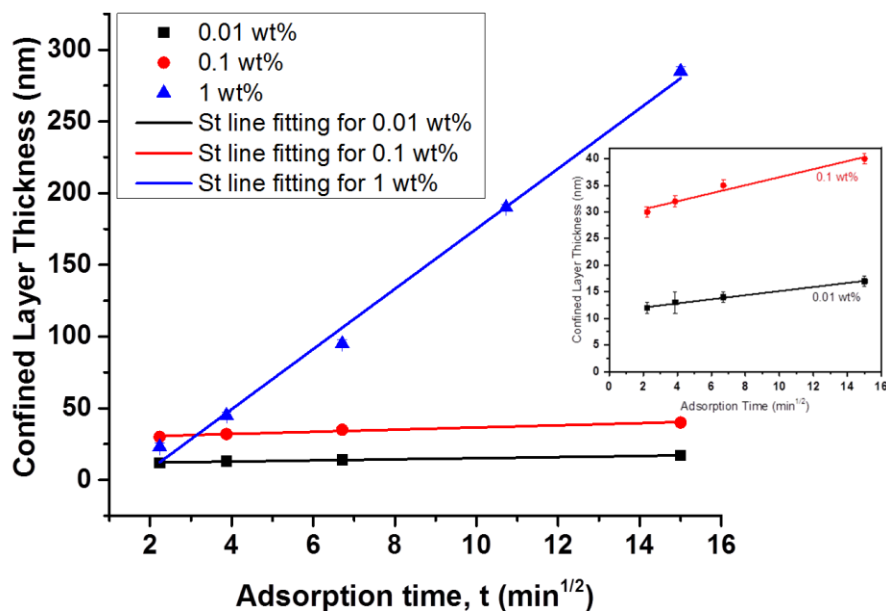
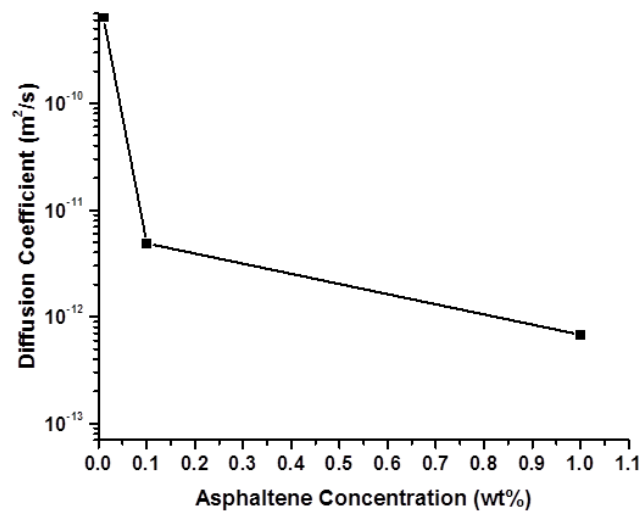


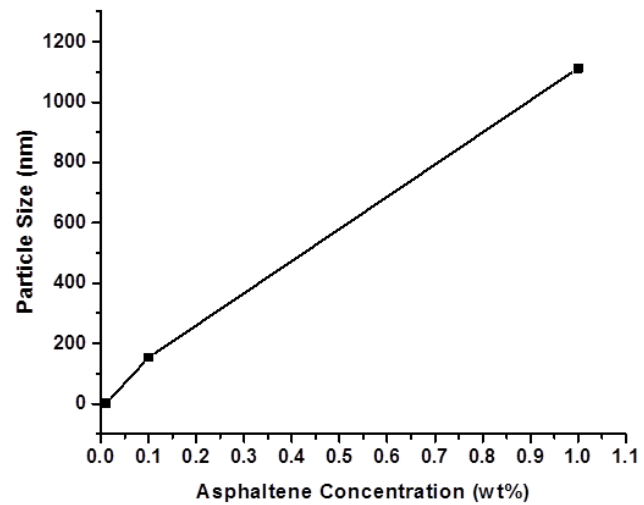
Figure 4-5 Confined layer thickness plotted as a function of square root of adsorption time for the three different concentrations of asphaltene-toluene solution (wt %). Insert: Expanded plots for the 0.01 wt% and 0.1 wt% asphaltene-toluene solution. Note: Only 0.01 wt% follows a perfectly linear relationship with square root of adsorption time.

$$S = 2C \left( \frac{D^*}{\pi} \right)^{1/2} \quad (4-4)$$

The estimated asphaltene diffusion coefficient for the lowest concentration is on the order of  $10^{-10} \text{ m}^2/\text{s}$ . Ostlund et al.<sup>45</sup> have reported diffusion coefficients of asphaltenes in toluene solutions to be on the order of  $10^{-10} \text{ m}^2/\text{s}$ , which is in good agreement with the current study. Figure 4-6A shows asphaltene diffusion coefficient for the different concentrations.



**A**



**B**

Figure 4-6 Asphaltene (A) diffusion coefficient and (B) particle size, as a function of concentration (wt%).

Assuming asphaltenes are spherical in shape, the apparent particle size can be calculated from the Stokes-Einstein equation:<sup>46</sup>

$$D^* = \frac{K_B T}{3\pi\mu d_0} \quad (4-5)$$

where  $D^*$  is the diffusion coefficient of the particles,  $d_0$  is the particle diameter,  $\mu$  is the solvent viscosity, and  $k_B$  is the Boltzmann's constant. At 0.01 wt% asphaltene concentration in toluene, the particle diameter is calculated to be ~1 nm (radius ~0.5 nm). Figure 4-6B shows the asphaltene particle size as a function of concentration. Comparing Figure 4-6A and B we can observe that as the diffusion coefficient decreases with increasing concentration, the particle size increases with increasing concentration. Asphaltene molecular size at 0.01 wt% suggests that asphaltenes are present at very low concentrations as single molecules or nanoaggregates. The bigger particle size for 0.1 wt% and 1 wt% asphaltene concentration indicates that asphaltenes exist as aggregates. For example, from Figure 4-2 b-In and c-In, we can observe that even at 225 min adsorption time the confined layer thickness is only around 35 nm and 270 nm respectively. However, our calculated size for the 0.1 wt% and 1 wt% suggest larger aggregates of 150 nm and 1.1  $\mu\text{m}$  respectively. Therefore, the calculated aggregate sizes do not agree with our SFA force measurements. From Figure 4-5 it is observed that the higher concentrations of asphaltene in toluene solution do not follow a linear relationship with the square root of adsorption time. This means that the above equations 4-3, 4-4 and 4-5 cannot be used to calculate the

particle diameter for higher concentrations. Furthermore, the assumption that the asphaltene particle is spherical in shape is a big stretch from reality and most likely introduces significant error in the calculation of particle diameter. Kawashima et. al.,<sup>41</sup> observed that the aggregation of asphaltenes proceeds stepwise, from monomer to nano aggregates and then cluster of aggregates before forming flocs or precipitates, as asphaltene concentration increases. At very low concentration of 0.1 g/L in chloroform (0.01 wt%), the calculated particle size (diameter) from the Stokes-Einstein equation was ~0.8-1.4 nm. Groenzin and Mullins,<sup>47</sup> studied rotational correlation times of individual asphaltene molecules using fluorescence depolarization techniques. Using simple theoretical models and model-independent comparisons with known chromophores, they obtained a range of molecular diameters of asphaltene molecules between 1-2 nm. The results from both these studies closely match the calculated asphaltene molecule diameter obtained in the present study.

## **4.6 Conclusion**

Asphaltene adsorption on mica surfaces has been carried out to better understand the interactions that can occur between crude oil components and solids surfaces during the extraction process. The SFA force measurements allowed a direct evaluation on molecular interactions of asphaltenes in organic solvents, providing insight of asphaltene interactions at interface, molecular conformations, re-arrangements and swelling of asphaltenes in toluene. AFM was used to obtain

complimentary information on the morphology change of the asphaltene films in organic solvents with time. The results of this study show that asphaltenes adsorb to the interface very quickly and form multilayers. The adsorption of asphaltenes onto mica surfaces strongly depend on the concentration of asphaltenes in the solution, adsorption time and load (pressure) applied to the mica substrates during the force measurement. The adsorption process is controlled by diffusion of asphaltenes from the bulk solution to mica surface with a diffusion coefficient on the order of  $10^{-10}$  m<sup>2</sup>/s at room temperature, which was found to be a function of concentration. This diffusion coefficient corresponds to a hydrodynamic radius of approximately 0.5 nm, indicating monomers at very low concentration (e.g. 0.01 wt%). In this study we use mica surfaces to mimic clay particles and asphaltenes surfaces to mimic bituminous particles. The interactions between bitumen and clay particles play a very important role in the oil sands extraction process. The results from this study provide an insight into the basic interaction mechanisms of asphaltenes and solids in organic media and hence in crude oil and bitumen production.

## 4.7 Reference

1. Zhang, L. Y.; Xu, Z.; Masliyah, J. H. *Langmuir* **2003**, *19*, 9730-9741.
2. Spiecker, P. M.; Kilpatrick, P. K. *Langmuir* **2004**, *20*, 4022-4032.
3. Horva'th-Szabo', G.; Masliyah, J. H.; Elliott, J. A. W.; Yarranton, H. W.; Czarnecki, J. J. *Colloid Interface Sci.* **2005**, *283*, 5-17.
4. Yarranton, H. W.; Hussein, H.; Masliyah, J. H. *J. Colloid Interface Sci.* **2000**, *228*, 52-63.
5. Taylor, S. D.; Czarnecki, J.; Masliyah, J. *J. Colloid Interface Sci.* **2002**, *252*, 149-160.
6. Wu, X. *Energy Fuels* **2003**, *17*, 179-190.
7. Friberg, S. E.; Yang, H. F.; Midttun, O.; Sjöblom, J.; Aikens, P. A. *Colloids Surf., A* **1998**, *136*, 43-49.
8. Sjöblom, J.; Mingyuan, L.; Christy, A. A.; Ronningsen, H. P. *Colloids Surf., A* **1995**, *96*, 261-272.
9. Rane, J. P.; Harbottle, D.; Pauchard, V.; Couzis, A.; Banerjee, S. *Langmuir* **2012**, *28*, 9986.
10. Mitchell, D. L.; Speight, J. G. *Fuel* **1973**, *52*, 149-152.
11. Yen, T. F.; Erdman, J. G.; Pollack, S. S. *Anal. Chem.* **1961**, *33*, 1587-1594.
12. Natarajan, A.; Xie, J.; Liu, Q.; Masliyah, J.; Zeng, H.; Xu, Z. *J. Phys. Chem. C* **2011**, *115*, 16043-16051.
13. Buckley, J. S.; Lord, D. L. *J. Pet. Sci. Eng.* **2003**, *39*, 261-273.

14. Hannisdal, A.; Ese, M. H.; Henningsen, P. V.; Sjöblom, J. *Colloids Surf. A* **2006**, 279, 45.
15. Gonzalez, G.; Travalloni-Louvisse, A. M. *SPE Production & Facilities* **1993**, 8, 91.
16. Kupai, M. ; M. ; Yang, F. ; Harbottle, D. ; Moran, K. ; Masliyah, J. ; Xu, Z. *Canadian Journal of Chemical Engineering* **2013**, 91, 1395.
17. Dudasova, D.; Simon, S.; Hemmingsen, P.; Sjöblom, J. *Colloid Surf. A* **2008**, 317, 1.
18. Alboudwarej, H.; Jakher, R. K.; Svrcek, W. Y.; Yarranton, H. W. *Pet. Sci. Tech.* **2004**, 22, 647.
19. Ekholm, p.; Blomberg, E.; Claesson, P.; Auflen, I. H.; Sjöblom, J.; Kornfeldt, A. *J. Colloid Interface Sci.* **2002**, 247, 342.
20. Goual, L.; Horvath-Szabo, G.; Masliyah, J. H.; Xu, Z. *Langmuir* **2005**, 21, 8278.
21. Acevedo, S.; Castillo, J.; Fernandez, A.; Goncalves, S.; Ranaudo, M. A. *Energy Fuels* **1998**, 12, 386.
22. Buckley, J. S.; Liu, Y. *J. Pet. Sci. Eng.* **1998**, 20, 155.
23. Gonzalez, G.; Middea, A. *J. Dispersion Sci. Technol.* **1987**, 8, 525.
24. Acevedo, S.; Ranaudo, M. A.; Escobar, G.; Gutierrez, L.; Ortega, P. *Fuel* **1995**, 74, 595.
25. Marczewski, A. W.; Szymula, M. *Colloids Sur., A* **2002**, 208, 259.

26. Labrador, H.; Fernandez, Y.; Tovar, J.; Munoz, R.; Pereira, J. C. *Energy Fuels* **2007**, *21*, 1226.
27. Acevedo, S.; Ranaudo, M. A.; Garcia, C.; Castillo, J.; Fernandez, A.; Caetano, M.; Goncalves, S. *Colloids Surf., A* **2000**, *166*, 145.
28. Xie, K.; Karan, K. *Energy Fuels* **2005**, *19*, 1252.
29. Israelachvili, J.; Min, Y.; Akbulut, M.; Alig, A.; Carver, G.; Greene, W.; Kristiansen, K.; Meyer, E.; Pesika, N.; Rosenberg, k.; Zeng, H. *Rep. Prog. Phys.* **2010**, *73*, 036601, 1-16.
30. Zhang, L. Y.; Lawrence, S.; Xu, Z.; Masliyah, J. H. *J. Colloid Interface Sci.* **2003**, *264*, 128-140.
31. Israelachvili, J. N.; Adams, G. E. *J. Chem. Soc. Faraday Trans.* **1978**, *174*, 975-1001.
32. Wang, J.; Lu, Q.; Harbottle, D.; Sjöblom, J.; Xu, Z.; Zeng, H. *J. Phys. Chem. B.* **2012**, *116*, 11187.
33. Israelachvili, J. N. *Intermolecular and Surface Forces*, 2nd ed.; Academic Press: New York, **1991**.
34. Israelachvili, J. N. *J. Colloid Interface Sci.* **1973**, *44*, 259-272.
35. Zeng, H. *Polymer Adhesion, Friction and Lubrication*, Somerset, NJ, USA: Wiley, **2013**.
36. Akbulut, M.; Alig, A. R. G.; Min, Y.; Belman, N.; Reynolds, M.; Golan, Y.; Israelachvili, J. *Langmuir* **2007**, *23*, 3961-3969.

37. Zeng, H.; Maeda, N.; Chen, N.; Tirrel, M.; Israelachvili, J. *Macromolecules* **2006**, 39, 2350.
38. Drummond, C.; Israelachvili, J. *J. Pet. Sci. Eng.* **2004**, 45, 61-81.
39. Jouault, N. ; Corvis, Y. ; Cousin, F. ; Jestin, J. ; Barré, L. *Langmuir* **2009**, 25, 2991-3998.
40. Andreatta, G.; Bostrom, N.; Mullins, C. *Langmuir* **2005**, 21, 2728.
41. Kawashima, H.; Takanohashi, T.; Iino, M.; Matsukawa, S. *Energy Fuels* **2008**, 22, 3989.
42. Vuillaume, K. ; Giasson, S. *J. Phys. Chem. C.* **2009**, 113, 3660-3665.
43. Ward, A. F. H.; Tordai, L. *J. Chem. Phys.* **1946**, 14, 453-461.
44. Abudu, A.; Goual, L. *Energy Fuels* **2009**, 23, 1237-1248.
45. Ostlund, J. A.; Lofroth, J. E.; Holmberg, K.; Nyden, M. *J. Colloid Interface Sci.* **2002**, 253, 150-158.
46. Cussler, E. L. *Diffusion Mass Transfer in Fluid System*, 2<sup>nd</sup> ed.; Cambridge University Press: New York, 1997.
47. Andrews, A. B.; Guerra, R. E. ; Mullins, O. C. ; Sen, P. N. *J. Phys. Chem. A* **2006**, 110, 8093-8097.

## **Chapter 5**

# **Understanding Molecular Interactions between Asphaltenes and Ethyl Cellulose immobilized on Hydrophilic Solids in Organic Solvent<sup>c</sup>**

From the previous chapters, we realize that in nonaqueous systems, the interaction of adsorbed molecules on the surfaces of dispersed phase plays a critical role. Better control of process performance in nonaqueous systems requires a good description of the molecular interactions between the different materials involved. In the present chapter we investigate the interactions between ethyl cellulose (EC) and asphaltenes immobilized on hydrophilic solids in organic solvent. EC is a proven demulsifier for water-in-diluted bitumen emulsions. A detailed history of the problem is describes below.

### **5.1 Introduction**

In heavy oil processing, the presence of oil-wet and biwetable solids create many challenging operational problems with the formation of stable water-in-oil (w/o) emulsions.<sup>1-5</sup> These solids along with the heavy components of bitumen such as asphaltenes readily partition at the water-oil interface forming a film that hinders droplet coalescence.<sup>6-9</sup> The hindered breakdown of emulsions can result in the

---

<sup>c</sup> A version of this chapter has been submitted for publication: Natarajan, A; Kuznicki, N.; Harbottle, D.; Zeng, H.; Xu, Z. *J. Phys. Chem. C* **2014**, Submitted.

formation of rag layers that are a complex mixture of oil, water and solids.<sup>10</sup> With the gradual accumulation of the rag, oil-wet solids and water can be carried over with the oil phase creating issues of equipment fouling and catalyst poisoning in the downstream refining process. The solids consist mainly of ultrafine aluminosilicate clay particles that are naturally hydrophilic. However, due to contamination by heavy oil fractions (asphaltenes and other organic matter) in the oil sands formation, the solids are often biwettable with large patches of hydrophobic surface contamination.

Asphaltene adsorption on hydrophilic surfaces is often considered an irreversible process with asphaltene-contaminated solids remaining hydrophobic even after excessive washing in good solvents such as toluene or naphtha.<sup>3</sup> Removal of highly contaminated and hence hydrophobic solids can be extremely challenging even with centrifuges, since the particle size of clays can be as small as a few tenths of a micron. Typically, a demulsifier is used to aid in the separation of these hydrophobic solids and destabilize the w/o emulsion. In a previous study from our group,<sup>11</sup> a biodegradable ethyl cellulose (EC) was found to be an effective demulsifier for breaking water-in-diluted bitumen emulsions.<sup>11,12</sup> The addition of EC to the organic phase was found to cause a significant reduction in diluted bitumen-water interfacial tension. Water droplets were shown to flocculate and coalesce in diluted bitumen solutions containing EC, depending on EC concentration. In a following study,<sup>13</sup> quartz crystal microbalance with dissipation (QCM-D) was used to determine the adsorption of asphaltenes and EC

on silica or alumina surface. EC was shown to decrease the surface hydrophobicity of organic-contaminated solids. The effect of EC on the wettability and morphology of the bitumen contaminated silica or alumina surface was determined by contact angle measurements and AFM images.

A fundamental understanding of the emulsion stabilization mechanism and the subsequent destabilization of the emulsion by demulsifier can only be realized by a good description of the interaction forces that act between asphaltenes, EC and mica. To that effect, in the current study, we use a surface forces apparatus (SFA) to measure the interaction force ( $F$ ) as a function of surface separation ( $D$ ) between the different materials in contact. SFA can achieve a force sensitivity of  $<10$  nN and an absolute distance resolution of  $<0.1$  nm when measured in situ and in real time. Here we mimic mica for the hydrophilic solids, asphaltenes for the stable interfacial film and EC for the demulsifier. Numerous studies in literature have used such an approach where a solid substrate coated with polymer or surfactant layers was used to mimic the interface between two phases or domains.<sup>14-18</sup> The force profiles obtained from SFA measurements would be able to provide valuable information on material properties such as interaction energies and molecular conformation changes of the interacting surfaces or films in a given solvent. AFM imaging was employed to provide complementary information on the surface morphology of the coated/adsorbed films.

## **5.2 Materials and Experimental Methods**

### **5.2.1 Materials**

Bitumen samples were provided by Syncrude Canada Ltd., Alberta, Canada. Asphaltenes were precipitated from bitumen by adding 40 times of n-heptane to bitumen by volume and repeatedly washed with n-heptane. Details on asphaltene precipitation are reported elsewhere.<sup>19</sup> High-performance liquid chromatography (HPLC)-grade toluene and heptane purchased from Fisher Scientific was used as received. Ruby mica sheets were purchased from S & J Trading Inc. (Glen Oaks, NY). Muscovite mica can be easily cleaved to obtain large atomically smooth surfaces whose exposed aluminosilicate lattice is similar to quartz and many clay basal surfaces. In that way, a clean reproducible substrate can be obtained. The surfaces were cleaved in a laminar hood and stored in vacuum before use.

### **5.2.2 Sample Preparation**

The sample preparation varied according to the different experimental set ups. Film-coating method was adopted to coat an asphaltene/EC film on a mica surface. Briefly, after gluing a freshly cleaved thin mica sheet on a silica disk used in SFA, several drops of the 0.5 wt% asphaltene or EC in toluene solution were placed and allowed to spread on the exposed mica surface. The solvent was evaporated for ~15 min to immobilize the surface layer on the mica. The sample was then washed with pure toluene and blow-dried with ultra-pure nitrogen before it was loaded in the SFA chamber. The film coated mica surfaces were then used

to measure interaction forces and image their topographic features by SFA and AFM, respectively. Alternatively, a solution of 0.5 wt% asphaltenes or EC in toluene was injected in-between two molecularly smooth mica surfaces loaded in the SFA chamber. The adsorption of the asphaltenes or EC from the bulk solution to mica was measured by SFA.

### 5.2.3 Force Measurement

A surface forces apparatus was used to measure the molecular interaction forces between confined EC and asphaltene films between mica surfaces. Detailed setup of SFA experiments has been reported elsewhere.<sup>14,20</sup> Briefly, thin mica sheets (1-5  $\mu\text{m}$  thick) were coated with a ~50 nm semi reflective layer of silver on the back surface. The silver coating is required to obtain multiple Beam Interference to produce fringes of equal chromatic order (FECO).<sup>23</sup> The FECO fringes were then used to determine the surface separation, surface geometry, deformations and the contact area in situ and in real time. The silver coated mica sheets were glued onto the cylindrical silica disks (radius  $R = 2$  cm). The choice of glue is very important. In our experiments we use glucose as glucose is insoluble in toluene. The prepared silica disks were then mounted into the SFA chamber in cross-cylinder geometry, which is equivalent to the interaction of a sphere of radius  $R$  approaching a flat surface locally when  $R$  is much larger than the surface separation  $D$ . The measured force  $F(D)$  between the two curved surfaces can be correlated to the interaction energy per unit area between two flat surfaces  $W(D)$  using the Derjaguin approximation:<sup>20-22</sup>

$$F(D) = 2\pi RW(D) \quad (5-1)$$

The adhesion energy per unit area between two surfaces of the same materials,  $W_{ad}$ , can be determined from the pull-off force,  $F_{ad}$  (the force required to separate the surfaces from adhesive contact), given by:<sup>20,22</sup>

$$W_{ad} = 2\gamma = F_{ad}/1.5\pi R \quad (5-2)$$

In each set of measurements, the reference distance ( $D = 0$ ) was determined at the adhesive contact between the two bare mica surfaces in air prior to introducing the solvents between the surfaces. For the force measurements, ~100  $\mu$ L of desired solvent/solution was injected between two closely placed coated mica surfaces in the SFA chamber. The chamber was sealed and saturated with the vapor of the same solvent. During a typical force measurement, the two mica surfaces are brought close together for an initial approach until the two surfaces do not move any closer followed by separation of the two surfaces. In this way we obtain the normal force-distance (F vs. D) profile. Note: “confined film thickness” in this study is defined as the mica-mica separation distance or thickness of confined asphaltenes/EC films which barely changed with increasing the normal load or pressure.

### **5.3 Results and Discussion**

We have previously studied the interactions of asphaltene films in toluene and heptane (good and poor solvents respectively) and the adsorption of asphaltenes on hydrophilic solid (mica) surface.<sup>24,25</sup> In pure toluene repulsive interaction was measured which was attributed to the steric repulsion of swollen asphaltene films. In aliphatic solvent adhesion force was measured between two asphaltene layers confirming the association of asphaltenes in poor solvents. Results of the adsorption study showed that the adsorption of asphaltenes onto mica surfaces strongly depends on the concentration of asphaltenes in the solution and adsorption time. Analysis of the adsorption process indicated that adsorption is controlled by diffusion of asphaltenes from the bulk solution to the mica surface.

#### **5.3.1 Topography of Sample Surfaces**

The topographical features of asphaltene and EC films immobilized on mica surfaces were imaged in air by an AFM operating in tapping mode. As shown in Figure 5-1, the AFM image of bare mica prior to film deposition showed a featureless flat surface with a root-mean-square roughness of  $\sim 0.22$  nm. The AFM image of coated EC and asphaltene films on mica are shown in Figure 5-1B & C, respectively. Image of EC films show a uniform and flatter surface morphology with an average surface roughness of  $\sim 0.9$  nm. In contrast, the asphaltenes are randomly distributed in the form of closely packed nanoaggregates,<sup>24-26</sup> with an average root mean square roughness of  $\sim 1.2$  nm.

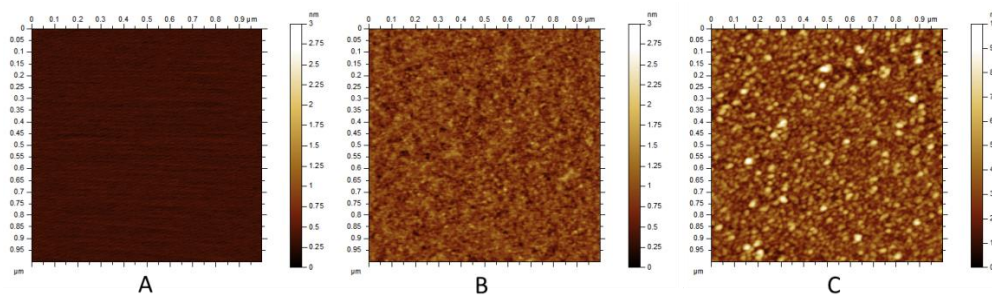


Figure 5-1 AFM images of (A) bare mica surface (B) coated EC film on mica surface (C) coated asphaltene film on mica surface. Note that the surfaces were gently dried with nitrogen before imaging.

### 5.3.2 Adsorption of Ethyl Cellulose to Mica

The force-distance profile between two bare mica surfaces immediately (in ~5 minutes) following the injection of 0.5 wt% EC in toluene solution is shown in Figure 5-2. It is evident from both the AFM image in Figure 5-1B and the force-distance profile in Figure 5-2 that EC molecules were able to irreversibly adsorb to mica surface and form a thin film very quickly (< 5 min). Dijt et. al.,<sup>27</sup> showed that the initial stages of polymer adsorption process is relatively fast. De-Gennes et. al.,<sup>28</sup> showed that for practical applications, the initial stages of the adsorption process is irreversible due to small probability of complete desorption of a chain attached to several surface sites. Repulsive force was observed during approach at ~30 nm with a confined film thickness of ~11 nm. This implies that the adsorbed EC film is ~5.5 nm on each mica surface. Since the electrical double-layer forces in toluene can be considered negligible, repulsive forces observed during the approach of the surfaces are attributed to steric repulsion of swollen EC films. The long-ranged repulsion is suggestive of loose (diffuse) polymer layers which

under compression, compact to a uniform thickness. The retracting force-distance profile in Figure 5-2 shows an adhesion force,  $F_{ad}/R \approx -1 \text{ mN/m}$ , most likely due to the interdigitation and bridging of EC molecules on the two surfaces when brought in contact during force measurements. Bridging adhesion can occur only when there are adsorption sites available on both the surfaces. In other words, when the coverage is below saturation.<sup>29</sup> EC molecules were stretched up to ~35 nm before the two surfaces were finally detached from each other. This is not only an indication of adhesion but also that the compacted EC films are compressible and deformable rather than rigid or solid like.

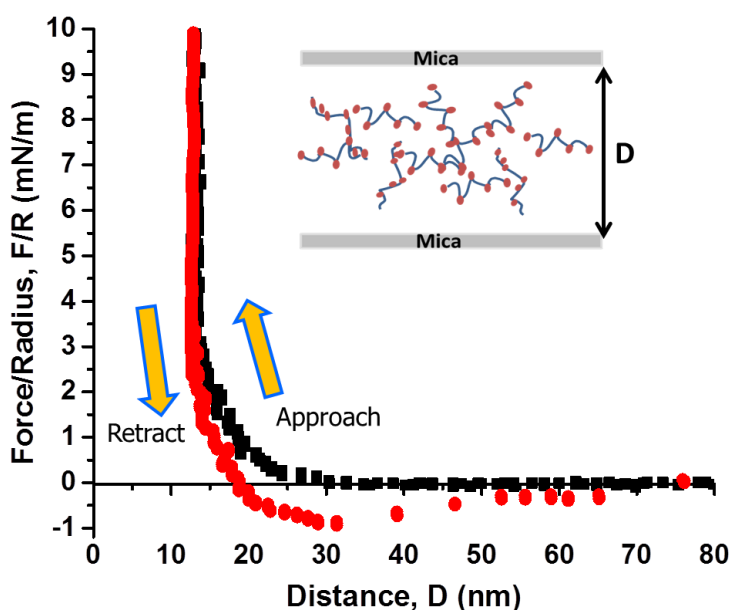


Figure 5-2 Force-distance profiles between two mica surfaces after immersed in 0.5 wt% EC-toluene solution for ~5 min. In this figure and all subsequent figures, “In” indicates approach of the two surfaces and “Out” indicates separation of the two surfaces.

### 5.3.3 Interaction between Asphaltene and EC Surfaces in Toluene

The intermolecular forces of asphaltenes and EC immobilized on mica in toluene were measured using a SFA as shown in Figure 5-3. The experimental set up consists of an asphaltene film coated on a mica surface interacting with EC film coated on the other mica surface. Figure 5-4 shows the interaction force measured after exposing the two immobilized films in toluene for ~10 min. The two surfaces were brought into contact and separated. Repulsive force was observed

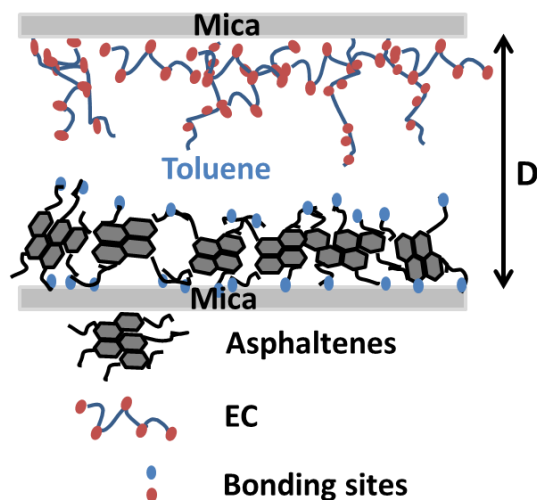


Figure 5-3 Experimental configuration for studying the surface interactions between asphaltene films and EC films coated mica surfaces in toluene (asymmetric case).

during approach at ~35 nm with a confined film thickness of ~23 nm. A strong adhesive force ( $F_{ad}/R \approx -2 \text{ mN/m}$ ;  $W_{ad} = 0.42 \text{ mJ/m}^2$ ) was observed during separation. Under high compression the confined film thickness shifted to ~12 nm, which corresponds to ~6 nm of immobilized films on each surface. This 6 nm film of asphaltenes on mica surface is close to the literature values.<sup>24</sup> This

indicates that asphaltenes and EC form approx. same size (height profile) films on mica from the film coating method.

The repulsive force observed during the approach of the two films in toluene is attributed to steric repulsion of swollen asphaltene/EC films. The strong adhesion measured during the separation is most likely due to interdigitation and bridging of asphaltene and EC molecules on the two surfaces. Such interactions resulted in stretching of the two films up to  $D \approx 40$  nm during separation before the two surfaces finally detached from each other.

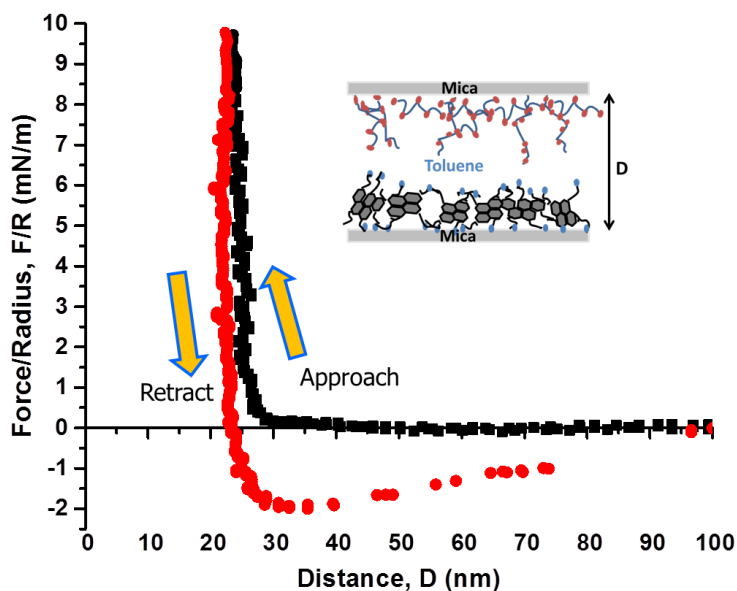


Figure 5-4 Force-distance profile of EC and asphaltene films coated on mica (asymmetric surfaces). When the surfaces are compressed, the confined film thickness shifted to about 12 nm indicating that the coated films of EC and asphaltenes in toluene swell and are flexible instead of rigid.

Toluene is a good solvent for both asphaltenes and EC. Hence the chains of the immobilized asphaltene and EC molecules on mica surface tend to stretch and act as a swollen brush. Therefore, the steric repulsion between these two layers could be described by Alexander—de Gennes (AdG) model on two interacting polymer brush layers.<sup>30-33</sup> When two polymer brush surfaces approach each other, at some distance the brushes/films start to overlap leading to an increase in the local density of polymer segments. This in turn leads to an increase in osmotic pressure and repulsive interaction energy. The repulsive pressure between two planar brush layers is given by:<sup>34</sup>

$$P(D) \approx \frac{kT}{s^3} \left[ \left( \frac{2L}{D} \right)^{\frac{9}{4}} - \left( \frac{D}{2L} \right)^{\frac{3}{4}} \right] \text{ for } D < 2L \quad (5-3)$$

Where  $s$  is the mean distance between anchoring (or grafting) sites on the surface,  $L$  is the brush layer thickness per surface,  $T$  is the temperature, and  $k$  is the Boltzmann constant. For the geometry of two crossed cylinders of radius  $R$  (used in our experiments), the force between them is given by first integrating the above equation and then using the Derjaguin approximation as:<sup>20,34</sup>

$$\frac{F(D)}{R} = 2\pi \int P(D)dD = \frac{16\pi kTL}{35s^3} \left[ 7 \left( \frac{2L}{D} \right)^{5/4} + 5 \left( \frac{D}{2L} \right)^{7/4} - 12 \right] \quad (5-4)$$

For the asymmetric case, the equation becomes

$$\frac{F(D)}{R} = \frac{8\pi kTl}{35s^3} \left[ 7 \left( \frac{L}{D} \right)^{5/4} + 5 \left( \frac{D}{L} \right)^{7/4} - 12 \right] \quad (5-5)$$

The fit of measured repulsive force for asphaltene and EC films in toluene (blue color) with the AdG model is shown in Figure 5-5. For reference, the fit for two EC films in toluene (green color) and two asphaltene films (red color) in toluene are also shown. It can be observed that the fit for the asphaltene-EC films falls right in the middle of two EC films and two asphaltene films. Also, for system containing asphaltenes, at short separation distances under high compression forces we observe that AdG model fits the measured force profile well. However, at longer separation distances under lower compression forces a significant deviation is observed. It appears that the swelling and stretching of the side chains on asphaltene brushes in toluene induces a weaker repulsive force over a much longer separation distance. This additional force is not considered in the AdJ model applicable to monodispersed brushes. However, the lower compression regime can be fitted with the AdG theory using an independent set of parameters as shown in Figure 5-5, indicating the possible presence of secondary brushes due to the polydispersity and complexity of asphaltene molecules or aggregates. These secondary structures disappear when there is no asphaltenes present in the system as seen for the two EC films in toluene system. The fitted parameters of  $s$  and  $L$  are listed in Table 5-1.

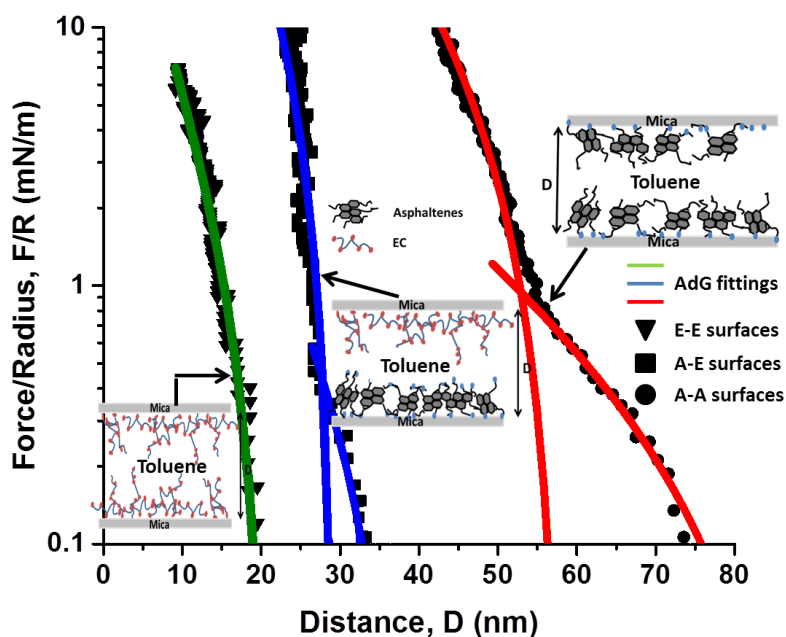


Figure 5-5 Experimentally measured repulsion forces and best fitted curves using the AdG theory for two EC films in toluene (E-E); asphaltene film against an EC film in toluene (A-E); and two asphaltene films in toluene (A-A).

Table 5-1 Fitting parameters using the AdG scaling model.

Asphaltene and EC surfaces in toluene			EC surfaces in toluene			
At ~10min	High Loading <sup>a</sup>		Low Loading <sup>b</sup>		At ~10min	
L (nm)	14.6		19.0		10.5	
S (nm)	2.0		6.9		4.3	
	A-A <sup>c</sup>		A-M <sup>c</sup>		E-E	E-M
	High load	Low load	High load	Low load		
L (nm)	17.6	33	8.8	16.5	10.5	5.3
S (nm)	2.8	12.5	2.8	12.5	4.3	4.3
A – Asphaltene			E – Ethyl Cellulose		M – Mica	

<sup>a</sup> High compression and short separation distance regime (solid fitting curve). <sup>b</sup> Low compression and long separation distance regime (dash fitting curve). <sup>c</sup> Previously published results.<sup>26</sup>

### 5.3.4 EC Coated Substrate and Asphaltene Solution

The intermolecular forces of asphaltene solution in between EC surfaces were measured using a SFA as shown in Figure 5-6. Force-distance profile of EC surfaces in asphaltene solution at different adsorption time are shown in Figure 5-7. On approach, Figure 5-7A, there is a long-ranged repulsion suggestive of loose (diffuse) polymer-like films which under compression compact to a uniform thickness which ranges from ~25 nm to ~85 nm during each approach and in ~4 hours. Note that the repulsive forces become long range, with increasing confined film thickness and adsorption time as shown in Figure 5-7A & B.

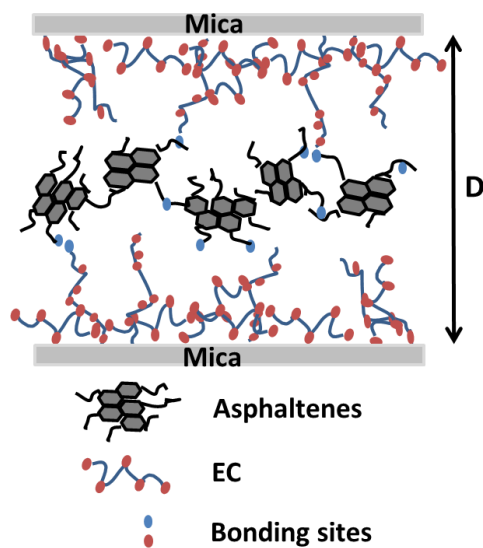
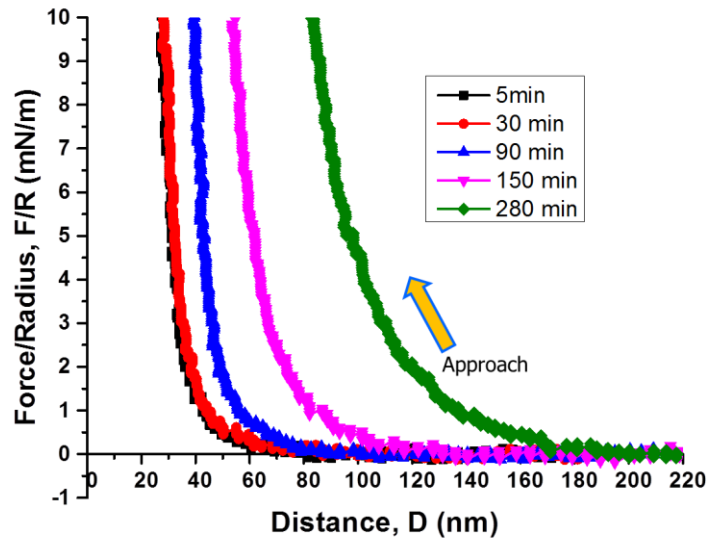
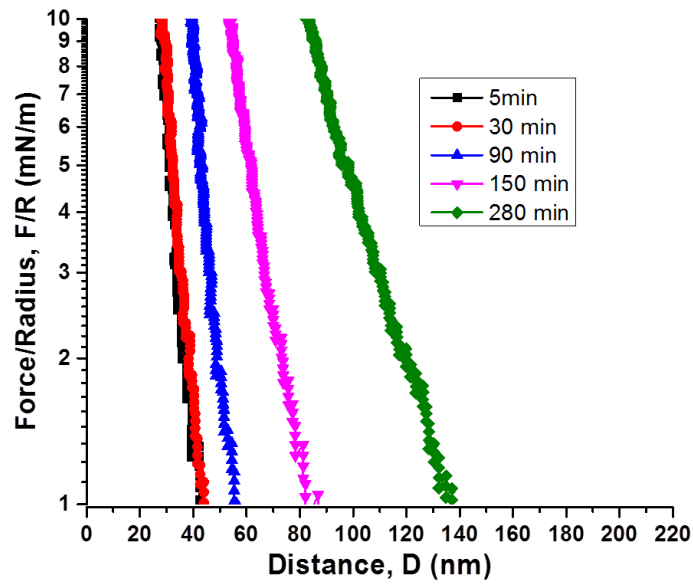


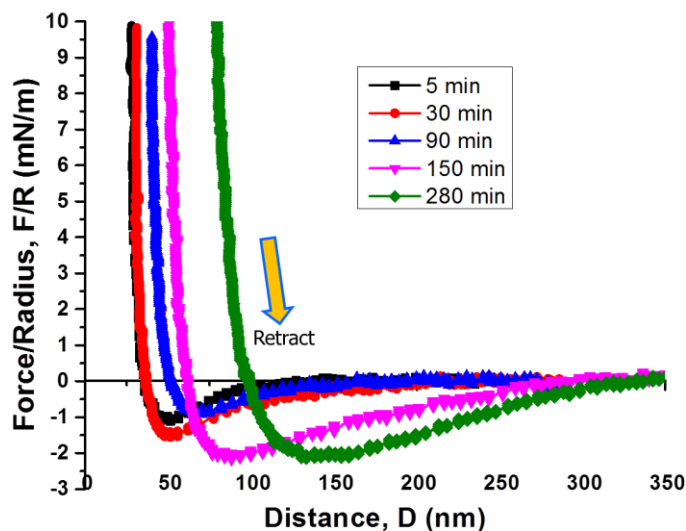
Figure 5-6 Experimental configuration for studying the surface interactions between EC films coated mica surfaces in asphaltene solution.



A



B



C

Figure 5-7 (A) Approaching force profile of two EC surfaces in 0.5 wt% asphaltene-toluene solution. (B) Same data on a semi log plot to illustrate the exponentially repulsive force-distance regime. (C) Separation force profile of two EC surfaces in asphaltene-toluene solution.

At smaller separations, as the surfaces are more compressed, the repulsive force rises more steeply. The increase in confined film thickness indicates adsorption of asphaltenes on EC surface. This observation agrees with our previous work on the same system studied by QCM-D.<sup>13</sup> Asphaltenes adsorption on mica surface is mainly through polar-polar bonding between asphaltene molecules and the hydrophilic solid surface. However, once EC is adsorbed on a hydrophilic solid surface, it occupies most of the available binding sites on the surface. Although polar groups on EC surface allow polar-polar bonding with asphaltenes in the bulk solution, the large hydrophobic block of asphaltene molecules and the

ethoxyl chains on EC molecules prevent effective polar-polar bonding between them, leaving opportunity mainly for physisorption of asphaltenes on EC surface.<sup>13</sup>

The adsorbed layers on mica and the asphaltenes in the solution contribute to strong bridging adhesion observed on the separation force profile as seen in Figure 5-7C. The strength of the adhesive force is  $F_{ad}/R \approx -2.2$  mN/m (for example, in figure 4C at 280 min) which corresponds to adhesion energy of  $W_{ad} = F_{ad}/1.5\pi R \approx 0.47$  mJ/m<sup>2</sup>. All the separation force-distance profiles show that the adsorbed films are stretched before the two surfaces detach from each other. The separation force-distance profiles are very similar to the force profile of asphaltene adsorption on mica surface.<sup>20</sup> Figure 5-8, shows that the adhesion energy increases steadily with adsorption time. The time dependent increase in the adhesion is due to asphaltene/EC chain interdigitation occurring across the interface coupled with the conformational changes of the adsorbed layers that enable effective bridging adhesion. The chain interdigitation increases the real contact area with time and thereby increases the adhesion above the value expected for perfectly flat surfaces. This type of effect is often seen with polymer and surfactant systems.<sup>20</sup>

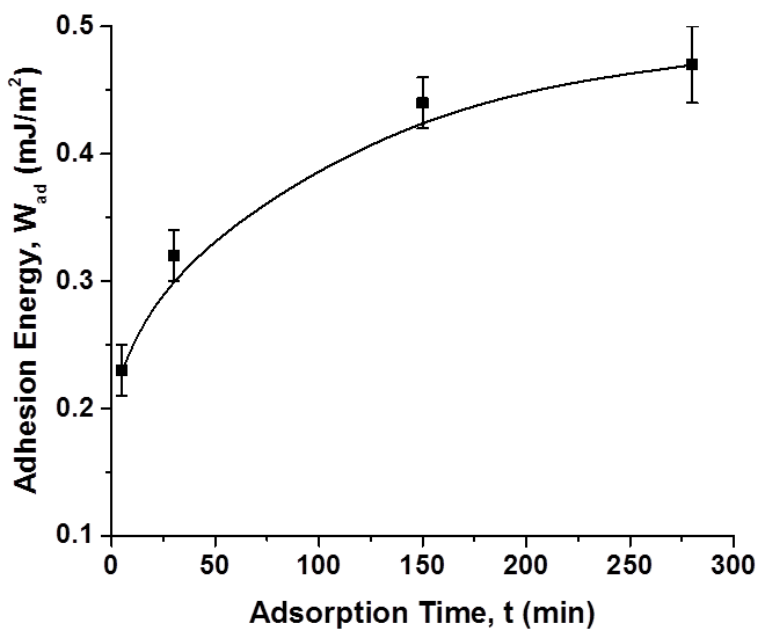


Figure 5-8 Adhesion energy  $W_{ad}$  between EC surfaces in asphaltene-toluene solution as a function of adsorption time at 24°C.

### 5.3.5 Asphaltene Coated Substrate and EC Solution.

The intermolecular forces of asphaltene solution in between EC surfaces were measured using a SFA as shown in Figure 5-9. Force-distance profile of film coated asphaltene surfaces in EC solution at different adsorption time are shown in Figure 5-10. The adsorption measurements were made by injecting 0.5 wt% EC solution between the asphaltene surfaces. On approach, Figure 5-10A, there is a long-ranged repulsion suggestive of loose (diffuse) polymer-like films which under compression compact to a uniform thickness which ranges around ~30 nm. Comparing Figure 5-7A and Figure 5-10A, there is a ~5 nm difference between the confined film thickness measurements at initial approach. Furthermore, unlike

the force-distance profile in Figure 5-7A, for subsequent measurements in Figure 5-10A, there was no significant change in the confined film thickness with increasing adsorption time. To interpret the results of this force profile, a good description of the structure of EC and asphaltene molecules and their interaction with mica is required.

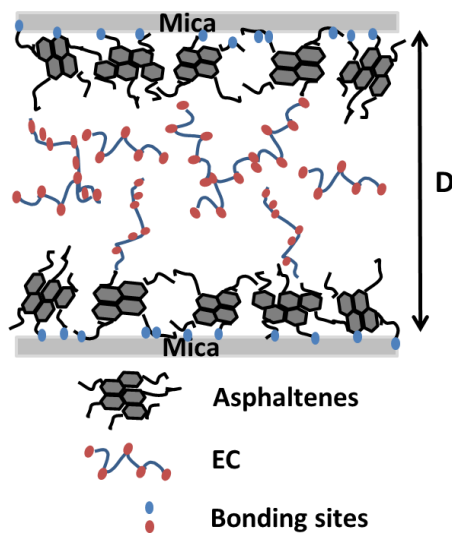
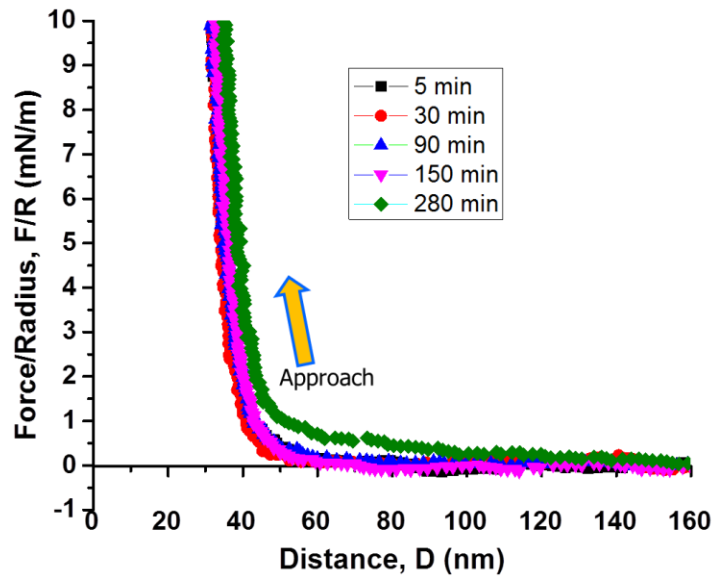
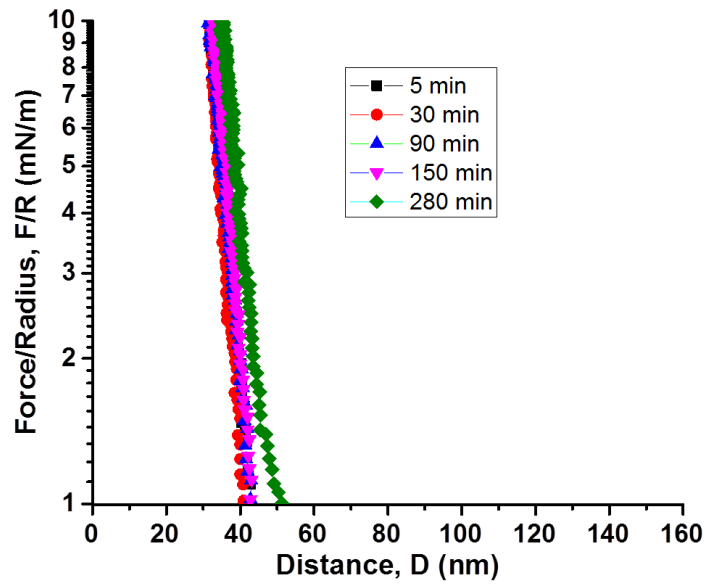


Figure 5-9 Experimental configuration for studying the surface interactions between asphaltene films coated mica surfaces in EC solution.



A



B

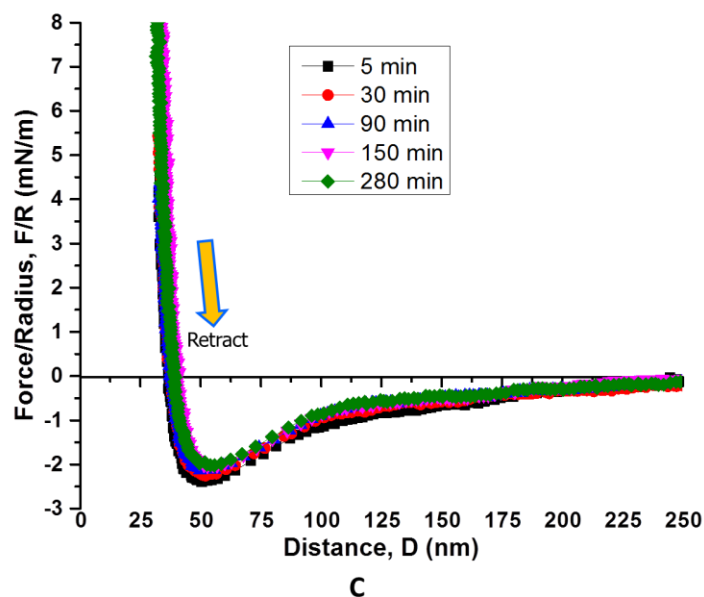


Figure 5-10 (A) Approaching force profile of two asphaltene surfaces in EC-toluene solution at different time intervals. (B) Same data on a semi log plot to illustrate the exponentially repulsive force-distance regime. (C) Separation force profile of two asphaltene surfaces in EC-toluene solution at different interval of time.

Asphaltene molecules are shaped with the fused aromatic ring system in the middle connected by aliphatic chains, with polar functional groups and heteroatoms scattered in the side chains.<sup>35-37</sup> As a result, the polar groups are separated by large hydrophobic aromatic ring systems and their distribution on asphaltenes is not dense and uniform. When adsorbing on the hydrophilic mica surfaces, asphaltenes cannot occupy all the binding sites on a solid surface, providing opportunities for sequential adsorption of EC. In contrast, the polar (e.g., hydroxyl) groups on EC molecules are more uniformly distributed along the polymeric chains and are of higher density. As a result, each EC molecule can

form multiple bonding with the hydrophilic solid surfaces.<sup>27</sup> Hence, once adsorbed, the EC molecules are likely to lie on the solid surface, although tails and loops of EC chains can also be present contributing to the interdigitation and bridging adhesion. In this manner, the adsorbed EC gradually expands to compete for more binding sites on the solid surface and pushes away the neighboring asphaltenes. The structural differences between asphaltenes and EC can be seen in AFM images (Figure 5-1), where asphaltenes are in the form of randomly distributed nanoaggregates on the mica surface while the mica surface with EC is more smooth and flatter. Surface topography of asphaltene-coated surfaces as a function of adsorption time in EC solution is shown in Figure 5-11. Asphaltene coated surface in pure toluene is shown in Figure 5-11a for reference. With increasing adsorption time, surface topography of asphaltene films on mica show two distinct changes: some nanoaggregates grew in size while the discrete flat areas expanded on the surface. Figure 5-11b, c and d show larger rough domains (large globule structures/aggregates) and much expanded flat open areas. The rms value at 240 min soaking time is almost equal to the rms value of EC coated on mica surface (comparing Figure 5-1b and Figure 5-11d). The AFM images suggest that EC displaced asphaltenes by pushing them to form larger globule structures/aggregates. The AFM height profile suggests that asphaltene aggregates on the mica/EC surface is ~15 nm. The confined film thickness from the force curve in Figure 5-10A is ~ 30 nm which is equivalent to a ~15 nm film on each surface. Hence the AFM and SFA data are in agreement.

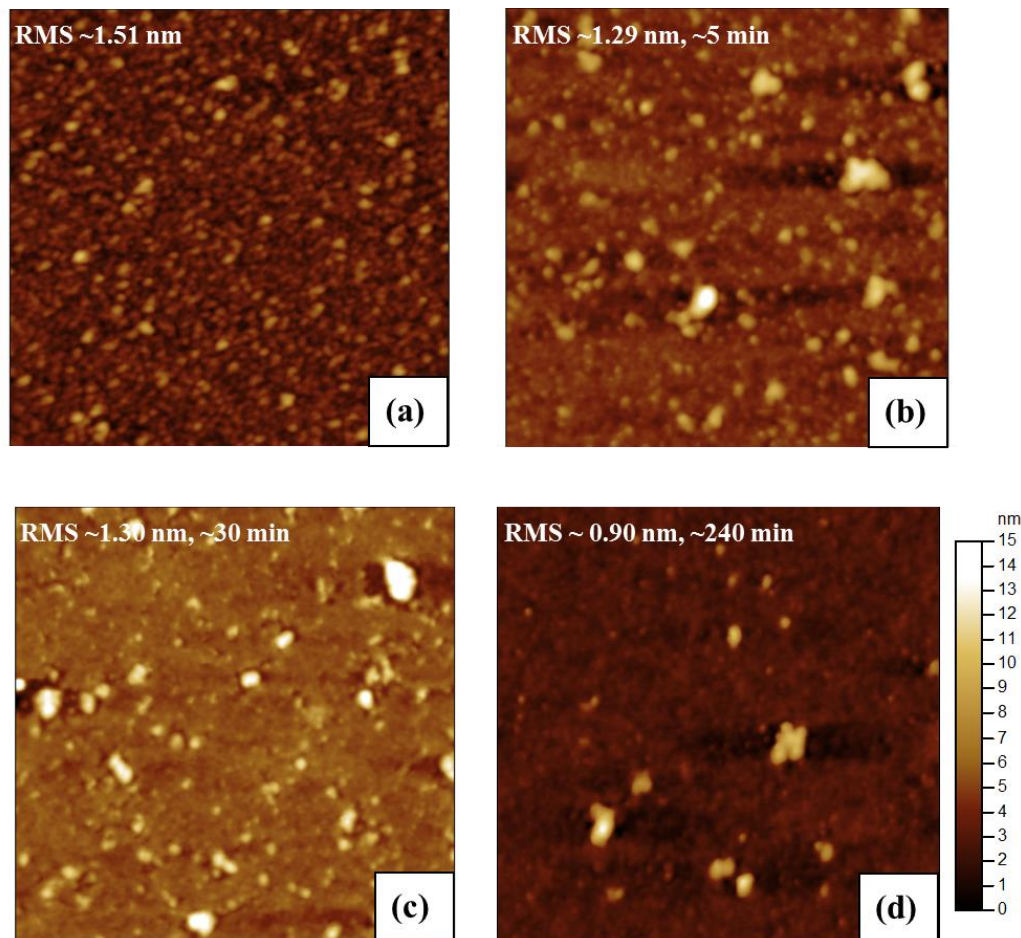


Figure 5-11 AFM topography images of asphaltene surface in EC solution at different adsorption time. (A) asphaltene coated mica surface in air. (B) asphaltene coated mica surface in EC solution for 5 min. (C) asphaltene coated mica surface in EC solution for 30 min. (D) asphaltene coated mica surface in EC solution for 280 min. Note: the time it takes for EC to displace asphaltene from the mica surface is very quick, within 5 min of adsorption time. The asphaltene height profile grows from ~10 nm to about ~20 nm in the first 5 min and remains almost consistent for the duration of the experiment. The dimension of images is  $1 \mu\text{m} \times 1 \mu\text{m}$ .

The displacement of asphaltenes from the surface, as seen from AFM images, correlates well with the force curves. The larger globule structures of asphaltenes contribute to the increase in long range repulsive force as observed in Figure

5-10A at 280 min. The EC molecules, now occupying most of the mica surfaces give limited binding sites for bridging adhesion. Bridging adhesion can occur only when adsorption sites are available on the opposing surfaces, i.e.; when the coverage is below saturation. As additional EC molecules adsorb onto the surfaces from the solution, the polymer will extend further out into the solution and fewer sites will be available for bridging. This gives rise to a longer ranged but progressively weaker adhesive force as seen in Figure 5-10C. Similar force curves have been measured in previous studies.<sup>38,39</sup> Figure 5-12 shows the decrease in adhesive energy with increase in adsorption time. The decrease in bridging adhesion also suggests that asphaltenes though pushed to form nanoaggregates and compete for binding sites with EC molecules, do not leave the surface. Because if they leave the surface and become part of the bulk solution, then similar to Figure 5-7 and previous literature results,<sup>25</sup> they will contribute towards increasing bridging adhesion with adsorption time. So for the duration of our experiment, asphaltenes do not leave the mica surface.

The driving force for EC to displace the adsorbed asphaltenes is therefore attributed to its higher number of stronger hydrogen bonding sites toward hydroxyl groups on hydrophilic solid surfaces as shown in Figure 5-13. For the duration of our experiment, Figure 5-13 also represents the possible final state of the film on mica surface. From the above discussion, the combined results of SFA and AFM suggest constant structural changes at the interface resulting in the

formation of these globule structures that enable EC to act as a wettability modifier.

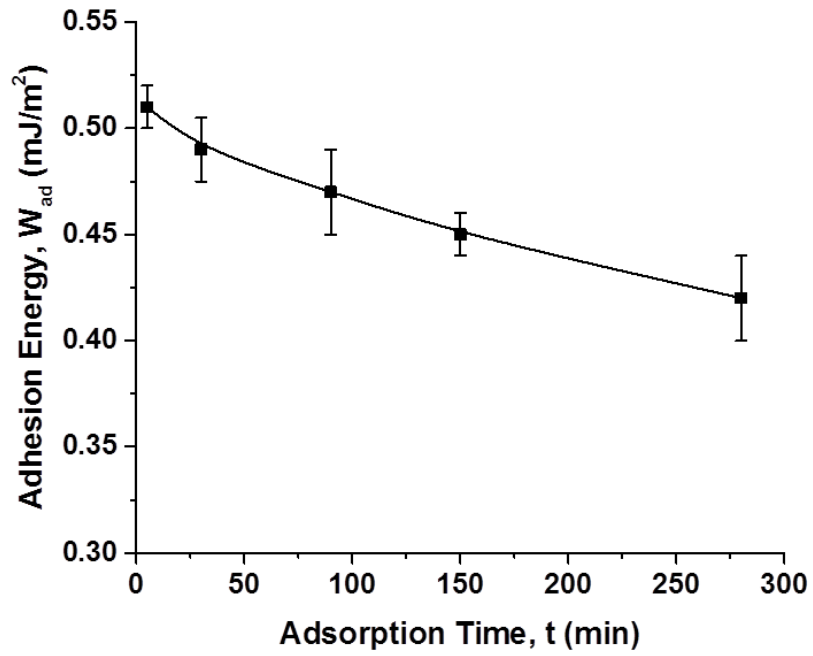


Figure 5-12 Adhesion energy  $W_{ad}$  between asphaltene surfaces in EC-toluene solution as a function of adsorption time at room temperature.

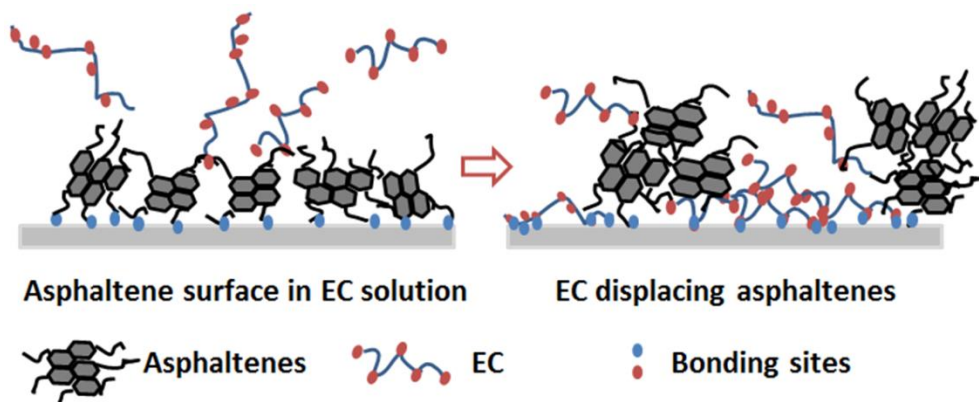


Figure 5-13 Schematic representation of asphaltene on mica being displaced by EC from solution.

## 5.4 Conclusion

The forces between EC and asphaltene films were measured using a SFA. SFA force measurements allowed a direct evaluation on molecular interactions of the adsorbed films on mica. AFM was used to obtain complimentary information on the morphology change of the adsorbed films with time. EC adsorb onto mica very quickly, less than 5 min and contribute to bridging adhesion between the surfaces. The long range repulsive interaction between EC and asphaltene surfaces in toluene is indicative of the interaction between the hydrophobic asphaltene molecules and the ethoxyl chains on EC that prevent the polar-polar bonding effectively. But when the surfaces are compressed, the interdigitation of the films gives rise to strong adhesive force.

The force profiles of asphaltene surfaces in EC solution and EC surfaces in asphaltene solution were completely different. Asphaltenes in the solution physisorb on EC surface and give rise to increasing long range repulsion and increasing confined film thickness. Once compressed, they contribute to bridging adhesion indicated by increasing adhesive force during separation. However, EC in the solution displaces asphaltenes from the surface and pushes them to form larger globule structures/aggregates which in turn improve dewatering. This is seen by combining the results from both the force measurements and AFM images. The interaction between EC and asphaltene played a minimal role in asphaltene displacement by EC. The displacement occurred because of the higher number of hydroxyl groups per EC molecule. Therefore, the EC molecule has a stronger affinity to the hydrophilic mica surface than asphaltenes. This study with SFA supports the major finding from our previous study on the wettability control of organic-contaminated solids using chemicals, especially appropriate demulsifiers of w/o emulsions, to improve processability of heavy oils.

## 5.5 References

1. Jiang, T. M.; Hirasaki, G. J.; Miller, C. A.; Ng, S. *Energy Fuels* **2011**, *25*, 2551.
2. Sparks, B. D.; Kotlyar, L. S.; O'Carroll, J. B.; Chung, K. H. *J. Pet. Sci. Eng.* **2003**, *39*, 417.
3. Kotlyar, L. S.; Sparks, B. D.; Woods, J. R.; Chung, K. H. *Energy Fuels* **1999**, *13*, 346.
4. Dudasova, D.; Simon, S.; Hemmingsen, v. P.; Sjoblom, Johan. *Colloids and Surfaces A* **2008**, *317*, 1.
5. Kotlyar, L. S.; Sparks, B. D.; Woods, J.; Capes, C. E.; Schuttle, R. *Fuel* **1995**, *74*, 1146.
6. Zhang, L. Y.; Xu, Z.; Masliyah, J. H. *Langmuir* **2003**, *19*, 9730.
7. Spiecker, O. M.; Kilpatrick, P. K. *Langmuir* **2004**, *20*, 4022.
8. Wu, X. *Energy Fuels* 2003, *17*, 179.
9. Yan, N. X.; Masliyah, J. H. *J. Colloid Interface Sci.* 1994, *168*, 386.
10. Kupai, M. ; M. ; Yang, F. ; Harbottle, D. ; Moran, K. ; Masliyah, J. ; Xu, Z. *Canadian Journal of Chemical Engineering* 2013, *91*, 1395.
11. Feng, X. M. P.; Gao, S.; Wang, S.; Wu, S. Y.; Masliyah, J. H.; Xu, Z. *Langmuir* 2010, *26*, 3050.
12. Feng, X. H.; Xu, Z.; Masliyah, J. *Energy Fuels* 2009, *23*, 451.
13. Wang, S.; Segin, N.; Wang K.; Masliyah, H. H.; Xu, Z. *J. Phys. Chem. C* 2011, *115*, 10576.

14. Israelachvili, J.; Min, Y.; Akbulut, M.; Alig, A.; Carver, G.; Greene, W.; Kristiansen, K.; Meyer, E.; Pesika, N.; Rosenberg, K.; Zeng, H. *Rep. Prog. Phys.* 2010, 73 (036601), 1.
15. Anderson, T. H.; Donaldson, S. H.; Zeng, H.; Israelachvili, J. N. *Langmuir* 2010, 26, 14458.
16. Hwang, D. S.; Zeng, H.; Masic, A.; Harrington, M. J.; Israelachvili, J. N. Waite, J. H. *J. Biol. Chem.* 2010, 285, 25850.
17. Zeng, H.; Hwang, D. S.; Israelachvili, J. N.; Waite, J. H. *Proc. Natl. Acad. Sci. U.S.A.* 2010, 107, 12850.
18. Blomberg, E.; Claesson, P. M.; Warnheim, T. *Colloids Surf. A* 1999, 159, 149.
19. Zhang, L. Y.; Lawrence, S.; Xu, Z.; Masliyah, J. H. *J. Colloid Interface Sci.* 2003, 264, 128.
20. Israelachvili, J. N. *Intermolecular and Surface Forces*, 2nd ed.; Academic Press: New York, 1991; p 291.
21. Akbulut, M.; Alig, A. R. G.; Min, Y.; Belman, N.; Reynolds, M.; Golan, Y.; Israelachvili, J. *Langmuir* 2007, 23, 3961.
22. Zeng, H. *Polymer Adhesion, Friction and Lubrication*, Somerset, NJ, USA: Wiley, 2013.
23. Israelachvili, J. N. *J. Colloid Interface Sci.* 1973, 44, 259.
24. Natarajan, A.; Xie, J.; Wang, S.; Liu, Q.; Masliyah, J.; Zeng, H.; Xu, Z. *J. Phys. Chem. C* 2011, 115, 16043.

25. Natarajan, A.; Kuznicki, N.; Harbottle, D.; Masliyah, J.; Zeng, H.; Xu, Z. *Langmuir* 2014, submitted.
26. Wang, S.; Liu, J.; Zhang, L.; Xu, Z.; Masliyah, J. *Energy Fuels* 2009, 23, 862.
27. Dijt, J. C.; Cohen Stuart, M. A.; Fleer, G. J. *Macromolecules* 1994, 27, 3207; 1994, 27, 3219; 1994, 27, 3229.
28. De Gennes, P. G. *Macromolecules* 1981, 14, 1637.
29. Scheutjens, J. M. H. M.; Fleer, G. J. *Macromolecules* 1985, 18, 1882.
30. de-Gennes, P. G. *Adv. Colloids Interface Sci.* 1987, 27, 189.
31. Kuhl, T. L.; Leckband, D. e.; Lasic, D. D.; Israelachvili, J. N. *Biophys. J.* 1994, 66, 1479.
32. Efremora, N. V.; Bondurant, B.; O'Brien, D. F.; Leckband, D. E. *Biochemistry* 2000, 39, 3441.
33. Butt, H. J.; Kappl, M.; Mueller, H.; Raiteri, R.; Meyer, W.; Ruhe, J. *Langmuir* 1999, 15, 2559.
34. Kamiyana, Y.; Israelachvili, J. *Macromolecules* 1992, 25, 5081.
35. Mullins, O. C.; Hammami, A.; Marshall, A. G. *Asphaltenes, heavy oils and petroleomics*: Springer: New York, 2007.
36. Sheremata, J. M.; Gray, M. R.; Dettman, H. D.; McCaffrey, W. C. *Energy Fuels* 2004, 18, 1377.
37. Strausz, O. P.; Mojelsky, T. W.; Lown, E. M. *Fuel* 1992, 71, 1355.

38. Ruths, M.; Israelachvili, J. N.; Ploehn, H. J. *Macromolecules* 1997, 30, 3329.
39. Hu, H. W.; Granick, S. *Macromolecules* 1990, 23, 613.

## **Chapter 6**

### **Summary**

#### **6.1 Overall Summary**

Stable water-in-bitumen emulsions are undesirable in the bitumen extraction process. The quality of the final product and the integrity of the equipment in both the upstream and downstream processes are challenged by stable w/o emulsions. Asphaltenes and fine solids contaminated by hydrocarbons are one of the primary causes of emulsion stability. Hence removal or destabilizing this stable emulsion is essential. In order to do that, we must first understand why and how these emulsions are stable in the first place. This requires a fundamental understanding of the molecular interactions between the different materials involved. To this effect, the present work measures the interactions between asphaltene surfaces in organic solvent, both good and poor. The adsorption mechanism of asphaltenes on mica is discussed. Molecular interactions between asphaltenes, EC and mica are measured to establish their implications on the observed wettability control mechanism. In all of the above cases, the asphaltene films on mica surfaces mimic the stable interfacial film and the mica surfaces mimic the water droplets or hydrophilic solid surface.

In Chapter 3, the SFA force measurements allowed a direct evaluation on molecular interactions of asphaltenes in organic solvents providing insight of

molecular aggregation, rearrangements and swelling of asphaltenes in toluene and heptane. The swelling of asphaltene films/layers in heptane, though small, illustrates the complexity of asphaltene structure. By fitting the measured force profiles with theoretical models, the presence of secondary structures of asphaltenes in toluene was observed, stemming from the polydispersity/complexity of asphaltene molecules/aggregates. Asphaltenes adsorb on mica irreversibly indicating strong adhesion force. In contrast, asphaltene surfaces swell significantly in toluene giving rise to strong steric repulsion. The results suggest that fine hydrophilic solids along with asphaltenes aggregate at the water-oil interface and form a semi-rigid interfacial film. The presence of such rigid interfacial film, coupled with the steric repulsion between asphaltene surfaces, lead to strong energy barrier preventing the water droplets from coalescing.

In Chapter 4, we analyze the adsorption mechanisms that enable asphaltenes to adsorb or coat the surface of fine solids to render them interfacially active. Adsorption of asphaltenes on mica is highly dependent on time and concentration of the solution. The experimental results show the following (1) asphaltenes rearrange their conformation at molecular level with time, (2) the thickness of the interfacial film grows suggesting multilayer formation with time, (3) the interfacial film thickness gradually approaches that of a loose and compressible solid if the concentration of asphaltenes in the bulk solution is sufficiently high, and (4) the adsorption process is controlled by diffusion of asphaltenes from the

bulk solution to the solids surface. The surface modification of fine solids by asphaltenes can lead to dramatically enhanced emulsion stability and the above experimental results highlight this important mechanism.

In Chapter 5, EC was observed to irreversibly adsorb on mica forming a much smoother and flatter morphology than asphaltene adsorption on mica. By virtue of the number of bonding sites (hydroxyl groups) in its structure, EC has a stronger affinity towards mica surface than asphaltenes whose large hydrophobic aromatic rings leave comparatively fewer available binding sites. This strong attraction for mica surface enables EC to penetrate the asphaltene films at the interface and bind to the solid surface. EC then gradually begins to expand and compete for the binding sites on the solid surface. The long-ranged repulsion between EC and asphaltenes that prevents polar-polar bonding effectively, forces asphaltenes on the solid surface to form globule structures/aggregates. In this way, EC is able to decrease the surface hydrophobicity of asphaltene-contaminated solids.

## **6.2 Major Contributions**

1. To the best of my knowledge, this is the first time the SFA has been used for a direct evaluation on molecular interactions of asphaltenes in both good and poor solvents. The force measurements provided insights into molecular aggregation, rearrangements, and swelling of asphaltenes in toluene and heptane.

2. The successful application of the scaling theory for polymer brushes to the steric repulsion forces between asphaltene surfaces at short separation distances under high compression forces supports the polymeric properties of asphaltene molecules adsorbed on a hydrophilic solid surface. The deviation of steric repulsion at large separation distances under lower compression forces from the scaling theory indicates the presence of secondary structures of asphaltenes in good solvents.
3. At dilute concentrations (0.01 wt%) the adsorption of asphaltenes from the bulk solution to a hydrophilic solid surface is controlled by diffusion.
4. The force measurements between EC and asphaltenes sheds light on the wettability control of organic-contaminated solids using chemicals, especially appropriate demulsifiers of w/o emulsions to improve processability of heavy oils.

### **6.3 Suggestions for Future Work**

It seems fairly clear from the evidence presented in this dissertation that asphaltenes and fine solids play an unambiguous and important role in water-in-oil emulsion stabilization. But in order to fully understand this emulsion stabilizing mechanism more work needs to be carried out to understand the interactions between all other players that contribute to emulsion stability:

- (1) Understanding the interactions between asphaltenes and aromatic and polyaromatic acids in stabilizing interfacial film could provide important clues to emulsion stability. Similarly, Interaction between asphaltenes and.
- (2) Interactions between asphaltenes and naphthenic acids, linear acids, or fused aromatic ring acids are an area of research that can provide useful information of emulsion stability. There are evidence in the literature that a low total acid number/high asphaltene crude oil forms stable and troublesome emulsions.
- (3) Surface force measurements in naphtha, which is the industrial choice of solvent in the extraction process. Defined as a fraction of crude oil, it is made up of complex mixtures of cyclic saturates and fused aromatic sheets. Toluene and heptane used in the present work cannot represent this complex structure.

## Appendix 1

### Preparation of Solid and Hollow Asphaltene Fibers by Single Step Electrospinning<sup>d</sup>

Electrospinning has been used to produce micrometer size fibers, both solid and hollow from non-covalently associate small molecules of a low grade hydrocarbon reject of crude oil, asphaltene. Asphaltene defined as a solubility class of crude oil is by no means a polymer but relatively large organic molecule of molecular weight ranging from 500 to 1000 Dalton. The production of asphaltene fibers is feasible by electrospinning because of its unique molecular structure which allows molecular aggregation. Fibers with diameter ranging from 2-20  $\mu\text{m}$  were successfully spun from an asphaltene in toluene solution. Adding 2% hydrogen peroxide enhances electrospinning, leading to formation of hollow fibers, whereas adding 2% water inhibits electrospinning. The structure and morphology of the electrospun fibers were investigated with optical microscopy, scanning electron microscopy, Fourier transform infrared spectroscopy and time-of-flight secondary ion mass spectroscopy. The electrospun asphaltene fibers offer

---

<sup>d</sup> Published Work: Natarajan, A.; Mahavadi, S. C.; Natarajan, T. S.; Masliyah, J. H.; Xu, Z. *Journal of Engineered Fibers and Fabrics* **2011**, 6, 1-6.

the potential for direct fabrication of membranes without use of multiple synthetic steps, complex electrospinning designs, or post processing surface treatments.

## **INTRODUCTION**

Asphaltenes are components found in crude oil and bitumen. Defined as solubility class: insoluble in n-alkanes, such as n-pentane or n-heptane, and soluble in toluene. According to their chemical structure, they are aromatic multicyclic molecules surrounded and linked by aliphatic chains and heteroatoms. They are a mixture of large number of molecular species and hence are extremely complex and difficult to characterize. Their complex structure and polarity lead to their self association, flocculation and precipitation, depending on the properties of solvents. Due to these effects and their amphiphilic nature asphaltenes create problems in every stage of heavy oil processing such as clogging of wells, flowlines and surface facilities, and hence are considered undesirable components.<sup>1,2</sup> Recently published molar mass data for crude oil asphaltenes ranges from 500 Dalton to 1000 Dalton.<sup>3</sup>

Electrospinning introduces electrostatic forces as the driving force to form ultra thin fibers. In this process, a polymer solution (in our case – asphaltenes) held by its surface tension at the end of a capillary tube is subjected to an electric field. With an increase in electric potential the charged pendent drop is deformed into a cone, known as “Taylor’s cone”.<sup>4</sup> At a critical field strength when the force due to the electric field overcomes the surface tension force holding the droplet, the

solution starts to flow in the form of a charged jet. The jet moves towards the collecting counter electrode. While in transit, most of the solvent evaporates and the different polymer strands in the jet separate out due to mutual repulsion, a phenomenon known as “splaying”. When these strands reach the collecting electrode their diameters are in the range of a few micrometers to nanometers. Continuous fibers are collected in the form of a nonwoven fabric.<sup>5-8</sup>

One of the suggested conditions necessary for electrospinning to occur is that the solution must consist of a polymer of sufficient molecular weight and minimum critical viscosity.<sup>9</sup> As the jet of polymer solution leaves the tip of needle during electrospinning, it is stretched as it travels towards the collection plate. During the stretching of the polymer solution, it is the entanglement of the molecular chains that prevents the electrically driven jet from breaking up and thus maintaining a continuous jet. As a result, monomeric polymer solution does not form fibers when electrospun.<sup>9,10</sup> Molecular weight of the polymer represents the length of the polymer chain, which in turn has an effect on the viscosity of the solution since the polymer molecular length is one of key properties determining the degree of entanglement of the polymer chains in a solvent. Hence, producing fibers of asphaltene with a molecular weight in the range of 500-1000 Dalton would be considered infeasible unless there is some kind of network or entanglement between the individual molecules.

It is postulated that in aromatic solvents, asphaltenes are highly soluble, but above a certain concentration, known as the critical nanoaggregate concentration (CNAC) they can form nanoaggregates.<sup>11</sup> The CNAC data for asphaltenes in toluene have been determined using a variety of methods, such as laser thermal lensing,<sup>12</sup> fluorescence measurements,<sup>13</sup> and high-quality-factor (high-Q) ultrasonic spectroscopy.<sup>14</sup> Studies on Index-of-refraction show the importance of van der Waals interactions in controlling the solubility of asphaltenes in various types of solvents.<sup>15</sup> It is well established now that the van der Waals attraction of aromatic rings balances with the steric repulsion of alkane chains, thereby determining the solubility of asphaltenes in various types of solvents.<sup>14,16</sup> It is suggested by Andreatta, et al.<sup>14</sup> that asphaltenes are shaped “like your hand” with aromatic rings being the palm and the alkane chains being the fingers. It is thought that the association of first few asphaltene molecules has fairly clear access to intermolecular interactions of the fused rings. The aromatic rings of different asphaltene molecules stack like “pancakes” to form nanoaggregates.<sup>14</sup> However, subsequent aggregation of more molecules becomes constrained, due to the presence of alkane substituents, impeding further stacking. As a result of this steric repulsion, at some point, the interaction between a nanoaggregate and additional molecules becomes rather weak. At this point, new nanoaggregates form with increasing concentration but not an increase in the size of a single nanoaggregate.<sup>14</sup> Finally, at very high asphaltenes concentrations, the nanoaggregates undergo clustering with low binding energy between them.<sup>14</sup>

Here, we discuss electrospinning of these non-covalently associating small molecules. Through interactions such as hydrogen bonding, van der Waals forces, a sufficient number of clusters of nanoaggregates is reached that allows asphaltenes to electrospin successfully. The only other small molecules that have been used in electrospinning are phospholipids and very recently peptides.<sup>17,18</sup> With careful variation and adjustment of the experimental parameters, we demonstrate the production of asphaltene solid and hollow fibers by electrospinning with diameter ranging from 2-20  $\mu\text{m}$ . Our study shows that molecular weight is not a major criterion for electrospinning, rather the intermolecular forces between the asphaltene aggregates and hence molecular association are sufficient to mimic the chain entanglements observed in polymer solutions. Similar conclusions were reached by McKee, et al.<sup>17</sup> while spinning phospholipids.

## **MATERIALS AND METHODS**

Vacuum distillation bitumen feed contains ca. 0.5 wt% solids which consist of fine clays, mineral matters and solid hydrocarbons which are insoluble in toluene. The solids were removed by centrifugation of toluene-diluted bitumen at a toluene to bitumen volumetric ratio of 5:1 for 30 min at 20,000 rpm. The toluene was then removed from the bitumen solution by natural evaporation. Heptane was mixed with the prepared bitumen at a volume ratio of 40:1 to extract the asphaltenes. The *n*-heptane and bitumen mixture was shaken for 2 hours on a laboratory shaker and

left overnight for asphaltene precipitation. The supernatant was then decanted and the asphaltene precipitates were repeatedly washed with *n*-heptane in a bottle until the supernatant became colorless. The solid asphaltenes were left overnight in a fume hood to evaporate the solvent. The asphaltene prepared as such is referred to as whole asphaltene. The mass of the whole asphaltene is about 11% of the original bitumen. Solutions with 10%, 15%, 20%, 30% and 40% (wt/wt) of asphaltene were prepared in toluene. The solutions were freshly prepared by adding a required amount of asphaltene into toluene under stirring at 20,000 rpm for 30 minutes. The resultant solution was sonicated for 30 minutes before electrospinning. In this study, silicon wafer was used as collector. The silicon wafer was made hydrophilic by thorough cleaning in a solution of hydrogen peroxide and sulphuric acid for about 30 minutes.

## **EXPERIMENTAL SETUP**

The experimental setup is shown in **Fig 1**. A 3 ml syringe was connected through the needle to the one end of a Teflon tube with an internal diameter of 0.7 mm, and a stainless steel needle of the same diameter as the the one on the syringe was connected to the other end of the tube. The substrate was mounted to an adjustable laboratory screw jack. The stainless steel needle was connected to the positive terminal and the substrate to the negative terminal of a high voltage power supplier. During the experiment, a pendent drop of asphaltene in toluene solution was formed at the tip of the needle just before the application of electric potential. The

applied voltage was gradually increased. With increasing applied potential the pendent drop elongated to form a Taylor cone at a critical voltage ( $\sim 8$  kV), at which a jet started from the tip of the cone. No good fibers were formed if electrospinning was performed at this critical voltage. In fact, there were more droplets rather than fibers deposited on the substrate collector. Therefore the voltage of electrospin was increased further to obtain better fibers.

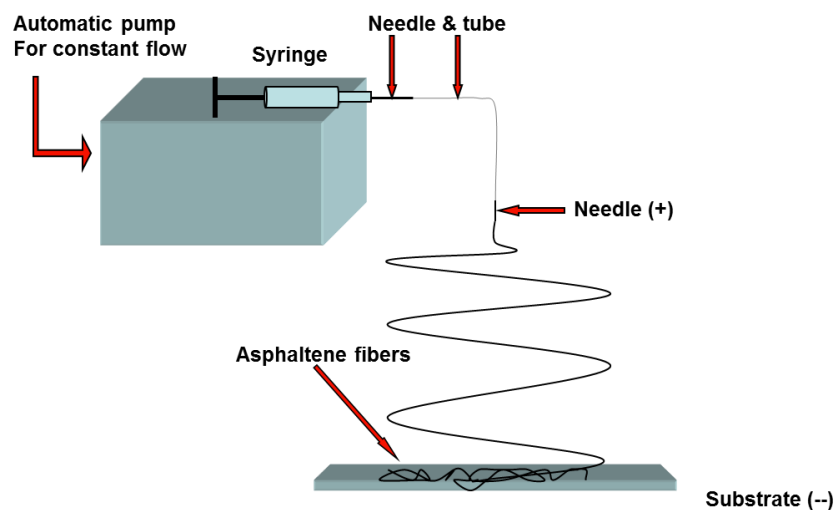


**Figure 1.** Experimental setup

## RESULTS AND DISCUSSIONS

We have previously described the importance of chain entanglements for the formation of electrospun fibers. Electrospun fiber formation would not be possible

if the asphaltenes did not aggregate and form clusters of aggregates in some form of entangled network, as individual asphaltene molecules are low molecular weight compounds and hence incapable of forming entanglements. Another way to facilitate aggregation and result in greater clustering of aggregates within the solution is to increase the asphaltene concentration, which is similar to increasing molecular weight of a polymer. Thus asphaltene concentration was chosen as a variable while other electrospun conditions were fixed at 50 kV/m electric field strength, 1  $\mu\text{L}/\text{min}$  syringe flow rate, and 30 cm working distance. Such preferred conditions were arrived at by trial and error.

Optical microscopy, scanning electron microscopy (SEM), Fourier transform infrared spectroscopy (FTIR) and time-of-flight-secondary ion mass spectroscopy (ToF-SIMS) were used for characterizing the fibers. Before taking electron micrographs, the electrospun fibers were observed by optical microscope to confirm the formation of fibers. The SEM micrographs were obtained using Hitachi S-2700 Scanning Electron Microscope, after sputtering a carbon film of thickness around 5 nm on the substrate. **Fig 2** shows SEM micrographs of electrospun fibers that were formed from various concentrations of asphaltenes in toluene. At 20 wt% of asphaltenes in toluene, droplets were formed because of insufficient concentration, or in other words, limited clustering of asphaltene aggregates to form sufficiently entangled network, which resulted in the breakage of the electrified jet (**Fig 2A**). All the formed droplets tend to collapse inward suggesting that they are hollow. When the concentration was increased to 30%

(Fig 2B), fibers were formed, many of them with beads. During the evaporation of solvents from the fiber, Li et al.<sup>19</sup> suggested that if the evaporation rate through the fiber surface is lower than the diffusion rate outwards the fiber, ballooning of the fiber is unavoidable; otherwise, no ballooning would occur and only dense fibers be obtained. For polymer solutions, reported studies indicated the requirement of a minimum critical viscosity to yield fibers without beads.<sup>9,10,20</sup> When the viscosity is low, equivalent to low asphaltene concentrations in our case, it is common to find beads along the fibers deposited on the collection plate.

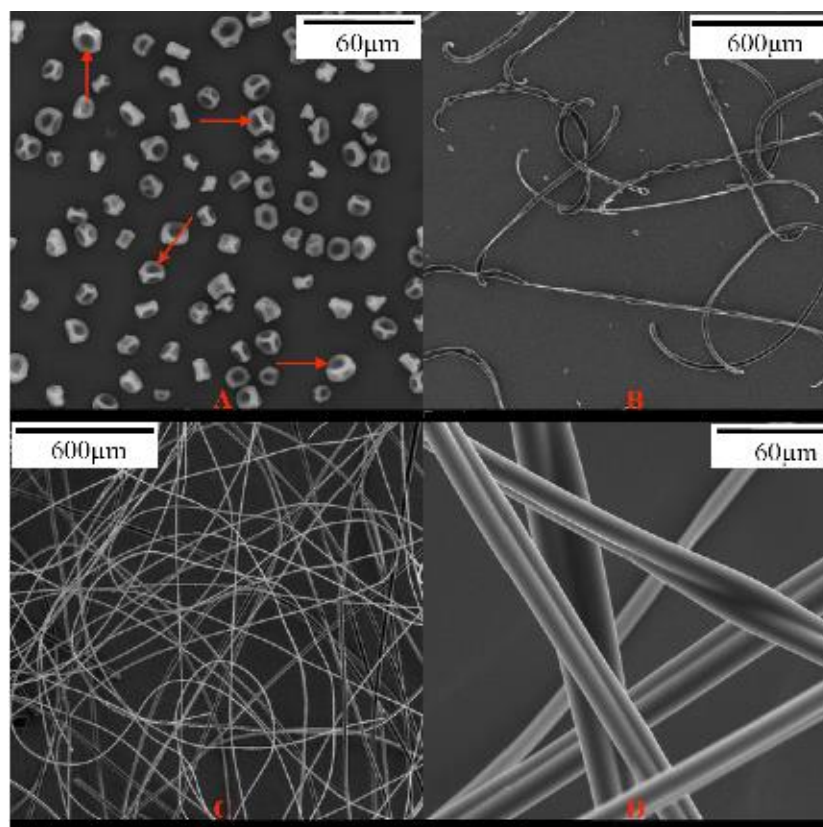


**Figure 2.** A is 20 wt% asphaltene in toluene. The surface of the droplets tends to collapse inward suggesting that they are all hollow (shown by arrow). B shows morphology of fibers formed from 40 wt% asphaltene in toluene solutions. C and D show morphologies of ribbon like fibers formed from 40 wt% asphaltene solutions.

A 35 wt% asphaltene concentration was still not sufficient for the formation of smooth fibers. However, at 40 wt%, uniform beadless fibers with an average diameter of 16  $\mu\text{m}$  were formed and they were ribbon shaped (**Fig 2C**). The fibers are shown at a higher resolution in (**Fig 2D**). One possible mechanism for the formation of fibers might be the accumulation of asphaltene aggregates at interfaces. When the electrically charged jet is initiated and is on its path towards the collection plate, toluene evaporates from the surface of the jet, thereby increasing asphaltene concentration at the jet surface leading to further asphaltene aggregation at the air- toluene interface. As a result, the asphaltene aggregates form a skin on the liquid jet. Koombhongse et al.<sup>21</sup> suggested that as the solvent diffuses out and evaporates, the atmospheric pressure tends to collapse the tube formed by the skin. The circular cross section, during the course of the collapse, initially becomes elliptical and then into ribbon-like shape with small tubes formed at each edge of the ribbon. This phenomenon was observed while spinning 10% poly(ether imide) in hexafluoro-2-propanol.

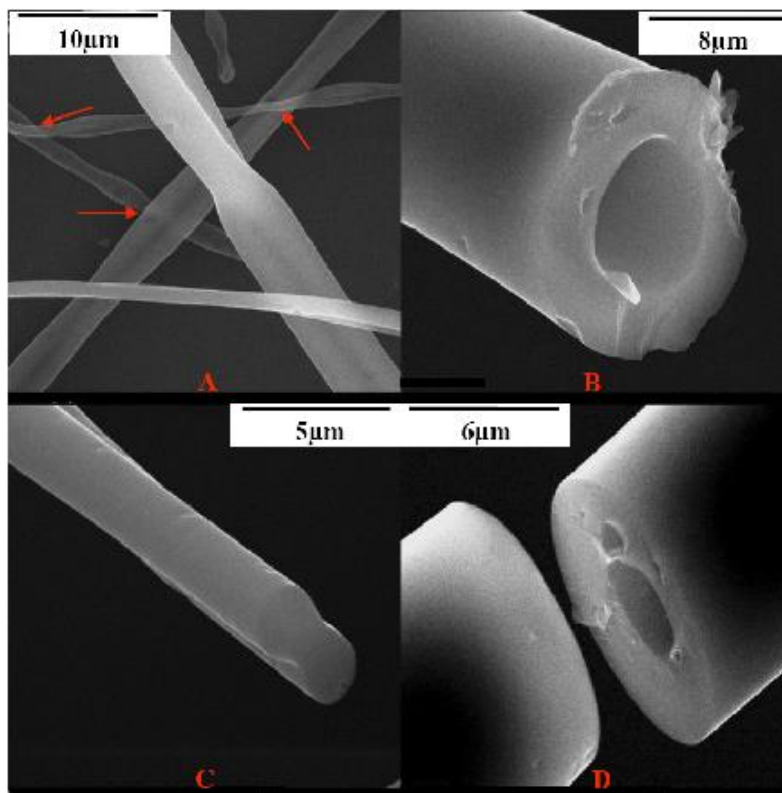


**Figure 3.** A and B are hollow fibers formed by the addition of hydrogen peroxide. The arrow marks in A indicate areas where we can clearly see that the fibers are translucent; C and D are formed by addition of water. Fiber in C is ribbon shaped and in D it is hollow with thick walls.

Hydrogen peroxide is a well-known oxidizing and a cross-linking agent used in polymerization reactions. It was speculated that addition of hydrogen peroxide to an asphaltene solution could improve the fiber morphology. A 2 wt% hydrogen peroxide (with 30% strength) was added to a 20 wt% asphaltene solution. Hollow fibers (**Fig 3A and 3B**) were formed instead of ribbon-like shape as shown in Fig 2. The arrow markings in Fig 3A indicate areas where we can clearly note that the fibers are translucent. Fig 3B is an image of a hollow fiber. Hollow fibers are generally produced using methods such as direct co-axial electrospinning,

chemical vapour deposition or by using special precursors. With these methods, annealing, sintering, calcination, etc. are often needed to achieve desired shapes.<sup>22-24</sup> Our method, however, only uses a single step electrospinning to produce hollow fibers of asphaltenes. To illustrate the role of hydrogen peroxide, the same experiment was conducted with the addition of 2 wt% deionised water. The water formed a water-in-oil emulsion with an average water droplet size of 4  $\mu\text{m}$ . When the mixture was electrospun, the fibers are a mixture of hollow and ribbon morphology (**Fig 3C and 3D**). Decreasing the average size of the droplets to 2  $\mu\text{m}$  inhibited fiber formation during electrospinning. This observation is attributed to aggregation or accumulation of asphaltenes at the water-oil interface rather than air-oil interface. In this case, as the surface area of the droplets increases with decreasing size of the water droplets, insufficient asphaltenes are available at the air-oil interface, thereby limiting the formation of the asphaltene skin on the liquid jet and hence formation of asphaltene fibers. **Fig 4A** and **4B** show a brittle fiber and a fiber that is broken into a large number of pieces. These fibers are formed while spinning 30 wt% asphaltene in toluene. The brittle nature of fibers suggest that the asphaltene fibers formed by electrospinning might be in the crystalline form. **Fig 4C** shows a wafer or foil of asphaltene formed while electrospinning 30 wt% asphaltene in toluene. **Fig 4D** shows the layered asphaltene skin on the surface of the fiber.

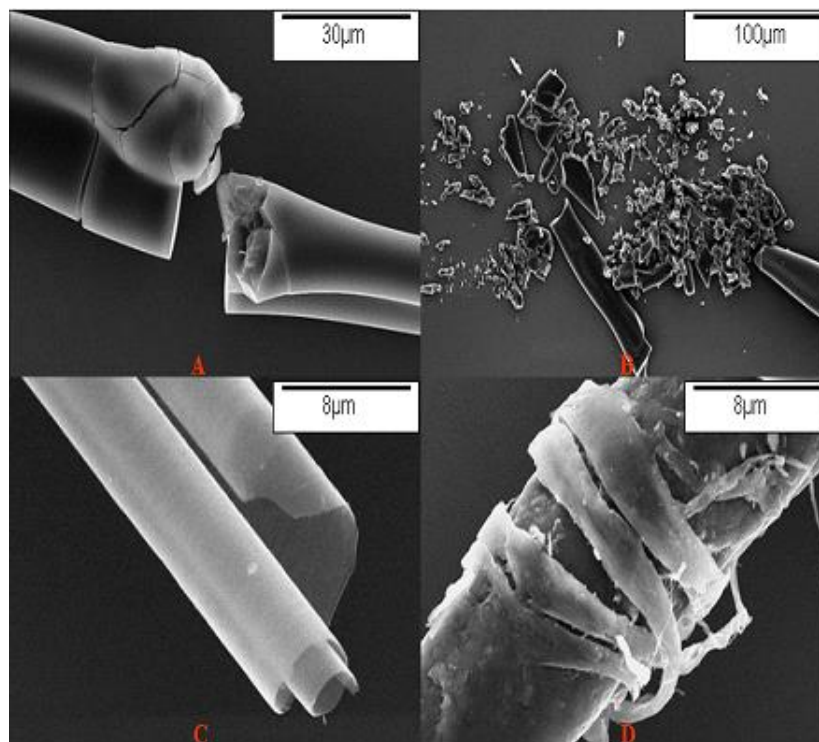


**Figure 4.** Different shapes of fibers formed during electrospinning of asphaltene. A and B show the evidence of fibers turning brittle after electrospinning. These fibers are formed by electrospinning 30 wt% asphaltene in toluene. C is a wafer or foil formed during electrospinning 30 wt% asphaltene in toluene. D shows the layers of asphaltene skin formation while spinning 20 wt% asphaltene with hydrogen peroxide in toluene.

FTIR spectroscopy, shown in **Fig 5**, was used to characterize asphaltene solutions before and after electrospinning. The concentration of asphaltenes in each sample was maintained at 30 wt%. For the bulk asphaltene sample, the bands at 738, 849 and 894  $\text{cm}^{-1}$  are attributed to aromatic C-H bending. Bands at 1378 and 1464  $\text{cm}^{-1}$  assigned to aliphatic C-H bending, and the band over 2700-2930  $\text{cm}^{-1}$  represents aliphatic C-H stretching. Similar band assignments are reported for bulk asphaltene samples.<sup>25</sup> For samples after electrospinning, there are slight indications of new bands at 2270  $\text{cm}^{-1}$  and 2580  $\text{cm}^{-1}$ . They are attributed to R-

N=C=O (isocyanates) and S-H stretching vibrations, respectively. We suspect that the high electric field employed during electrospinning changed the conformation of some of these bonds, which has been reported in literature for other systems.<sup>26</sup>

The nature of these changes needs to be studied further.

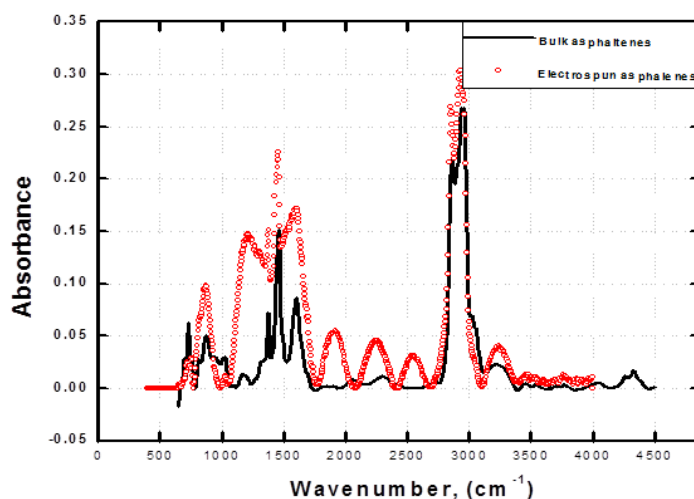


**Figure 5.** FTIR analysis of bulk asphaltene (black solid line) and electrospun asphaltene fibers (red open circles).

**Fig 6** shows ToF-SIMS results for 35 wt% asphaltene samples. During electrospinning, samples for ToF-SIMS analysis were selected from the top, bottom, right, left and center of the substrate, to identify any pattern in the variation of the elemental compositions after electrospinning. The images in Fig 6 show that the fibers are mainly consisted of carbon and hydrogen with small amount of oxygen, sulfur and marginal amount of nitrogen, as anticipated. It was also found that the carbon to sulphur ratio in the fibers varied when moving from

the edges of the collector towards the center. This observation indicates chemical alterations of asphaltenes after electrospinning. Systematic study is needed to investigate changes in structure and stacking sequence of asphaltene aggregates after electrospinning.

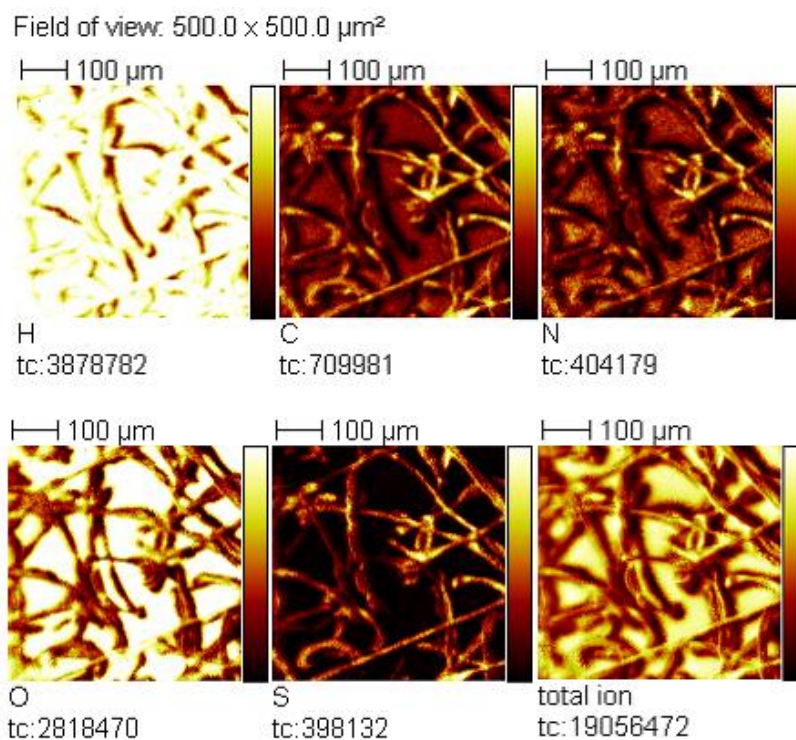


**Figure 6.** ToF-SIMS results for 35% asphaltene fibers. The image shows the elemental composition on the fibers. The bright colour indicates abundance of the substance and the dark colour signifies scarcity. Here H, C, N, O, S mean hydrogen, carbon, nitrogen, oxygen and sulphur. Also, tc is the total intensity of the individual element. The substrate here is silicon wafer.

## **CONCLUSION**

This study shows that the intermolecular forces between asphaltene molecules are sufficient to form smooth fibers by electrospinning. Asphaltene fibers with an average diameter of 16  $\mu\text{m}$  were successfully electrospun. Hollow fibers were observed when 2 wt% hydrogen peroxide was added to the asphaltene solution. Adding 2 wt% of water was found to inhibit electrospinning. There is indication that the high electric field employed during electrospinning caused chemical alterations of ashaltenes in the formed fibers.

## REFERENCES

1. G. V. Chilingarian, T. F. Yen, *Bitumens, Asphalts, and Tar Sands*, Elsevier Scientific Publishing Co., New York, **1978**.
2. J. W. Bunger, N. C. Li, *Chemistry of Asphaltenes*, Eds, American Chemical Society, Washington DC, **1984**.
3. O. C. Mullins, E. Y. Sheu, A. Hammami, A. G. Marshall, *Asphaltenes, heavy oils and petroleomics*, Springer Science+Business Media, **2007**.
4. A. L. Yarin, S. Koombhongse, D. H. Reneker, *J. Appl. Phys*, 2001, **90**, 9, 4836-4846.
5. Dan Li and Younan Xia, *Adv. Mater.* 2004, **16**, 14, 1151-1170.
6. J. Doshi, D. H. Reneker, *J. Electrostatics*, 1995, **35**, 151- 160.
7. B. Sundaray, V. Subramanian, T. S. Natarajan, R. Z. Xiang, C. C. Chang, W. S. Fann, *Appl. Phys. Lett*, 2004, **84**, 7, 1222-1224.
8. J. H. Yu, S. V. Fridrikh, G. C. Rutledge, *Adv. Mater*, 2004, **16**, 1562-1566.
9. S. Ramakrishna, K. Fujihara, W. E. Teo, T. C. Lim, Z. Ma, *Introduction to Electrospinning and Nanofibers*, World Scientific Publishing Co. Pte. Ltd., Singapore, **2005**.
10. H. Fong, I. Chun, D. H. Reneker, *Polymer*, 2004, **40**, 4585-4592.
11. Gaelle Andreatta, Cristiane Carla Goncalves, Gabriel Buffin, Neil Bostrom, Cristina M. Quintella, Fabricio Arteaga-Larios, Elas Prez and Oliver C. Mullins, *Energy Fuels*, 2005, **19**, 4, 1282-1289.

12. S. Acevedo, M. A. Ranaudo, J. C. Pereira, J. Castillo, A. Fernandez, P. Perez, M. Caetano, *Fuel*, 1999, **78**, 997-1003.
13. S. Goncalves, J. Castillo, A. Fernandez, J. Hung, *Fuel*, 2004, **83**, 1823-1828.
14. G. Andreatta, N. Bostrom, O. C. Mullins, *Langmuir*, 2005, **21**, 7, 2728-2736.
15. J. Buckley, *Energy Fuels*, 1999, **13**, 328-332.
16. E. Buenrostro-Gonzalez, H. Groenzin, C. Lira-Galeana, O. C. Mullins, *Energy Fuels*, 2001, **15**, 972-978.
17. M. G. McKee, J. M. Layman, M. P. Cashion, T. E. Long, *Science*, 2006, **311**, 353-355.
18. Gurvinder Singh, Alexander M. Bittner, Sebastian Loscher, Nikola Malinowski and Klaus Kern, *Adv. Mater*, 2008, **20**, 2332-2336.
19. Jianyin Li, Hui Dai, Xinghua Zhong, Yaufei Zhang and Xueqiang Cao, *Adv. Mater*, 2007, **9**, 3, 205-207.
20. S. Megelski, J. S. Stephens, D. B. Chase, J. F. Rabolt, *Macromolecules*, 2002, **35**, 8456-8466.
21. S. Koombhongse, W. Liu, D. H. Reneker, *J. Polym. Sci., Part B; Polym. Phys*, 2001, **39**, 2598-2606.
22. D. Li and Y. Xia, *Nano Lett*, 2004, **4**, 933-938.
23. M. Bognitzki, H. Hou, M. Ishaque, T. Frese, M. Hellwig, C. Schwarte, A. Schaper, J. H. Wendorff, A. Greiner, *Adv Mater*, 2000, **12**, 9, 637-640.

24. Y. Dror, W. Salalha, R. Avrahami, E. Zussman, A. L. Yarin, R. Dersch, A. Greiner, J. H. Wendorff, *Small*, 2007, **3**, 6, 1064-1073.
25. L. Y. Zhang, R. Lopetinsky, Z. Xu, J. H. Masliyah, *Energy Fuels*, 2005, **19**, 1330-1336.
26. J. S. Stephens, D. B. Chase, J. F. Rabolt, *Macromolecules*, 2004, **37**, 877-881.